

8. SITE 1014¹

Shipboard Scientific Party²

HOLE 1014A

Date occupied: 8 May 1996
Date departed: 10 May 1996
Time on hole: 2 days, 13 hr, 15 min
Position: 32°49.994'N, 119°58.903'W
Drill pipe measurement from rig floor to seafloor (m): 1175.8
Distance between rig floor and sea level (m): 11.0
Water depth (drill pipe measurement from sea level, m): 1164.8
Total depth (from rig floor, m): 1624.8
Penetration (m): 449.0
Number of cores (including cores having no recovery): 50
Total length of cored section (m): 449.0
Total core recovered (m): 404.4
Core recovery (%): 90.0
Oldest sediment cored:
Depth (mbsf): 449.0
Nature: Clay with silt, nannofossil chalk with clay
Age: late Miocene

HOLE 1014B

Date occupied: 10 May 1996
Date departed: 11 May 1996
Time on hole: 18 hr, 00 min
Position: 32°50.045'N, 119°58.874'W
Drill pipe measurement from rig floor to seafloor (m): 1177.7
Distance between rig floor and sea level (m): 11.0
Water depth (drill pipe measurement from sea level, m): 1166.7
Total depth (from rig floor, m): 1422.7
Penetration (m): 245.0
Number of cores (including cores having no recovery): 27
Total length of cored section (m): 245.0
Total core recovered (m): 224.7
Core recovery (%): 91.0
Oldest sediment cored:
Depth (mbsf): 245.0
Nature: Nannofossil ooze with clay, clayey nannofossil ooze with carbonate
Age: late Pliocene

HOLE 1014C

Date occupied: 11 May 1996
Date departed: 11 May 1996
Time on hole: 01 hr, 15 min
Position: 32°50.044'N, 119°58.881'W
Drill pipe measurement from rig floor to seafloor (m): 1176.4
Distance between rig floor and sea level (m): 11.0
Water depth (drill pipe measurement from sea level, m): 1165.4
Total depth (from rig floor, m): 1195.4
Penetration (m): 19.0
Number of cores (including cores having no recovery): 2
Total length of cored section (m): 19.0
Total core recovered (m): 19.5
Core recovery (%): 102.0
Oldest sediment cored:
Depth (mbsf): 19.0
Nature: Silty clay with foraminifers, nannofossil ooze with clay, clay nannofossil mixed sediment
Age: Quaternary

HOLE 1014D

Date occupied: 11 May 1996
Date departed: 11 May 1996
Time on hole: 07 hr, 45 min
Position: 32°50.046'N, 119°58.879'W
Drill pipe measurement from rig floor to seafloor (m): 1177.0
Distance between rig floor and sea level (m): 11.0
Water depth (drill pipe measurement from sea level, m): 1166.0
Total depth (from rig floor, m): 1297.9
Penetration (m): 120.9
Number of cores (including cores having no recovery): 13
Total length of cored section (m): 120.9
Total core recovered (m): 119.0
Core recovery (%): 98.0
Oldest sediment cored:
Depth (mbsf): 120.9
Nature: Silty clay, nannofossil clay mixed sediment
Age: Quaternary

Principal results: Site 1014 is located in Tanner Basin, within the outer band of California Borderland basins. The primary objective of drilling at this site was to sample a high-resolution section from the late Miocene to Quaternary to study the evolution of the California Current system and to study oceanographic processes in intermediate waters as Northern Hemi-

¹Lyle, M., Koizumi, I., Richter, C., et al., 1997. *Proc. ODP, Init. Repts.*, 167: Col-lege Station, TX (Ocean Drilling Program).

²Shipboard Scientific Party is given in the list preceding the Table of Contents.

sphere glaciations expanded. The site will also provide important information about organic carbon diagenesis and about minor element geochemistry through interstitial water profiles and through solid phase analyses.

Four holes were cored with the APC/XCB at Site 1014 to a maximum depth of 449.0 mbsf, recovering an apparently continuous interval of Quaternary to lower Pliocene sediments, underlain by a poorly dated upper Miocene(?) sequence (Fig. 1). Hole 1014A was cored with the APC to 50.6 mbsf and extended with the XCB to 449.0 mbsf. The hole was logged with the density-porosity combination tool (density, neutron porosity, resistivity, and natural gamma ray), the GHMT magnetic tool, and the sonic-Formation MicroScanner. Hole 1014B was cored with the APC to 114.7 mbsf and deepened with the XCB to 245.0 mbsf. Two APC cores were taken at Hole 1014C down to 19.5 mbsf. Hole 1014D was cored with the APC to 92.0 mbsf and deepened with the XCB to 120.9 mbsf. Detailed comparisons between the magnetic susceptibility and GRAPE density record generated on the MST and the high-resolution color reflectance measured with the Oregon State University system demonstrated complete recovery of the sedimentary sequence down to 160 mbsf.

The sediments consist predominantly of calcareous nannofossils, foraminifers, and siliciclastic clays. The top of the section is characterized by ~140 m of Quaternary interbedded clay and nannofossil ooze. An increase in the amount of calcareous nannofossils marks the top of 310 m of nannofossil ooze and nannofossil chalk alternating with clay-rich intervals. This unit is late to early Pliocene from 140 to 372 mbsf and late Miocene below 372 mbsf. The sedimentation rate throughout the uppermost part of this section is around 79 m/m.y. Ash layers, thin dolostone beds, and glauconite occur in the lower part of the sequence.

Biostratigraphic age control was provided by a combination of calcareous nannofossil, planktonic foraminifer, and radiolarian datums for the upper Pliocene and Quaternary. The base of the sequence is not well dated, but calcareous nannofossils suggest a late Miocene age of between 5 and 7 Ma.

Microfossil assemblages suggest weak to strong upwelling cycles during the late Pliocene leading to high productivity episodes on the continental margin and relative warmth from the early Pliocene through the late Pliocene until 2.5 Ma. Cooling at thermocline depths is suggested after 3.0 Ma by changes in radiolarian fauna. Low oxygen concentrations in basinal bottom waters during the earliest Quaternary through latest Pliocene coincided with strong upwelling. During the Quaternary, benthic foraminifer assemblages change in association with glacial-interglacial oscillations. This suggests changes in upper intermediate water circulation during late Quaternary climatic cycles.

Paleomagnetic investigations revealed a good magnetostratigraphic record down to 100 mbsf (Fig. 1 in "Site 1012" chapter, this volume) and allowed the identification of the Brunhes and Jaramillo normal polarity intervals. The interstitial water geochemistry reflects the influence of organic carbon diagenesis by sulfate reduction, biogenic opal dissolution, and possible authigenic mineralization reactions. Opal dissolution is indicated by the increase of dissolved silicate to values >1000 μM by 136.6 mbsf. Nonconservative profiles of calcium and magnesium indicate the potential importance of authigenic mineralization. Calcium carbonate content steadily increases from 30 wt% at the top to about 55 wt% at 250 mbsf and decreases again towards the bottom of the section. The organic carbon concentration is very high (2–9 wt%) and mainly of marine origin. Thermal conductivity is low, 0.842 W/(m·K) on average, and yields a heat-flow estimate of 49 mW/m².

BACKGROUND AND OBJECTIVES

General Description

Site 1014 is located ~150 km west of San Diego, California, in Tanner Basin, within the outer band of the California Borderland basin (Fig 2). It is west of Site 1013 (San Nicolas Basin), over the Santa Rosa–Cortes Ridge. Water depth at the drill site is shallow (1176 mbsl), and the sill depth for waters entering the deep basin is 1164

mbsl, similar to the sill for San Nicolas Basin (Emery, 1960). Deep water flowing into the basin, however, comes not from the south, but instead travels over a sill to the northwest near the San Miguel Gap (Fig. 3). It is almost directly in communication with pelagic intermediate waters and should suffer little loss of oxygen or addition of nutrients relative to these pelagic waters.

The site was surveyed in detail with the *Maurice Ewing* on cruise EW9504 in 1995 (Lyle et al., 1995a, 1995b; Fig. 4). Because of the proximity to major banks that become islands during low sea-level stands (Fig. 3), the deepest part of Tanner Basin (about 1500 mbsl) has significant turbidite deposition. We located Site 1014 in a shallow sub-basin to the west to avoid turbidites and to sample a hemipelagic section. Site 1014 is located near the central axis of this sub-basin (Fig. 4). The sediments exhibit a seismically transparent layer that extends 270 ms TWT below the seafloor (210–215 m) over more layered sequences below. An upper Miocene to Quaternary section was recovered.

Site Objectives

Site 1014 was drilled to sample a high-resolution section from the upper Miocene to Quaternary in the Tanner Basin to study the evolution of the California Current system and to study oceanographic processes in intermediate waters as Northern Hemisphere glaciation expanded. Benthic foraminiferal isotope data at Site 1014 should reflect intermediate-water characteristics at the sill depth (1164 mbsl), especially as the connection to offshore waters is close to the drill site. Planktonic microfossil data primarily will be influenced by waters traveling south in the California Current when it exists regionally. The sill depth of Tanner Basin approaches the modern depth of the oxygen minimum (~700 mbsl).

Site 1014 will also provide important new information about organic carbon diagenesis and about minor element geochemistry through interstitial water profiles and through solid phase analyses. Organic carbon content of Tanner Basin sediments is high, although there is little terrestrial input because of the location of the site. Interstitial water sampling, especially within the upper 100 m, will be used to define organic matter diagenesis and the removal of oxidants from interstitial waters and sediments, whereas organic geochemical analysis will provide data on organic matter preservation in a low-oxygen environment. Because of its location away from the turbidites that fill the inner California Borderland basins, we expect most of the organic matter in the basin to be marine in origin.

OPERATIONS

Transit from San Diego to Site 1014

The 151.0-nmi transit from San Diego to Site 1014 was accomplished in 15.5 hr at an average speed of 10.4 kt. A 3.5-kHz precision depth recorder (PDR) survey was performed while approaching the site. The *JOIDES Resolution* arrived at Site 1014 at 0530 hr on 8 May.

Hole 1014A

Hole 1014A was spudded at 0900 hr on 8 May. APC Cores 167-1014A-1H through 6H were taken from 0 to 50.6 mbsf with 100.8% recovery (Table 1; see Table 2 on CD-ROM in the back pocket of this volume for a more detailed coring summary). Oriented cores were obtained starting with 3H. APC refusal was reached at 50.6 mbsf when 70,000 lb of overpull was required to free the barrel. XCB Cores 167-1014A-7X through 50X were taken down to 449.0 mbsf with 88.7% recovery. Hole 1014A was logged with the combined sonic-Formation MicroScanner (FMS) and the GHMT toolstrings

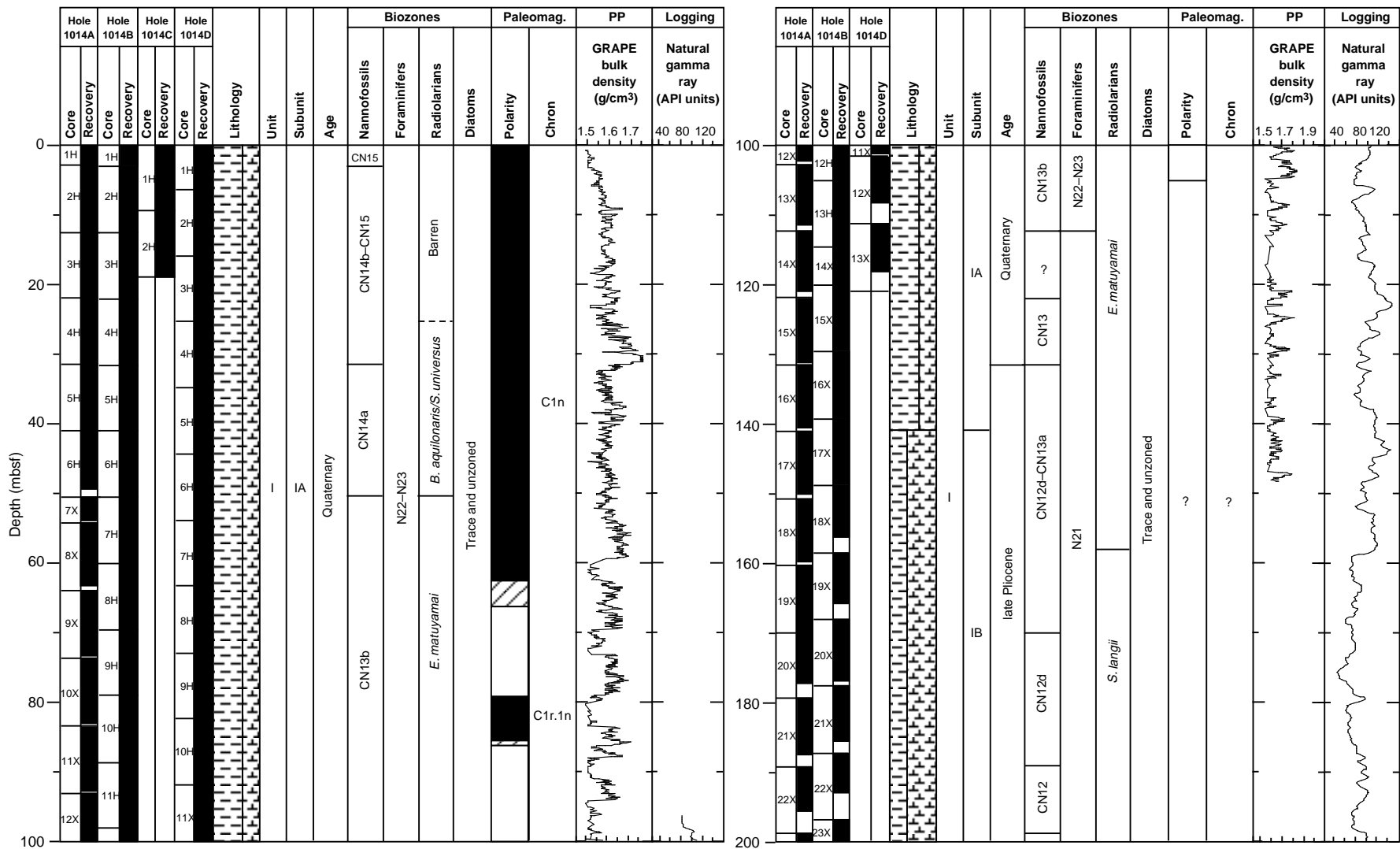


Figure 1. Site 1014 master column.

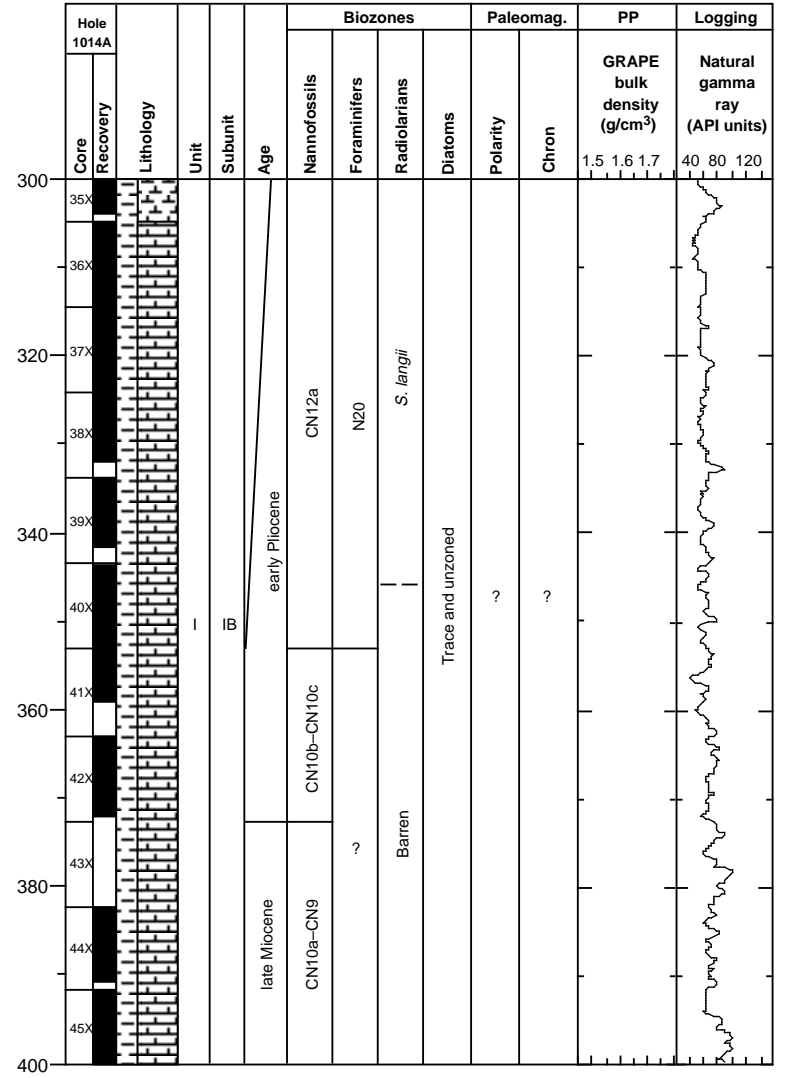
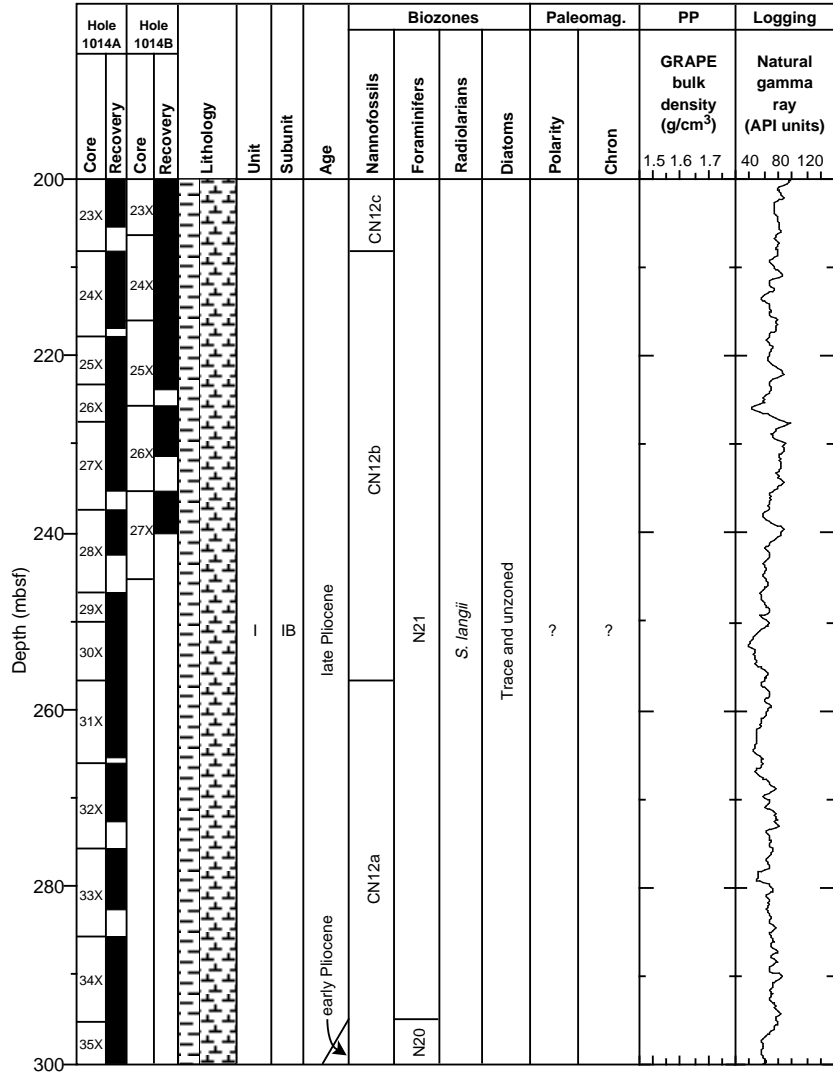


Figure 1 (continued).

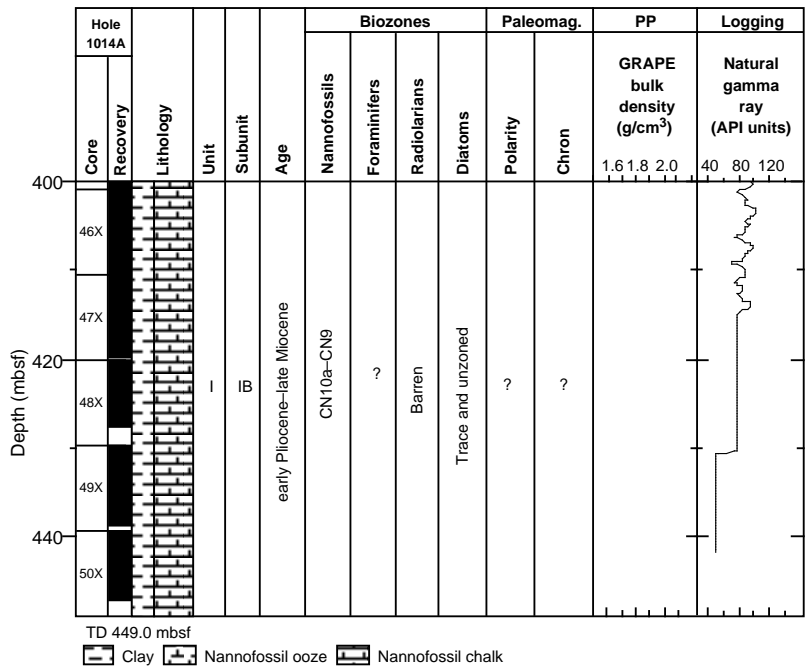


Figure 1 (continued).

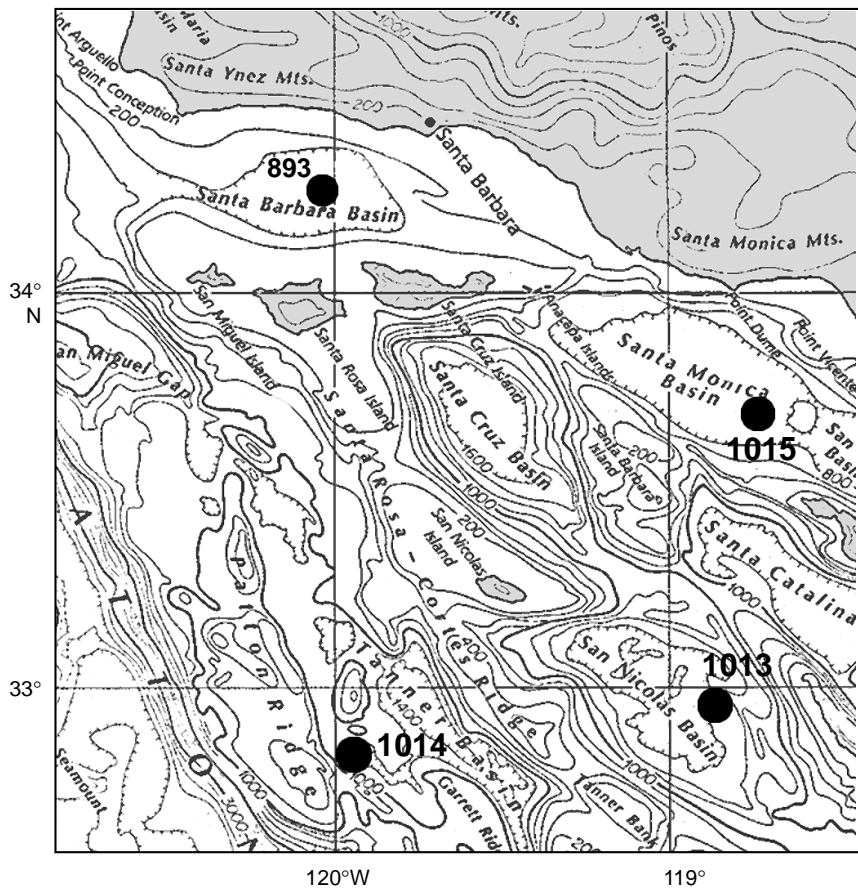


Figure 2. Location map for Site 1014, showing its position with respect to other northern California Borderland drill sites. Site 1013 is located in San Nicolas Basin, to the east of Site 1014 over the Santa Rosa-Cortes Ridge.

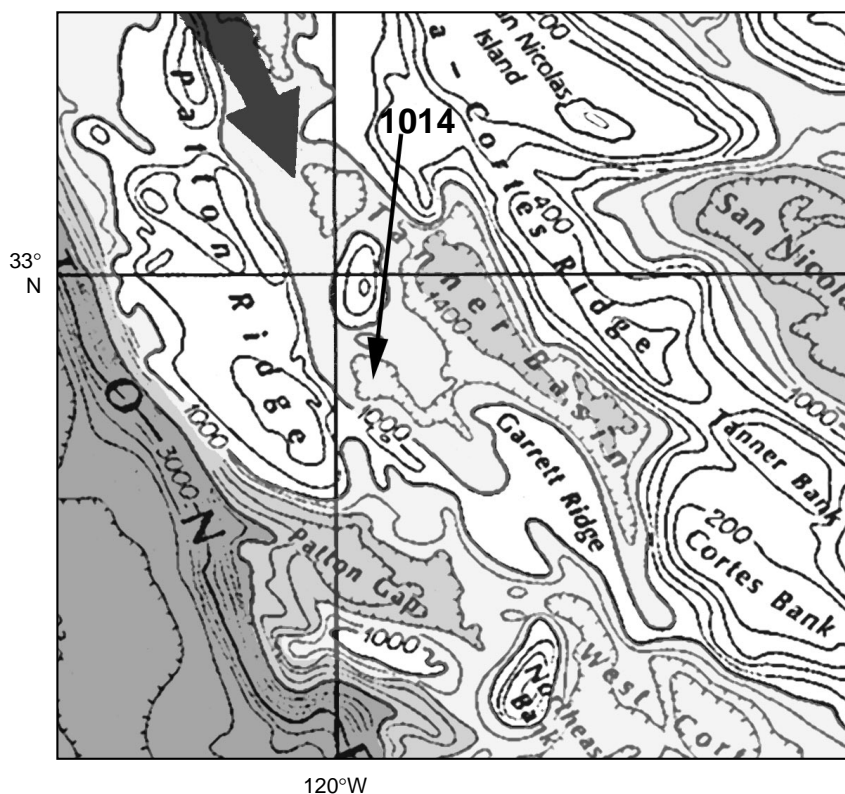


Figure 3. Bathymetry in the vicinity of Site 1014, showing the deep-water path into Tanner Basin from the northwest. Site 1014 is located in a sub-basin within Tanner Basin to the west of the deepest section. The deepest part of Tanner Basin was avoided because of turbidites from the nearby Santa Rosa–Cortes Ridge.

from 443 to 58 mbsf with good results. The vessel was offset 100 m to the east in an attempt to find an area more conducive to APC coring.

Hole 1014B

Hole 1014B was spudded at 1915 hr on 10 May. APC Cores 167-1014B-1H through 13H were taken from 0 to 114.7 mbsf with 100.8% recovery (Table 1). Apparently, the 100-m offset was enough to allow the piston coring to continue deeper than at Hole 1014A before APC refusal was encountered. Adara temperature measurements were taken on Cores 4H, 6H, and 8H (see “Physical Properties” section, this chapter). While pulling the core liner from the core barrel following Core 13H, the first meter of the liner exploded. The remaining liner was still inside the core barrel and shattered, but enough remained intact to be pulled out of the core barrel. The exploded liner caused part of the core to fall on the rig floor. XCB coring continued with Cores 167-1014B-14X through 27X, and the hole was taken down to 245.0 mbsf with 83.6% recovery.

Hole 1014C

Hole 1014C was spudded at 1315 hr on 11 May. APC Cores 167-1014C-1H and 2H were taken down to 19.5 mbsf with 102.8% recovery (Table 1).

Hole 1014D

Hole 1014D was spudded at 1400 hr on 11 May. APC Cores 167-1014D-1H through 10H were taken down to 92.0 mbsf with 104.5% recovery (Table 1). XCB Cores 167-1014D-11X through 13X were taken down to 120.9 mbsf with 83.8% recovery. The drill string was tripped back to the surface and secured for the 8-hr transit to Site 1015 by 2145 hr on 11 May.

LITHOSTRATIGRAPHY

Introduction

A Quaternary upper Miocene/lower Pliocene (0.0 to >5 Ma) sedimentary sequence was recovered at Site 1014. Biogenic assemblages (calcareous nannofossils and foraminifers) and siliciclastic clays dominate the composition of the sediment. The sequence was divided into two lithostratigraphic subunits based on visual core description and sediment composition obtained from smear slides, supplemented by multisensor track measurements, downhole logging, physical properties, and sediment chemistry (Fig. 5).

Subunit IA (0–140 mbsf) consists of clay with foraminifers interbedded with nannofossil ooze with foraminifers and clay. Subunit IB (140–449 mbsf) is distinguished by its increased calcareous nannofossil component. The dominant lithology of this subunit is nannofossil ooze and nannofossil chalk alternating with intervals of clay or clay with foraminifers. Discrete ash layers and lithified dolostone beds occur in the lower part of the sequence. A trace amount of glauconite grains are disseminated through the sediments from 276 mbsf to the bottom of the hole.

Description of Units

Unit I

Subunit IA

- Hole 1014A, intervals 167-1014A-1H through 17X-4, 100 cm; 0–146.7 mbsf;
- Hole 1014B, intervals 167-1014A-1H through 17X-2, 100 cm; 0–141.8 mbsf;
- Hole 1014C, intervals 167-1014A-1H through 2H; 0–19 mbsf (base of hole);
- Hole 1014D, intervals 167-1014A-1H through 13X; 0–120.9 mbsf (base of hole).

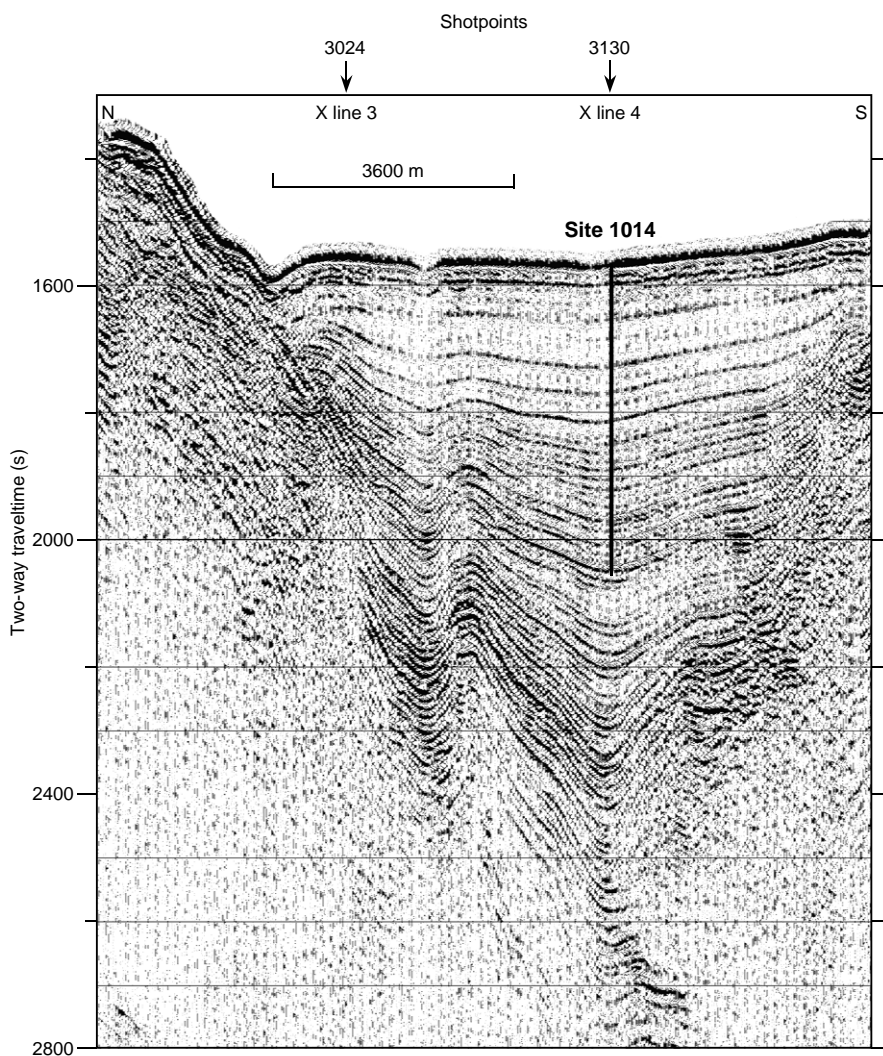


Figure 4. Seismic reflection profile through Site 1014 (Line EW9504 CA15-6; Lyle et al., 1995a, 1995b). The sub-basin, while narrow, has a thick sedimentary sequence within it. Site 1014 was drilled to a depth of 450 mbsf, which samples the upper, more seismically transparent sediment package and continues into the more layered sequence below. On y-axis, (s) = milliseconds.

Age: Quaternary, 1.77 to 0.0 Ma.

In Subunit IA, clay with foraminifers alternates with nannofossil ooze at a scale of 30–120 cm. Bedding contacts are gradational and the sediments are slightly bioturbated. Clay forms up to 60% of the sediment in several beds and organic matter composes 2% to 9% (see “Organic Geochemistry” section, this chapter). Color is generally dark olive gray (5Y 3/2) to very dark gray (5Y 3/1) or dark grayish brown (2.5Y 4/2).

Intervals of olive (5Y 5/3) to olive gray (5Y 4/2) nannofossil ooze with foraminifers and nannofossil ooze with clay occur throughout Subunit IA interbedded with the clay-rich lithologies. Based on smear-slide estimates, nannofossils form 60%–70% of the sediment, foraminifers make up 10%–25%, and trace quantities of opaque minerals and pyrite are present. Small pods of pure foraminifer sand occur between 52 and 49 mbsf. Overall, the sediment is moderately bioturbated; however, XCB coring in the lower portion of this subunit has disrupted most sedimentary features.

Subunit IB

Hole 1014A, intervals 167-1014A-17X-4, 100 cm, through 50X; 146.7–449 mbsf;

Hole 1014B, intervals 167-1014A-17X-2, 100 cm, through 27X; 141.8–245 mbsf (base of hole).

Age: late Miocene to late Pliocene, 7(?)–5 to 1.77 Ma.

The transition between Subunit IA and Subunit IB is marked by a gradual increase in nannofossils and total percentage of CaCO_3 (estimated by color reflectance spectrometry), a decrease in the natural gamma-ray value of the sediments, and an increase of the bulk density (see “Physical Properties” section, this chapter). Subunit IB consists chiefly of moderately bioturbated olive (5Y 5/3) and pale olive (5Y 6/3) nannofossil-rich lithologies (nannofossil ooze or nannofossil-rich lithologies) alternating with slightly bioturbated dark gray (5Y 3/1 and 5Y 4/1) foraminifer clay and olive gray (5Y 4/2 and 5Y 5/2) nannofossil clay mixed sediments.

Smear-slide estimates of composition vary widely, reflecting the differences between interbedded lithologies. Overall trends in carbonate content are confirmed by coulometric CaCO_3 measurements (see “Inorganic Geochemistry” section, this chapter). Three indurated dolostone beds and two volcanic ash layers occur between 354 mbsf and 260 mbsf. The lowermost interval (449 to 276 mbsf) is characterized by the presence of disseminated medium-grain-size glauconite. Below 370 mbsf, the concentration of foraminifers decreases significantly from 20% to 5%.

Depositional History

The recovered sequence at Site 1014 provides a continuous Pliocene to Quaternary record of hemipelagic sedimentation in a dis-

Table 1. Coring summary for Site 1014.

Core	Date (May 1996)	Time	Top (mbsf)	Bottom (mbsf)	Length cored (m)	Length recovered (m)	Recovery (%)
167-1014A-							
1H	08	1610	0.0	3.1	3.1	3.13	101.0
2H	08	1630	3.1	12.6	9.5	10.07	106.0
3H	08	1710	12.6	22.1	9.5	9.72	102.0
4H	08	1740	22.1	31.6	9.5	9.88	104.0
5H	08	1820	31.6	41.1	9.5	9.77	103.0
6H	08	1910	41.1	50.6	9.5	8.41	88.5
7X	08	2030	50.6	54.3	3.7	3.51	94.8
8X	08	2115	54.3	64.0	9.7	9.13	94.1
9X	08	2150	64.0	73.8	9.8	9.58	97.7
10X	08	2220	73.8	83.5	9.7	9.21	94.9
11X	08	2250	83.5	93.1	9.6	9.37	97.6
12X	08	2330	93.1	102.8	9.7	9.39	96.8
13X	09	0015	102.8	112.4	9.6	8.82	91.9
14X	09	0055	112.4	122.0	9.6	8.64	90.0
15X	09	0140	122.0	131.6	9.6	9.30	96.9
16X	09	0220	131.6	141.2	9.6	8.97	93.4
17X	09	0250	141.2	150.8	9.6	9.01	93.8
18X	09	0325	150.8	160.4	9.6	9.06	94.4
19X	09	0400	160.4	170.0	9.6	9.66	100.0
20X	09	0430	170.0	179.6	9.6	7.27	75.7
21X	09	0500	179.6	189.2	9.6	7.96	82.9
22X	09	0535	189.2	198.8	9.6	6.42	66.9
23X	09	0615	198.8	208.4	9.6	6.92	72.1
24X	09	0650	208.4	218.0	9.6	8.63	89.9
25X	09	0750	218.0	223.5	5.5	5.89	107.0
26X	09	0840	223.5	227.7	4.2	6.16	146.0
27X	09	0930	227.7	237.3	9.6	8.58	89.4
28X	09	1000	237.3	246.9	9.6	5.04	52.5
29X	09	1100	246.9	250.1	3.2	3.53	110.0
30X	09	1155	250.1	256.6	6.5	6.58	101.0
31X	09	1235	256.6	266.2	9.6	8.71	90.7
32X	09	1315	266.2	275.8	9.6	6.56	68.3
33X	09	1350	275.8	285.5	9.7	6.89	71.0
34X	09	1440	285.5	295.1	9.6	9.63	100.0
35X	09	1520	295.1	304.8	9.7	9.00	92.8
36X	09	1610	304.8	314.4	9.6	9.59	99.9
37X	09	1650	314.4	324.1	9.7	9.66	99.6
38X	09	1740	324.1	333.7	9.6	9.27	96.5
39X	09	1830	333.7	343.4	9.7	8.19	84.4
40X	09	1900	343.4	353.0	9.6	9.56	99.6
41X	09	1950	353.0	362.6	9.6	6.84	71.2
42X	09	2030	362.6	372.2	9.6	9.58	99.8
43X	09	2100	372.2	381.8	9.6	0.00	0.0
44X	09	2250	381.8	391.3	9.5	10.13	106.6
45X	10	0005	391.3	401.0	9.7	9.68	99.8
46X	10	0125	401.0	410.5	9.5	9.61	101.0
47X	10	0230	410.5	420.2	9.7	9.41	97.0
48X	10	0335	420.2	429.8	9.6	7.39	77.0
49X	10	0450	429.8	439.4	9.6	9.04	94.1
50X	10	0620	439.4	449.0	9.6	8.00	83.3
167-1014B-							
1H	11	0225	0.0	3.2	3.2	3.15	98.4
2H	11	0245	3.2	12.7	9.5	9.91	104.0
3H	11	0330	12.7	22.2	9.5	9.74	102.0
4H	11	0415	22.2	31.7	9.5	9.84	103.0
5H	11	0445	31.7	41.2	9.5	9.85	103.0
6H	11	0530	41.2	50.7	9.5	10.09	106.2
7H	11	0555	50.7	60.2	9.5	10.04	105.7
8H	11	0635	60.2	69.7	9.5	9.99	105.0
9H	11	0705	69.7	79.2	9.5	9.93	104.0
10H	11	0730	79.2	88.7	9.5	10.10	106.3
11H	11	0755	88.7	98.2	9.5	10.11	106.4
12H	11	0820	98.2	105.2	7.0	7.12	102.0
13H	11	0910	105.2	114.7	9.5	5.72	60.2
14X	11	1015	114.7	120.1	5.4	6.10	113.0
15X	11	1050	120.1	129.7	9.6	9.46	98.5
16X	11	1130	129.7	139.3	9.6	9.54	99.4
17X	11	1205	139.3	148.9	9.6	9.46	98.5
18X	11	1240	148.9	158.6	9.7	7.53	77.6
19X	11	1315	158.6	168.1	9.5	7.29	76.7
20X	11	1400	168.1	177.7	9.6	8.76	91.2
21X	11	1435	177.7	187.3	9.6	7.91	82.4
22X	11	1515	187.3	196.9	9.6	5.62	58.5
23X	11	1600	196.9	206.5	9.6	9.67	101.0
24X	11	1635	206.5	216.1	9.6	9.78	102.0
25X	11	1705	216.1	225.8	9.7	7.88	81.2
26X	11	1745	225.8	235.4	9.6	5.60	58.3
27X	11	1835	235.4	245.0	9.6	4.50	46.9
167-1014C-							
1H	11	2030	0.0	9.5	9.5	9.63	101.0
2H	11	2045	9.5	19.0	9.5	9.90	104.0
167-1014D-							
1H	11	2105	0.0	6.5	6.5	6.46	99.4
2H	11	2130	6.5	16.0	9.5	9.81	103.0
3H	11	2145	16.0	25.5	9.5	9.94	104.0

Table 1 (continued).

Core	Date (May 1996)	Time	Top (mbsf)	Bottom (mbsf)	Length cored (m)	Length recovered (m)	Recovery (%)
4H	11	2200	25.5	35.0	9.5	9.68	102.0
5H	11	2230	35.0	44.5	9.5	10.07	106.0
6H	11	2250	44.5	54.0	9.5	10.00	105.2
7H	11	2310	54.0	63.5	9.5	10.10	106.3
8H	11	2345	63.5	73.0	9.5	10.01	105.3
9H	12	0005	73.0	82.5	9.5	10.05	105.8
10H	12	0035	82.5	92.0	9.5	9.99	105.0
11X	12	0125	92.0	101.7	9.7	9.26	95.4
12X	12	0145	101.7	111.3	9.6	6.73	70.1
13X	12	0225	111.3	120.9	9.6	6.86	71.4

Note: Table 2, on the CD-ROM in the back pocket, this volume, is a more detailed coring summary.

tal basin of the California Borderland underlain by a poorly dated upper Miocene sequence. Miocene and Pliocene sedimentation (Subunit IB) is dominated by cyclic alternation between calcareous nanofossil-rich ooze or chalk and nanofossil-poor clay and mixed sediments. Much of this sediment also contains small amounts of glauconite documenting the contribution of reworked sediments from a shallower suboxic environment on nearby bank tops or slopes. Three dolostone horizons likely reflect short-term pauses in sediment accumulation. Near the Pliocene/Pleistocene boundary, accumulation of carbonate decreased significantly, shifting the sediments to more clay-rich compositions, and simultaneously decreasing the overall sedimentation rate for the remainder of the Quaternary (Subunit IA).

BIOSTRATIGRAPHY

The sedimentary sequence recovered from the four holes at Site 1014 consists of a well-dated, apparently continuous 325-m-thick interval of upper Pliocene to Quaternary sediments, underlain by a relatively poorly dated 124-m-thick sequence of lower Pliocene to possibly uppermost Miocene age. A well-constrained biostratigraphy and chronology for all holes of Site 1014 is provided by a combination of calcareous nanofossil, planktonic foraminifer, and radiolarian datums for the upper Pliocene and Quaternary. The base of the sequence is not well dated, but calcareous nanofossils suggest a late Miocene age of between 5 and 7 Ma. An age/depth plot for Hole 1014A shows downward increases in sedimentation rates in three steps from the Quaternary to the upper and middle upper Pliocene and to the lower upper Pliocene. Below this, sedimentation rates decrease drastically (Fig. 6). The middle and upper Quaternary (0–110 mbsf) sediment contains common to abundant well-preserved calcareous nanofossils, abundant well-preserved planktonic foraminifers, and rare diatoms and radiolarians. The lower Quaternary and uppermost Pliocene sequence between about 110 and 190 mbsf contains few poorly preserved calcareous nanofossils, common to absent and relatively poorly preserved planktonic foraminifers, and few diatoms and radiolarians. The underlying middle and lower upper Pliocene contains abundant and generally well-preserved calcareous nanofossils, often common to abundant moderately well-preserved planktonic foraminifers, common well-preserved radiolarians, and traces of diatoms. In the lower part of the sequence below 353 mbsf, microfossils are poorly represented. Planktonic foraminifers and diatoms are completely absent below 353 mbsf. Diatoms occur only in traces, radiolarians are absent below 391 mbsf, while calcareous nanofossils are abundant to very rare and moderate to poorly preserved below 353 mbsf.

Site 1014 offers much potential for the study of paleoceanographic/paleoclimatic history from about 3.6 Ma to the Quaternary. Diatom and radiolarian assemblages suggest weak to strong upwelling cycles during the late Pliocene leading to high productivity episodes on the

continental margin. Middle to upper Miocene diatom and radiolarian species suggest a persistent input of reworked material throughout this sequence. Planktonic foraminifer and radiolarian assemblages indicate relative warmth from the early Pliocene through the late Pliocene until 2.5 Ma. Cooling at thermocline depths is suggested after 3.0 Ma by cooler radiolarian assemblages. This was followed at 2.5 Ma by a major surface-water cooling, indicated by the first appearance of dominant sinistrally coiled *Neogloboquadrina pachyderma*. Low oxygen concentrations in basinal bottom waters during the earliest Quaternary through latest Pliocene coincided with strong upwelling conditions. During the Quaternary, benthic foraminifer assemblages change in association with glacial-interglacial oscillations. This suggests changes in upper intermediate water circulation during late Quaternary climatic cycles.

Planktonic Foraminifers

Site 1014 contains an excellent planktonic foraminifer sequence in the upper 353 mbsf (from Sample 167-1014A-40X-CC to top of sequence) that ranges in age from the late early Pliocene (~3.6 Ma) through the Quaternary. Below 353 mbsf (Samples 167-1014A-41X-CC to 50X-CC), the sequence is completely barren of planktonic foraminifers. The assemblages are abundant and very well preserved in the middle and upper Quaternary. They are less well preserved and are variable, but less abundant in the early Quaternary through the Pliocene. The Pliocene through early Quaternary assemblages are marked by high test fragmentation and are often dominated by robust forms. An interval from the uppermost Pliocene through the lowest Quaternary exhibits especially poor preservation and low abundances of planktonic foraminifers. This report is largely based on observations and tabulations of species in assemblages in core-catcher samples from Hole 1014A (Table 3). Each core-catcher sample from Hole 1014B was examined to determine the dominant coiling direction of *N. pachyderma* (Table 4) and to check the position of planktonic foraminifer datums. The biostratigraphy of planktonic foraminifers at Site 1014 is similar to that of Site 1012. Because Site 1014 is marked by higher sedimentation rates than at Sites 1010 through 1013, the stratigraphic ranges of species are well exhibited. The Quaternary at Site 1014 is special because of its thickness (~112 m) and because of the quality of preservation of the planktonic and benthic foraminifers. Also, the planktonic foraminifer assemblages clearly exhibit glacial to interglacial climatic oscillations and the benthic foraminifers reflect associated changes in oxygen concentrations of basin bottom waters.

The base of the Quaternary at Site 1014 is not well delineated because of the absence of *Globorotalia truncatulinoides* in this interval. Correlation with Site 1011, however, indicates that the boundary occurs within the upper range of *Neogloboquadrina humerosa* in the interval above the LO of *Neogloboquadrina asanoi*. We tentatively place the Quaternary/Pliocene boundary (and the boundary between Zones N21 and N22) between Samples 167-1014A-13X-CC and

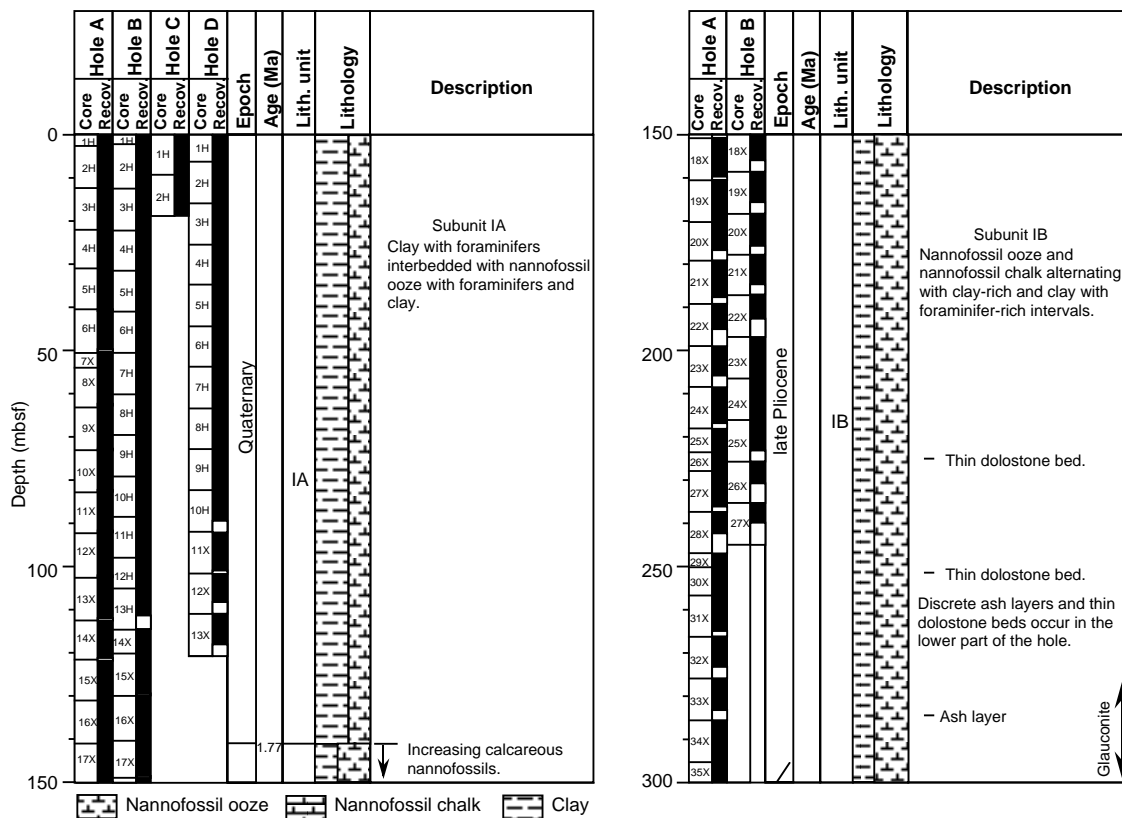


Figure 5. Site 1014 lithologic summary (0–449 mbsf).

14X-CC. The upper part of the Quaternary is marked by the occurrence of *Neogloboquadrina duterrei*, with the FO dated at 1.0 Ma. The lower part of the Quaternary is marked by *N. humerosa*, with the LO dated at 1.2 Ma.

Late Pliocene Zone N21 ranges from the FO of *Globorotalia inflata* at 3.3 Ma (FO in Sample 167-1014A-34X-CC) to the Quaternary/Pliocene boundary. Within Zone N21, three datum levels are recognized that are consistent with the biostratigraphy at Sites 1012 and 1013. These datums are the LO of *N. asanoi* dated at 1.9 Ma, the LO of *Neogloboquadrina* sp. (rounded) dated at 2.25 Ma, and the LO of *Globorotalia puncticulata* dated at 2.50 Ma. The FO of modern morphotypes of *G. inflata* appear above the LO of *G. puncticulata*. Morphotypes of *G. inflata* that overlap the range of *G. puncticulata* are more primitive forms with four chambers in the final whorl, less inflation, and a more quadrate shape. The first appearance of consistent, and often abundant, *N. pachyderma* (sinistral) coincides with the LO of *G. puncticulata*.

The boundary between the early and late Pliocene is taken at the FO of *G. inflata* at 3.3 Ma, marking the boundary between Zones N20 and N21. Within upper lower Pliocene Zone N20, the short range zone of *Globorotalia* cf. *conoidea* has not been previously recognized.

Planktonic foraminifers are absent in all samples below Sample 167-1014A-14X-CC. These samples do contain consistent and often abundant benthic foraminifer assemblages.

Site 1014 offers much potential for the study of paleoceanographic and paleoclimatic history from about 3.6 Ma to the Quaternary. The planktonic foraminifer assemblages indicate relative warmth from the late early Pliocene through the late Pliocene until 2.5 Ma (Sample 167-1014A-22X-CC). At that time *N. pachyderma* (sinistral) appeared as a fairly consistent and often abundant element of the planktonic foraminifer assemblage, marking the initiation of cooler California Current waters at Site 1014. This event is associated with

the well-known development of the Northern Hemisphere ice sheets. From this time, planktonic foraminifers record strong glacial-interglacial oscillations.

Benthic foraminifers are abundant, diverse, and extremely well preserved throughout the middle and late Quaternary at Site 1014. As at Santa Barbara Basin Site 893 (Kennett, Baldauf, Lyle et al., 1995), benthic foraminifer assemblages change in association with glacial-interglacial oscillations. Glacial episodes are dominated by *Uvigerina* in association with such forms as *Buliminella*, *Globulimina*, *Bolivina*, *Nonionellina*, *Epistominella*, *Hoeglundina*, *Cibicides*, and *Pyrgo*. Such assemblages suggest bottom waters of moderately low oxygen concentrations. Interglacial episodes are marked by benthic foraminifer assemblages dominated by *Bolivina* associated with forms such as *Uvigerina* and *Globobulimina*. Such assemblages are indicative of very low oxygen concentrations of basin bottom waters. Benthic foraminifers are less abundant and well preserved below the middle Quaternary. Robust species and specimens often dominate. Nevertheless, benthic foraminifers are consistently present and often common to abundant throughout this interval. Assemblages are often dominated by *Bolivina*, *Bulimina*, and *Uvigerina* indicating relatively low oxygen concentrations in basinal waters. Very high dominance of *Bolivina* in Samples 167-1014A-13X-CC to 19X-CC indicate very low oxygen concentrations in basinal bottom waters during the earliest Quaternary through latest Pliocene.

Hole 1014B

The position of planktonic foraminifer datums based on core-catcher samples in Hole 1014B are essentially the same as in Hole 1014A. In Hole 1014B the LO of *N. humerosa* is in Sample 167-1014B-11H-CC compared with Sample 167-1014A-10X-CC in Hole 1014A. The pattern of coiling direction change in *N. pachyderma* is also very similar between both holes (Tables 3, 4). In both holes, the

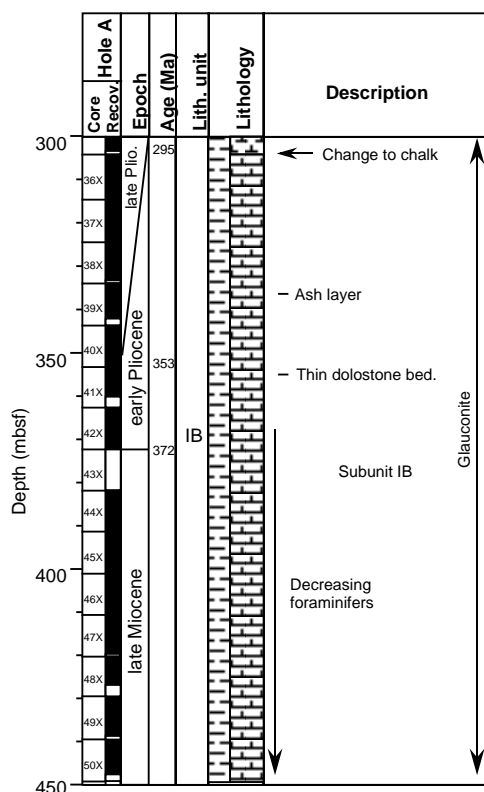


Figure 5 (continued).

FO of dominantly sinistrally coiled *N. pachyderma* occurs at about 200 mbsf reflecting the beginning of major surface-water cooling in the late Pliocene. The benthic foraminiferal sequences are also similar between the holes.

Calcareous Nannofossils

Nannofossils are generally common to abundant and well preserved through the Quaternary. In the upper upper Pliocene and lower Pliocene, the preservation is poor and specimens often are broken. Therefore, identification is difficult and *Discoaster* spp. are not recognized in the upper Pliocene (Table 5). An interval spanning the upper Miocene/lower Pliocene Zone CN10a-CN9 to the upper Pleistocene Zone CN 15 is recognized in Hole 1014A. Hole 1014B encompassed an interval from the upper upper Pliocene Zone CN12b to the upper Pleistocene Zone CN15.

In the Quaternary of both holes, nannofossil assemblages are marked by the presence of *Emiliania huxleyi*, *Pseudoemiliania lacunosa*, *Calcidiscus leptoporus*, *Helicosphaera carteri*, *Helicosphaera sellii*, and several morphotypes of *Gephyrocapsa* spp. and *Ceratolithoides*. An expanded Quaternary sequence allows recognition of most of the Pleistocene nannofossil datums.

In Hole 1014A, rare and poorly preserved calcareous nannofossils do not permit accurate placement of the Pliocene to Pleistocene boundary. The LO of *C. calcidiscus macintyreii* at 141.20 mbsf (Sample 167-1014A-16X-CC) provides an approximate position for this boundary. In Hole 1014B, the Pliocene/Pleistocene boundary is placed at 114.70 mbsf (167-1014B-13H-CC) by the FO of *Gephyrocapsa oceanica* s.l.

Pliocene nannofossil assemblages are marked by an association of *Helicosphaera carteri*, *Discoaster brouweri*, *D. tamalis*, *D. pentaradiatus*, *D. surculus*, *Amaurolithis delicatus*, and several morphotypes of *Reticulofenestra* and *Ceratolithus*. The upper/lower Pliocene boundary is placed at 353 mbsf (Sample 167-1014A-40X-CC) by the

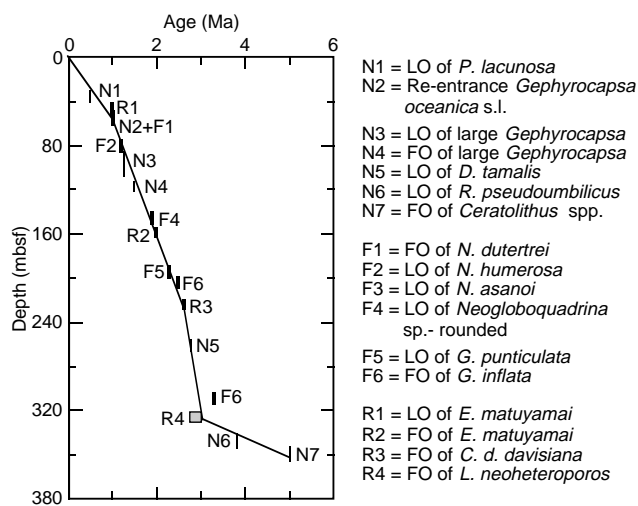


Figure 6. Age/depth plot for Hole 1014A.

LO of *Reticulofenestra pseudoumbilicus*, which marks the base of Zone CN12a. The presence of *Amaurolithus* spp. and *Ceratolithus* spp. in Samples 167-1014A-40X-CC and 42X-CC allows assignment of this interval to the lower Pliocene Zone CN10c/CN10b. The FO of *Ceratolithus* spp. between Samples 167-1014A-42X-CC and 43X-CC (372.2 mbsf) marks the Miocene/Pliocene boundary. Below this level, calcareous nannofossil assemblages are marked by the presence of *Amaurolithus* spp., which indicates lower Pliocene to upper Miocene Zones CN10a and CN9. This suggests a latest Miocene age for this interval, but an absence of *Discoaster quinqueramus/bergrenii* (Zone CN9) does not necessarily confirm this age.

Diatoms

Few diatoms occur in the Pliocene and Quaternary section at Site 1014. All diatom assemblages are poorly preserved, and, as well as at Sites 1012 and 1013, neither the Leg 167 North Pacific diatom zonation, nor the standard diatom datum levels were recognized in Holes 1014A and 1014B. Poorly preserved assemblages are commonly accompanied by abundant fresh sponge spicules, rare radiolarians, and reworked planktonic diatoms, forming an unusual biosiliceous assemblage.

Sparse occurrences of *Actinocyclus oculatus* in Samples 167-1014A-27H-CC and 38H-CC suggest a range of late Pliocene to early Pleistocene (~3.9–1.4 Ma), but cannot be used to recognize any zones (Table 6). The diatom assemblage in Sample 167-1014A-39X-CC contains *Hemidiscus cuneiformis*, *Thalassiosira* cf. *leptopus*, *Coscinodiscus* sp., but lacks *Neodenticula* spp., *Nitzschia reinholdii*, and another *Nitzschia* sp. The assemblage is typical of neither the subarctic North Pacific nor equatorial East Pacific Ocean, but rather of the relatively warm-temperate surface water that might be extended along the west coast of California at the time.

More than 20 m of the section from 196 to 216 mbsf includes abundant to few representatives of both *Coscinodiscus marginatus* and *Rhizosolenia barboi* (Samples 167-1014A-22X-CC and 167-1014B-22X through 24X-CC). These diatom elements are characteristic of marginal upwelling, indicative of high continental margin productivity (Tables 6, 7).

Persistent reworking of many diagnostic cool-water taxa such as *Actinocyclus ingens*, *A. ingens nodus*, and *Denticulopsis* spp., documented in the Pleistocene through upper Pliocene section from Site 1014 (Tables 6, 7), represents strong incursions of marginal shallow waters inducing seafloor erosion. Reworked specimens, which are commonly dissolved and fragmented, suggest that they might be de-

Table 3. Distribution and relative abundance of planktonic foraminifers in Hole 1014A.

Zone	Core, section, interval	Depth (mbsf)	Abundance	Preservation	<i>Neogloboquadrina duterrei</i>	<i>Globorotalia tosaensis</i>	<i>Neogloboquadrina humerosa</i>	<i>Globorotalia inflata</i>	<i>Globorotalia punctulata</i>	<i>Globorotalia crassaformis</i>	<i>Neogloboquadrina asanoi</i>	<i>Neogloboquadrina</i> sp. "rounded"	<i>Sphaeroidinella delticensis</i>	<i>Neogloboquadrina pachyderma</i> dex. sin.	<i>Neogloboquadrina pachyderma</i> sin.	<i>Globigerina bulloides</i>	<i>Orbulina universa</i>	<i>Globigerinoides conglobatus</i>	<i>Globigerinoides ruber</i>	<i>Globorotalia tumida</i>	<i>Sphaeroidinellopsis seminulina</i>	<i>Globorotalia scitula</i>	<i>Globigerinita glutinata</i>	<i>Globigerina quinqueloba</i>	<i>Globigerina umbilicata</i>	<i>Globigerina apertura</i>	<i>Globorotalia truncatulinoides</i>	<i>Globorotalia hirsuta</i>	<i>Globorotalia</i> cf. <i>conoides</i>				
N22/23	167-1014A-1H-CC	3.0	A	G	C																												
	2H-CC	13.0	A	G	A			A						A	A	F						F		A					R	F			
	3H-CC	22.0	A	G										A	A	F						F											
	4H-CC	32.0	A	G										A	A	F								A									
	5H-CC	41.0	C/A	M										A	A	F																	
	6H-top	51.0	A	G										A	A	F																	
	7X-CC	54.0	A	G						R				A	A	F																	
	8X-CC	64.0	A	G										A	A	F																	
	9X-CC	74.0	A	G										A	A	F																	
	10X-CC	84.0	A	G										A	A	F																	
	11X-CC	93.0	C	M						R				A	A	F																	
	11X-CC	93.0	C	M										A	A	F																	
	12X-CC	102.8	A	G										A	A	F																	
	13X-CC	112.4	C	M										A	A	F																	
N21	14X-CC	122.0	B																														
	15X-CC	132.0	C	M		M																											
	16X-CC	141.0	B																														
	17X-CC	151.0	F	M																													
	18X-CC	160.0	A	G			F							A	A	F																	
	19X-CC	170.0	C	M				R						A	A	F																	
	20X-CC	179.6	C	M										A	A	F																	
	21X-CC	189.2	B											A	A	F																	
	22X-CC	198.8	A	G										A	A	F																	
	23X-CC	208.4	A	G			C	A	A					A	A	F																	
	24X-CC	218.0	F	P										A	A	F																	
	25X-CC	223.5	A	M										A	A	F																	
	26X-CC	227.7	F/C	M										A	A	F																	
	27X-CC	237.3	F	P/M										A	A	F																	
	28X-CC	246.9	C	M										A	A	F																	
	29X-CC	250.1	A	G										A	A	F																	
	30X-CC	256.6	F	M			C							A	A	F																	
31X-CC	266.0	A	G			C		R	R				A	A	F																		
32X-CC	275.8	C	M										A	A	F																		
33X-CC	285.5	F	M										A	A	F																		
34X-CC	295.1	C	M										A	A	F																		
35X-CC	304.8	F	M										A	A	F																		
N20	36X-CC	314.4	F	M						R	A	C																					
	37X-CC	324.1	F	M						R	A	C																					
	38X-CC	333.7	B/R	M						R	A	C																					
	39X-CC	343.4	F/C	G						R	A	C																					
	40X-CC	353.0	F	M						R	A	C																					
?	41X-CC	362.6	B																														
	42X-CC	372.2	B																														
	44X-CC	391.0	B																														
	45X-CC	401.0	B																														
	46X-CC	410.5	B																														
	47X-CC	420.2	B																														
	48X-CC	430.0	B																														
	49X-CC	439.0	B																														
50X-CC	449.0	B																															

Note: See "Explanatory Notes" chapter for abbreviations.

rived from the corresponding sediment sequences of Luisian through Mohnian age in the Monterey Formation of California (Poore et al., 1981).

Radiolarians

Radiolarians are absent to abundant in Holes 1014A and 1014B. Most of the upper Quaternary is absent. Assemblages are better preserved in the lower Quaternary and upper Pliocene. Below 400 mbsf, radiolarians are absent.

Consistent occurrence of *Eucyrtidium matuyamai* and the LO of *Lamprocyrtis heteroporos* permits location of the Quaternary/

Pliocene boundary between 150.8 and 170.0 mbsf in Hole 1014A and between 148.9 and 158.6 mbsf in Hole 1014B (Tables 8, 9). The main radiolarian events are (1) the LO of *E. matuyamai* (1.0 Ma) between 41.4 and 50.6 mbsf in Hole 1014A and between 50.7 and 60.2 mbsf in Hole 1014B; (2) the LO of *L. heteroporos* (1.7 Ma) between 139.3 and 148.9 mbsf in Hole 1014B; (3) the LO of *Cycladophora d. davisi* (2.7/2.9 Ma) between 223.5 and 227.7 mbsf in Hole 1014A and between 206.5 and 216.2 mbsf in Hole 1014B; (4) the FO of *Lamprocyrtis neoheteroporos* (2.6-3.0 Ma) between 324.1 and 333.7 mbsf in Hole 1014A.

Rare and poorly preserved assemblages are composed of radiolarian debris of middle to late Miocene age, which indicate a persistent

Table 4. Coiling dominance of *Neogloboquadrina pachyderma* in Hole 1014B.

Core, section, interval	Depth (mbsf)	<i>Neogloboquadrina pachyderma</i> coiling dominance
167-1014B-		
1H-CC	3	Sinistral
2H-CC	13	Dextral
3H-CC	22	Sinistral
4H-CC	32	Sinistral
5H-CC	41	Sinistral
6H-CC	51	Sinistral
7H-CC	60	Sinistral
8H-CC	70	Sinistral
9H-CC	79	Sinistral
10H-CC	89	Sinistral
11H-CC	98	Dextral
12H-CC	105	Dextral
13H-CC	115	Dextral
14X-CC	120	Barren
15X-CC	130	Barren
16X-CC	139	Sinistral
17X-CC	149	Sinistral/Dextral
18X-CC	159	Sinistral
19X-CC	168	Dextral/Sinistral
20X-CC	178	Sinistral
21X-CC	187	Sinistral
22X-CC	197	Barren
23X-CC	207	Dextral
24X-CC	216	Dextral
25X-CC	226	Dextral
26X-CC	235	Dextral
27X-CC	245	Dextral

input of reworked material throughout the sequence. Abundant and well-preserved assemblages contain species that are indicative of upwelling conditions. Alternating occurrences of poor and well-preserved assemblages suggest weak and strong upwelling cycles through the upper Pliocene and early Quaternary. Persistent occurrence of many subtropical species in assemblages below Sample 167-1014A-36X-CC (314.4 mbsf) suggest an age slightly younger than 3 Ma for the beginning of major thermocline-water cooling at Site 1014.

PALEOMAGNETISM

Laboratory Procedures and Results

We made magnetic measurements using the pass-through cryogenic magnetometer on the archive halves of 6 APC cores and 3 XCB cores from Hole 1014A and 12 APC cores from Hole 1014B, applying alternating field (AF) demagnetization at 20 mT. While no magnetic reversal was found in Hole 1014A, there is a good magnetostratigraphy in the APC cores from Hole 1014B. The inclination record from the working halves of Cores 167-1014D-6H to 10H after AF demagnetization at 25 mT confirms the magnetostratigraphy from Hole 1014B.

The results from Hole 1014A are shown in Figure 7. The inclinations of the APC cores after AF demagnetization range between 40° and 60°, which is consistent with the direction of the geocentric axial dipole field at this site (52° at 32°50'N). The 3 XCB cores have similar inclination values of normal polarity. Their declinations are distributed uniformly around 0°, which suggests that the XCB cores have a strong drilling-induced overprint even after AF demagnetization.

After the early switch from APC to XCB coring in Hole 1014A, 13 APC cores were drilled in Hole 1014B. Core 167-1014B-13H could not be measured because it had exploded in the core barrel and the core's integrity was disturbed. Most intervals of Cores 167-1014B-8H to 12H showed negative inclinations after AF demagnetization

at 20 mT (Fig. 8). The AF demagnetization results from the interval between 52 and 93 mbsf in Hole 1014D are shown in Figure 9.

Discussion

The interpretation of the inclination record of Hole 1014B after AF demagnetization in terms of geomagnetic polarity chrons is shown in Figure 8. A reversal of magnetic polarity occurs at about 65 mbsf in Core 167-1014B-8H. We assign this transition to the Brunhes/Matuyama boundary, the onset of Chron C1n. The Jaramillo subchronozone (C1r.1n) covers an interval of about 6 m in Core 167-1014B-10H. The polarity changes of the Brunhes/Matuyama and the onset and termination of the Jaramillo subchron are equally well defined in Hole 1014D (Fig. 9). The magnetozone boundaries occur in the two holes at the same horizons with respect to the correlation by whole-core magnetic susceptibility (see "Composite Depths and Sedimentation Rates" section, this chapter). The magnetostratigraphic datum levels in Holes 1014B and 1014D are summarized in Table 10.

An age/depth plot of the magnetostratigraphic datums in Hole 1014B, based on the time scale of Cande and Kent (1995), is shown in Figure 10. A linear fit to the three magnetic reversals and to all nanofossil datums except the one at 1.02 Ma gives a sedimentation rate of 79 m/m.y. for the past 2.6 Ma. Our age assignment is consistent with the biostratigraphic datums, except for the nanofossil and planktonic foraminiferal datum levels at about 1.0 Ma (Fig. 10; also see "Biostratigraphy" section, this chapter).

The magnetic inclinations of Core 167-1014A-9X are contradicted by the results from the APC Cores 167-1014B-8H and 9H recovered from the same depth interval. We interpret the difference as caused by an intense overprint from drilling the XCB cores, which is probably too strong to be removed at 20 mT AF. The reworked parts of the XCB cores might have suffered mechanical realignment of magnetic particles in the strong magnetic field of the drill string. Even if the small drilling biscuits in the XCB cores carry a magnetization of reverse polarity, the remagnetized slurry surrounding them is probably strongly magnetized in the normal direction with almost uniform declinations.

COMPOSITE DEPTHS AND SEDIMENTATION RATES

Multisensor track (MST) data collected at 4- to 5-cm intervals from Holes 1014A through 1014D and color reflectance data collected at 6- to 8-cm intervals from Holes 1014A, 1014B, and 1014D were used to determine depth offsets in the composite section. On the composite depth scale (expressed as mcd, meters composite depth), features of the plotted MST and color reflectance data present in adjacent holes are aligned so that they occur at approximately the same depth. Working from the top of the sedimentary sequence, a constant was added to the mbsf (meters below sea floor) depth for each core in each hole to arrive at a mcd depth for that core. The depths offsets that compose the composite depth section are given in Table 11, also on CD-ROM, back pocket. Continuity of the sedimentary sequence was documented for the upper 150 mcd.

Magnetic susceptibility and color reflectance measurements were the primary parameters used for interhole correlation purposes. GRAPE bulk density measurements were not useful in interhole correlations because gas expansion in the cores severely affected the high-resolution bulk density data. Natural gamma-ray activity measurements were made throughout the entire section in Holes 1014A and 1014B, but the sampling interval of 12–20 cm was insufficient for interhole correlation.

The color reflectance and magnetic susceptibility records used to verify core overlap for Site 1014 are shown on a composite depth scale in Figure 11. The GRAPE bulk-density data were used to iden-

Table 5. Distribution and relative abundances of calcareous nannofossils in Holes 1014A and 1014B.

Zone	Core, section, interval	Depth (msbf)	Preservation	Abundance	<i>Enitiania huxleyi</i>	<i>Pseudoemiliania lacunosa</i>	<i>Helicosphaera carteri</i>	<i>Helicosphaera sellii</i>	<i>Gephyrocapsa oceanica</i> s.l.	<i>Gephyrocapsa</i> sp. 3	<i>Gephyrocapsa</i> small	<i>Gephyrocapsa</i> large	<i>Discoaster brouweri</i>	<i>Discoaster triradiatus</i>	<i>Discoaster pentaradiatus</i>	<i>Discoaster surculus</i>	<i>Discoaster tamalis</i>	<i>Sphenolithus</i> spp.	<i>Reticulofenestra pseudoumbilicus</i>	<i>Ceratalolithus</i> spp.	<i>Ceratalolithus telesmus</i>	<i>Ceratalolithus acutus</i>	<i>Ceratalolithus rugosus</i>	<i>Amaurolithus</i> spp.	<i>Coccolithus pelagicus</i>	<i>Calcidiscus macintyreii</i> >11 µm	<i>Calcidiscus leptoporus</i>	<i>Cyclicargolithus floridanus</i>	<i>Sphenolithus heteromorphus</i>	Reworking				
CN15	167-1014A-1H-CC	3.1	G	A	P		C																											
CN15-CN14b	2H-CC	12.6	G	A			C			P	A									R														
	3H-CC	22.1		B							C																							
CN15-CN14b	4H-CC	31.6	G	F/C																														
CN14a	5H-CC	41.1	G	A		C	F				A																							
CN14a	6H-top		G	A		C																												
CN14a	6H-CC	50.6	M	C/A						F	A																							
CN13b	7X-CC	54.3	G	A		C	P				D																							
CN13b	8X-CC	64.0	G	A		C	R				A																							
	9X-CC	73.8	P	R		P																												
CN13b?	10X-CC	83.5	G	A		A	C				A									R														
	11X-CC	93.1	P	R		P																												
CN13b	12X-CC	102.8	G	A		C																												
CN13b	13X-CC	112.4	G	A		P	P	C/F	C		C	P	R																					
	14X-CC	120.0	P	R		P																												
CN13a-CN13b	15X-CC	131.6	P	F		C																												
CN13a-CN12d	16X-CC	141.2	P	F		P		R																										
CN13a-CN12d	17X-CC	150.8	P	F		P		R																										
CN13a-CN12d	18X-CC	160.4	P	F/C		P		R																										
CN13a-CN12d	19X-CC	164.4	P	F/C		P		C																										
CN12d	20X-CC	179.6	P	F/C		C							RR	RR				R	R															
CN12d	21X-CC	189.2	P	F		P							R	RR																				
CN12	167-1011B-22X-CC	198.8	M	C		C		C																										
CN12c	23X-CC	208.4	G	A		P		C							F																			
CN12b	167-1014A-24X-CC	218.0	P	F		P							P																					
CN12b	25X-CC	223.5	P/M	F/C		P									P	P																		
CN12b	26X-CC	227.7	P	F/C		P									P	F/C																		
CN12b	27X-CC	237.3	P	F		P							P		P	P	R																	
CN12b	28X-CC	246.9	G	A		P									P	P																		
CN12b	29X-CC	250.1	G	A			P								P	P				P														
CN12b	30X-CC	256.6	M/G	A		P		P							P	F				R														
CN12a	31X-CC	266.2	G	A											P	F																		
CN12a	32X-CC	275.8	G	A											P	F					R													
CN12a	33X-CC	285.5	G	A		R									P	F																		
CN12a	34X-CC	295.1	G	A				P							R	R																		
CN12a	35X-CC	304.8	G	A		P									R	R																		
CN12a	36X-CC	314.4	M	A											P	P																		
CN12a	37X-CC	324.1	M/G	A		P									R	R																		
CN12a	38X-CC	333.7	G	A		P									R	R																		
CN12a	39X-CC	343.4	G	A		P		R							R	R																		
CN10c-CN10b	40X-CC	353.0	M/G	A		P									R	R																		
CN10c-CN10b	41X-CC	362.6	M	A																														
CN10c-CN10b	42X-CC	372.2	G	A											R																			
CN10a-CN9	44X-CC	391.0	M	A																														
CN10a-CN9	45X-CC	401.0	M	A																														
CN10a-CN9	46X-CC	410.5	P/M	C/A																														
CN10a-CN9	47X-CC	420.2	P	R																														

Table 5 (continued).

Zone	Core, section, interval	Depth (mbsf)	Preservation	Abundance	<i>Emiliana huxleyi</i>	<i>Pseudoemiliana lacunosa</i>	<i>Helicosphaera carteri</i>	<i>Helicosphaera sellii</i>	<i>Gephyrocapsa oceanica</i> s.l.	<i>Gephyrocapsa</i> sp. 3	<i>Gephyrocapsa</i> small	<i>Gephyrocapsa</i> large	<i>Discoaster brouweri</i>	<i>Discoaster triadriatus</i>	<i>Discoaster pentaradiatus</i>	<i>Discoaster surculus</i>	<i>Discoaster tamalis</i>	<i>Sphenolithus</i> spp.	<i>Reticulofenestra pseudoumbilicus</i>	<i>Ceratholithus</i> spp.	<i>Ceratholithus telesmus</i>	<i>Ceratholithus acutus</i>	<i>Ceratulithus rugosus</i>	<i>Amaurolithus</i> spp.	<i>Coccolithus pelagicus</i>	<i>Calcidiscus macintyreii</i> >11 µm	<i>Calcidiscus leptopus</i>	<i>Cyclargolithus floridanus</i>	<i>Sphenolithus heteromorphus</i>	Reworking						
CN10a–CN9	48X-CC	429.8	P	RR																																
CN10a–CN9	49X-CC	439.4	P	R																																
CN10a–CN9	50X-CC	449.0	P	RR																																
	167-1014B-																																			
CN15	1H-CC	3.2	G	A	P				C	C																										
CN15–CN14b	2H-CC	12.7	M/G	A		RR	R		C	C	R									P					C											
	3H-CC	22.2	P	F		R	F		C	P								R							A											
CN15–CN14b	4H-CC	31.7	G	A			F/C		F/R	A										R					C											
CN14a	5H-CC	41.2	G	A		C	R		F/R	A															A											
CN14a	6H-CC	50.7	G	A		P	R		R	A															C											
CN13b	7H-CC	60.2	P	F		P				A															C											
CN13b	8H-CC	69.7	G	A		P	R			P																										
CN13b	9H-CC	79.2	M	C		C				A																										
CN13b	10H-CC	88.7	P	F		P				A															P											
CN13b	11H-CC	98.2	M	C/A		C		R		P															P											
CN13b	12H-CC	105.2	M/G	A		C	F		P											R					P											
CN13b	13H-CC	114.7	P	F		C			P																C											
	14X-CC	120.1		B																																
	15X-CC	129.7	P	R/F		P																														
CN13a?	16X-CC	139.3	P	F		C																														
CN12d?	17X-CC	148.9	G	A		C		P		A			RR	RR						R																
CN12	18X-CC	158.8	M	A		P	P	R	C																											
CN12	19X-CC	168.1	A	P/M		P	R		C																											
	20X-CC	177.7	P	R																																
CN12	21X-CC	187.3	P/M	C																																
	22X-CC	196.9	P	F		P																														
CN12c	23X-CC	206.5	G	A		P	C	C																												
CN12b	24X-CC	21.1	M/G	C/A		P	P								F																					
CN12b	25X-CC	225.8	G	A											R																					
CN12b	26X-CC	235.4	P	C/A											C																					
CN12b	27X-CC	245.0	M	A		R									R					P																

Note: See "Explanatory Notes" chapter for abbreviations.

Table 6. Distribution and relative abundances of diatoms in Hole 1014A.

Core, section, interval	Depth (mbsf)	Abundance	Preservation	Marginal upwelling	Diatom fragments	<i>Actinocyclus ingens</i>	<i>Actinocyclus ingens nodus</i>	<i>Actinocyclus oculatus</i>	<i>Actinocyclus tsugaruensis</i>	<i>Actinopychus senarius</i>	<i>Coscinodiscus marginatus</i>	<i>Coscinodiscus nodulifer</i>	<i>Coscinodiscus</i> sp.	<i>Denticulopsis dimorpha</i>	<i>Denticulopsis hustedii</i>	<i>Denticulopsis hyalina</i>	<i>Denticulopsis lauta</i>	<i>Denticulopsis lauta</i> s.l.	<i>Denticulopsis praedimorpha</i>	<i>Denticulopsis prae lauta</i>	<i>Hemiaulus polymorphus</i>	<i>Hemidiscus cuneiformis</i>	<i>Neodenticula kamtschatica</i>	<i>Neodenticula koizumii</i>	<i>Neodenticula cf. seminae</i>
167-1014A-1H-CC	3.1	T	P			P	P			P													P		
2H-CC	12.6	T	P		T											P									
3H-CC	22.1	T	P		R	P				P						P									
4H-CC	31.6	T	P			P						P													
5H-CC	41.4	T	P		T																				
6H-CC	50.6	R	P		R	P										P		P	P		P				
7X-CC	54.3	T	P		P																				
8X-CC	64.0	T	P		R										P										
9X-CC	73.8	T	P		R												P				P				
10X-CC	83.5	T	P		P					P							P								
11X-CC	93.1	T	P		R	P																			
12X-CC	102.8	T	P		R	P			P																
13X-CC	112.4	T	P		R					P							P								
14X-CC	122.0	T	P		P	P				P		P													
15X-CC	131.6	T	P		P												P								
16X-CC	141.2	T	P																						
17X-CC	150.8	T	P							P															
18X-CC	160.4	T	P							P									P						
19X-CC	170.0	T	P		P	P																			
20X-CC	179.6	R	P														P								
21X-CC	189.2	R	P			P				P															
22X-CC	198.8	C	P	Up							P														
23X-CC	208.4	R	P		R	P				P						P	P								
24X-CC	218.0	T	P																						
25X-CC	223.5	R	P							P				P									P		
26X-CC	227.7	R	P		R	P	P												P						
27X-CC	237.3	T	P																P						
28X-CC	246.9	T	P				P												P						
29X-CC	250.1	R	P							P					P		P							P	
30X-CC	256.6	C	P						P								P	P			P				
31X-CC	266.2	T	P			P								P											
32X-CC	275.8	F	P			P				P					P										
33X-CC	285.5	R	P			P																P		P	
34X-CC	295.1	R	P																						
35X-CC	304.8	T	P		T	P																			
36X-CC	314.4	T	P			P									P	P			P						
37X-CC	324.1	R	P			P											P								
38X-CC	333.7	T	P							P															
39X-CC	343.4	F	P				P	P				F				P						F		P	
40X-CC	353.0	T	P		P																				
41X-CC	362.6	T	P			P																			
42X-CC	372.2	T	P			P				P															
43X-CC	381.8																								
44X-CC	391.0	T	P												P				P						
45X-CC	401.0	T	P								P		P		P										
46X-CC	410.5	T	P				P			P															
47X-CC	420.5	T	P							P															
48X-CC	429.8	T	P				P			P							P								
49X-CC	439.4	T	P							P															
50X-CC	449.0	T	P							P															

Notes: P = present; more detailed abundance information not available. See "Explanatory Notes" chapter for other abbreviations.

tify intervals of voids and highly disturbed sediments (values less than 1.4 g/cm³), and all MST and color reflectance data from these intervals were culled. The cores from Holes 1014A, 1014B, and 1014D provide continuous overlap to about 150 mcd. Between 150 and 240 mcd, the cores from Holes 1014A and 1014B were placed into the composite depth scale, but core gaps could not be covered between many of the cores. The composite records suggest that up to 2 m of material may be missing between cores down to about 150 mcd, al-

though the average gap is less than one meter. As there are no data to fill possible core gaps below 150 mcd, an assessment of core gap length below this depth is not possible.

Following construction of the composite depth section for Site 1014, a single spliced record was assembled from the aligned cores. Hole 1014B was used as the backbone of the sampling splice. Holes 1014A and 1014D were used to splice across core gaps in Hole 1014B. The composite depths were aligned so that tie points between

Table 6 (continued).

Core, section, interval	Depth (mbsf)	Abundance	Preservation	Marginal upwelling	<i>Nitzschia rolandii</i>	<i>Paralia sulcata</i>	<i>Rhizosolenia barboi</i>	<i>Stephanopyxis turris</i>	<i>Synedra jouseana</i>	<i>Synedra</i> sp.	<i>Thalassionema hirotsakiensis</i>	<i>Thalassionema nitzschoides</i>	<i>Thalassionema nitzschoides parva</i>	<i>Thalassionema schraderei</i>	<i>Thalassiosira convexa</i>	<i>Thalassiosira</i> cf. <i>leptopus</i>	<i>Thalassiosira oestrupii</i>	<i>Thalassiosira</i> spp. (native type)	<i>Thalassiosira yabei</i>	<i>Thalassiothrix longissima</i>	<i>Thalassiothrix</i> spp.	Silicoflagellates specimens	Sponge spicules
167-1014A-1H-CC	3.1	T	P																				C
2H-CC	12.6	T	P																				F
3H-CC	22.1	T	P							P													C
4H-CC	31.6	T	P																				C
5H-CC	41.4	T	P																				C
6H-CC	50.6	R	P																				R
7X-CC	54.3	T	P																				F
8X-CC	64.0	T	P																				F
9X-CC	73.8	T	P																				F
10X-CC	83.5	T	P																				P
11X-CC	93.1	T	P																				F
12X-CC	102.8	T	P																				F
13X-CC	112.4	T	P																				F
14X-CC	122.0	T	P																				P
15X-CC	131.6	T	P																				R
16X-CC	141.2	T	P																				A
17X-CC	150.8	T	P																				R
18X-CC	160.4	T	P																				P
19X-CC	170.0	T	P																				P
20X-CC	179.6	R	P		P														P				
21X-CC	189.2	T	P																				P
22X-CC	198.8	C	P	Up																			
23X-CC	208.4	R	P																				F
24X-CC	218.0	T	P																				C
25X-CC	223.5	R	P																				C
26X-CC	227.7	R	P																				
27X-CC	237.3	T	P																				F
28X-CC	246.9	T	P																				R
29X-CC	250.1	R	P																				P
30X-CC	256.6	C	P																				P
31X-CC	266.2	T	P																				R
32X-CC	275.8	F	P																				C
33X-CC	285.5	R	P																				P
34X-CC	295.1	R	P																				P
35X-CC	304.8	T	P																				C
36X-CC	314.4	T	P																				
37X-CC	324.1	R	P																				P
38X-CC	333.7	T	P																				P
39X-CC	343.4	F	P																				
40X-CC	353.0	T	P																				R
41X-CC	362.6	T	P																				T
42X-CC	372.2	T	P																				P
43X-CC	381.8																						
44X-CC	391.0	T	P																				
45X-CC	401.0	T	P																				
46X-CC	410.5	T	P																				
47X-CC	420.5	T	P																				F
48X-CC	429.8	T	P																				P
49X-CC	439.4	T	P																				F
50X-CC	449.0	T	P																				F

adjacent holes occurred at exactly the same depths in meters composite depth. Intervals having significant disturbance or distortion were avoided if possible. The Site 1014 splice (Table 12, also on CD-ROM, back pocket) can be used as a sampling guide to recover a single continuous sedimentary sequence between 0 and 150 mcd.

A preliminary age model (Table 13) was constructed to estimate sedimentation rates (Fig. 12). The age model was applied to the spliced records of GRAPE bulk-density, magnetic susceptibility, and color reflectance shown in Figure 13.

INORGANIC GEOCHEMISTRY

We collected 20 interstitial water samples from Hole 1014A at depths ranging from 1.45 to 443.51 mbsf. Chemical gradients in the interstitial waters at this site (Table 14) reflect organic matter diagenesis via sulfate reduction, the dissolution of biogenic opal, and the influence of authigenic mineral precipitation and ion exchange reactions.

Table 7. Distribution and relative abundances of diatoms in Hole 1014B.

Core, section, interval	Depth (mbsf)	Group abundance	Preservation	Marginal upwelling	Diatom fragments	<i>Actinocyclus ingens</i>	<i>Actinocyclus ingens nodus</i>	<i>Actinocyclus tsugarnensis</i>	<i>Aulacostira granulata</i>	<i>Coscinodiscus marginatus</i>	<i>Coscinodiscus cf. marginatus</i>	<i>Coscinodiscus nodulifer</i>	<i>Coscinodiscus radiatus</i>	<i>Coscinodiscus temperei</i>	<i>Coscinodiscus</i> sp.	<i>Denticulopsis dimorpha</i>	<i>Denticulopsis hustedii</i>	<i>Denticulopsis hyalina</i>	<i>Denticulopsis lauta</i>	<i>Denticulopsis lauta</i> s.l.	<i>Denticulopsis</i> sp.	<i>Diploneis</i> sp.	<i>Grammatophora</i> sp.	<i>Neodenticula seminiae</i>	<i>Rhizosolenia barboi</i>	<i>Stephanopyxis turris</i>	<i>Synedra jouseana</i>	<i>Synedra</i> sp.	<i>Thalassionema nitzschioides</i>	<i>Thalassionema schraderi</i>	<i>Thalassiosira</i> spp. (native type)	<i>Thalassiothrix longissima</i>	Sponge spicules					
167-1014B-1H-CC	3.2	T	P						P											P																		
2H-CC	12.7	T	P		P																																	
3H-CC	22.2	T	P		P																																	
4H-CC	31.7	T	P		P	P																																
5H-CC	41.2	T	P		P																																	
6H-CC	50.7	T	P			P				P						P	P																					
7H-CC	60.2	T	P																																			
8H-CC	69.7	T	P		P			P																														
9H-CC	79.2	T	P		P																																	
10H-CC	88.7	T	P				P																															
11H-CC	98.2	T	P																																			
12H-CC	105.2	T	P			P				P																												
13H-CC	114.7	T	P							P																												
14X-CC	120.1	T	P		P																																	
15X-CC	129.7	T	P																																			
16X-CC	139.3	T	P								P																											
17X-CC	148.9	T	P																																			
18X-CC	158.6	T	P		P																																	
19X-CC	168.1	T	P		P	P				P																												
20X-CC	177.7	T	P							P		P																										
21X-CC	187.3	T	P																																			
22X-CC	196.9	C	P	Up	C		P			A																												
23X-CC	206.5	C	P	Up						C																												
24X-CC	216.1	C	P	Up						C																												
25X-CC	225.8	T	P				R																															
26X-CC	235.4	F	P					P																														
27X-CC	245.0	T	P				P																															

Notes: P = present; more detailed abundance information not available. See "Explanatory Notes" chapter for other abbreviations.

Chlorinity increases by nearly 3% from 1.45 to 17.05 mbsf, then decreases to a value similar to that in the shallowest sample by 26.55 mbsf, then decreases by approximately 1% by 443.51 mbsf (Fig. 14). Salinity, measured refractively as total dissolved solids, ranges from 34 to 40. Sodium concentrations by charge balance (Table 14) increase from around 482 mM in the upper 40 mbsf to >500 mM deeper than 150 mbsf.

Alkalinity increases to values >100 mM from 136.63 to 222.45 mbsf, then decreases to values <80 mM from 317.75 to 384.90 mbsf, then increases to values >90 mM in the two deepest samples (Fig. 14). The broad alkalinity maximum begins at a depth corresponding to the base of an organic carbon rich zone (see “Organic Geochemistry” section, this chapter). Sulfate concentrations decrease rapidly in the uppermost sediments to values below the detection limit (approximately 1 mM) by 17.05 mbsf. Phosphate concentrations increase to a broad maximum >150 μ M and up to 200 μ M from 26.55 to 190.65 mbsf, then decrease with increasing depth to 40 μ M below 346.72 mbsf. Ammonium concentrations increase with increasing depth to values greater than 35 mM from 346.72 to 443.51 mbsf.

Dissolved silicate concentrations increase with depth to values >1000 μ M by 136.63 mbsf (Fig. 14), indicative of the dissolution of biogenic opal. Strontium concentrations increase with depth to >200 μ M by 384.90 mbsf.

Calcium concentrations decrease to 2.82 mM at 36.05 mbsf, then generally increase with increasing depth to 9.5 mM in the deepest sample at 443.51 mbsf (Fig. 14). Magnesium concentrations increase to a broad maximum between >60 and 68 mM from 78.25 to 190.65 mbsf, then generally decrease to around 42 mM in the five deepest samples from 317.75 to 443.51 mbsf. The increase in magnesium, around the zone of maximum alkalinity values, may be caused by ion exchange reactions involving ammonium ions and clay minerals, whereas magnesium concentrations decrease across the depth interval marked by thin dolostone beds, observed at approximately 225, 252, and 355 mbsf (see “Lithostratigraphy” section, this chapter). Along with the decrease in dissolved calcium in the upper sediment and the nonlinear relationship of calcium and magnesium, this suggests that authigenic mineral precipitation is significant in influencing these profiles. Lithium concentrations increase with depth to 278 μ M at 443.51 mbsf (Fig. 14).

ORGANIC GEOCHEMISTRY

We conducted measurements of elemental composition and volatile hydrocarbons in sediments from Site 1014 (for methods see “Organic Geochemistry” section, “Explanatory Notes” chapter, this volume).

Volatile Hydrocarbons

The concentrations of methane, ethane, and propane were routinely monitored at Hole 1014A because of shipboard safety and pollution prevention considerations. The results are displayed in Figure 15 and Table 15. Headspace methane concentration increases to 50,000 ppm within the uppermost 30 mbsf. Below 35 mbsf, the concentration decreases gradually with little fluctuation to values of ~1000–3000 ppm. Some higher amounts of ethane were recorded (8–27 ppm) in the lowermost part of this hole. Methane/ethane ratios show a gradual decrease from top to bottom of the hole, to values of ~100–200 in the lowest 100 mbsf (Fig. 15). These low ratios are normally considered significant for safety concerns. However, the gradual decrease and the fact that no higher weight molecular hydrocarbons (> C_2) were observed indicate that the methane is probably a mixture of biogenic- and thermogenic-produced gas. No indications for migrated gas could be found. The first obvious gas voids occurred at about 90 mbsf, and vacutainer samples were taken whenever voids were observed on the catwalk. Because of the direct gas sampling

method, the values of the vacutainer samples were higher but showed the same pattern as the headspace samples.

Elemental Analysis

At Site 1014, 237 sediment samples were analyzed for total carbon, inorganic carbon, total nitrogen, and total sulfur. Results are presented in Table 16 (also on the CD-ROM in the back pocket of this volume) and Figure 16.

The percentage of calcium carbonate ($CaCO_3$) was calculated from the inorganic carbon concentrations by assuming that all carbonate occurs in the form of calcite. The average $CaCO_3$ concentration increases from the top (~35 wt%) to about 200 mbsf (~60 wt%) and decreases again to ~30 wt% at the bottom of the hole. Throughout the entire hole, the $CaCO_3$ concentration record shows a very high amplitude fluctuation of about 20–30 wt%. In the upper 110 mbsf, well-preserved foraminifers and nannofossils indicate that the cyclicity is the result of changes in surface-water productivity (see “Biostratigraphy” section, this chapter). Decreased preservation of calcareous microfossils in the lower part, however, points to dissolution of carbonate as the reason for the observed cyclicity.

The organic carbon record is characterized by high concentrations between 2 and 9 wt% throughout the sequence (Table 16; Fig. 16B). Typical total organic carbon (TOC) contents are 4–5 wt%, but between 100 and 150 mbsf and from 360 to 440 mbsf, high values of up to 9 wt% dominate. The high TOC intervals probably resulted from strong upwelling and tropical climatic conditions (see “Biostratigraphy” section, this chapter).

Total nitrogen values at Site 1014 vary between 0.2 and 0.7 wt%. Total sulfur content ranges from 0 to ~2.6 wt% (Table 16). Total organic carbon/total nitrogen (TOC/TN) ratios were used to characterize the type of organic matter in the sediments. The TOC/TN values generally range between 9 and 12, which suggests to a dominance of marine organic matter (Fig. 16C; Bordovskiy, 1965; Emerson and Hedges, 1988). In the interval influenced by enhanced upwelling (100–150 mbsf), TOC/TN ratios show a remarkably low fluctuation, that may be a result of a more uniform composition of the organic material. A slight positive correlation between TOC and TOC/TN ratio (Fig. 17) may indicate that episodic supply of terrigenous organic matter led to increased TOC values.

PHYSICAL PROPERTIES

Multisensor Track Measurements

The shipboard physical properties program at Site 1014 included nondestructive measurements of bulk density, magnetic susceptibility, *P*-wave velocity, and natural gamma-ray activity on whole sections of all cores using the MST. Magnetic susceptibility was measured in all Site 1014 holes at low sensitivity (1-s measuring time), at 4-cm intervals in Holes 1014A and 1014B and at 5-cm intervals in Holes 1014C and 1014D. GRAPE wet-bulk density measurements were made at 4-cm intervals in Holes 1014A and 1014B and 5-cm intervals in Holes 1014C and 1014D. Whole-round density estimates from the GRAPE show a drop in density values at about 50 mbsf, coinciding with the switch from APC to XCB coring (Fig. 18). This is most likely due to the addition of lower density drilling slurry. The three intervals of very high density (approximately 2.4 g/cm³) at 223, 250, and 353 mbsf are associated with the occurrence of dolostone (see “Lithostratigraphy” section, this chapter).

PWL measurements were made at 4-cm intervals in Holes 1014A and 1014B, at 5-cm intervals throughout Hole 1014C, and at 20-cm intervals in Hole 1014D but gave poor results because of signal attenuation and sediment cracking from high gas content deeper in Holes 1014A, 1014B, and 1014D (see “Organic Geochemistry” section,

Table 8. Distribution and relative abundances of radiolarians in Hole 1014A.

Zone	Core, section, interval	Depth (mbsf)	Abundance	Preservation	<i>Acrosphaera murrayana</i>	<i>Actinomma popofskii</i>	<i>Amphimelissa setosa</i>	<i>Anthocyrtidium nosticae</i>	<i>Anthocyrtidium pliocenica</i>	<i>Botryostrobus aquilonaris</i>	<i>Botryostrobus praetumidulus</i>	<i>Botryostrobus tumidulus</i>	<i>Ceratocyrtis histricosa</i>	<i>Ceratospyrus hyperborea</i>	<i>Cycladophora bicincta</i>	<i>Clathrocyclas bicornis</i>	<i>Cycladophora davisiana davisiana</i>	<i>Cyrtocapsella japonica</i>	<i>Diartus petterssoni</i>	<i>Eucyrtidium aderees</i>	<i>Eucyrtidium calvertense</i>	<i>Eucyrtidium erythromystax</i>	<i>Eucyrtidium matuyamai</i>	<i>Eucyrtidium teuscheri</i>	<i>Gondwanaria dogeli</i>	<i>Lamprocyclas gamphorycha</i>	<i>Lamprocyclas hadros</i>	<i>Lamprocyclas junonis</i>		
Unzoned	167-1014A-1H-CC	3.1	B																											
	2H-CC	12.6	B																											
	3H-CC	22.1	B																											
<i>B. aquilonaris</i> / <i>S. universus</i>	4H-CC	31.6	R	P						P																				
	5H-CC	41.4	R	G								P	P	P	P		P				P									
<i>E. matuyamai</i>	6H-CC	50.6	R	M						P																				
	7X-CC	54.3	R	P							P																			
	8X-CC	64.0	R	M								P																		
	9X-CC	73.8	F	G								P																		
	10X-CC	83.5	R	P								P																		
	11X-CC	93.1	R	P																										
	12X-CC	102.8	F	G				P		P		P	P	P															P	
	13X-CC	112.4	R	P																										
	14X-CC	122.0	R	G									P				P	P												P
	15X-CC	131.6	R	P																										
	16X-CC	141.2	A	G							P	P					P	P			P	P	P	P		P				P
17X-CC	150.8	A	G				P		P	P			P		P	P				P	P	P	P		P				P	
<i>S. langii</i>	18X-CC	160.4	C	M						P						P	P													
	19X-CC	170.0	A	G						P						P	P													
	20X-CC	179.6	A	G	P						P					P	P													
	21X-CC	189.2	C	M												P	P													
	22X-CC	198.8	A	G						P		P	P	P																
	23X-CC	208.4	R	M			P																							
	24X-CC	218.0	F	M																										
	25X-CC	223.5	A	G																										
	26X-CC	227.7	R	P																										
	27X-CC	237.3	R	M																										
	28X-CC	246.9	R	P																										
	29X-CC	250.1	C	G																										
	30X-CC	256.6	A	G																										
	31X-CC	266.2	R	P																										
	32X-CC	275.8	F	M																										
	33X-CC	285.5	R	M																										
	34X-CC	295.1	A	G																										
	35X-CC	304.8	R	P																										
	36X-CC	314.4	R	P																										
	37X-CC	324.1	A	G																										
38X-CC	333.7	A	G																											
39X-CC	343.4	C	G																											
Unzoned	40X-CC	353.0	R	P																										
	41X-CC	362.6	R	P																										
	42X-CC	372.2	R	P																										
	44X-CC	391.0	R	P																										
	45X-CC	401.0	B																											
	46X-CC	410.5	B																											
	47X-CC	420.2	B																											
48X-CC	429.8	B																												
49X-CC	439.4	B																												
50X-CC	449.0	B																												

Note: P = present; more detailed abundance information not available. See "Explanatory Notes" chapter for other abbreviations.

this chapter) and was therefore discontinued after Cores 167-1014A-38X and 167-1014B-6H and Section 167-1014D-4H-6. Natural gamma-ray activity was measured with a 15-s count every 12 cm in Holes 1014A and 1014B, but measurement was reduced to a 15-s count every 15 cm after Core 167-1014A-38X, a 15-s count every 20 cm after Core 167-1014B-10H, and deactivated for Holes 1014C and 1014D.

Index Properties

Index properties measurements were made at one sample per working section in all cores to total depth (TD) in Hole 1014A. Index properties of wet-bulk density, void ratio, porosity, water content, dry density, and grain density were determined by the gravimetric Meth-

od C (see "Physical Properties" section, "Explanatory Notes" chapter, this volume) and presented in Table 17 on CD-ROM in the back pocket of this volume. The necessity to switch from APC to XCB coring at only 50.6 mbsf is perhaps related to the abrupt increase in the bulk density and associated decrease in void ratio, porosity, and water content (Fig. 19). Below this depth, the downhole physical properties changes are gradual, with few fluctuations that most likely correspond to changing amounts of clay and calcium carbonate. However, at approximately 140 mbsf, density measurements shift to higher values, whereas void ratio, porosity, and water content values drop. At this depth, an increase in calcium carbonate content marks the change from lithostratigraphic Subunit IA to IB (see "Litho-

Table 8 (continued).

Zone	Core, section, interval	Depth (mbsf)	Abundance	Preservation	<i>Lanprocyclus margatense</i>	<i>Lanprocyrtis heteroporos</i>	<i>Lanprocyrtis neoheteroporos</i>	<i>Lithelius</i> sp.	<i>Lychnocanoma nipponica sakai</i>	<i>Phormostichoartus crustula</i>	<i>Phormostichoartus intermedium</i>	<i>Pseudocubus warreni</i>	<i>Pterocanium auritum</i>	<i>Pterocorys clausus</i>	<i>Rhizosphaera aquatica</i>	<i>Rhopalastrium profunda</i>	<i>Siphocampe arachnea</i>	<i>Siphocampe quadrata</i>	<i>Sphaeropyle langii</i>	<i>Stichocorys delmontensis</i>	<i>Stichocorys peregrina</i>	<i>Syloactinarium acquilonium</i>	<i>Sylatractus universus</i>	<i>Sylocthamidium venustum</i>	<i>Sylocticya validispina</i>
Unzoned	167-1014A-1H-CC	3.1	B																						
	2H-CC	12.6	B																						
	3H-CC	22.1	B																						
<i>B. aquilonaris</i> / <i>S. universus</i>	4H-CC	31.6	R	P											P	P				P					
	5H-CC	41.4	R	G			P															P	P	P	
<i>E. matuyamai</i>	6H-CC	50.6	R	M															P						
	7X-CC	54.3	R	P																					
	8X-CC	64.0	R	M																					
	9X-CC	73.8	F	G			P																		
	10X-CC	83.5	R	P																					
	11X-CC	93.1	R	P																					
	12X-CC	102.8	F	G			P	P																	
	13X-CC	112.4	R	P						P															
	14X-CC	122.0	R	G			P																		
	15X-CC	131.6	R	P																					
	16X-CC	141.2	A	G			P					P	P	P										P	
	17X-CC	150.8	A	G			P		P																P
	<i>S. langii</i>	18X-CC	160.4	C	M			P																	
19X-CC		170.0	A	G		P	P			P					P									P	
20X-CC		179.6	A	G			P		P								P							P	
21X-CC		189.2	C	M		P	P			P	P													P	
22X-CC		198.8	A	G		P	P	P	P																P
23X-CC		208.4	R	M			P																		P
24X-CC		218.0	F	M			P																		P
25X-CC		223.5	A	G			P																		P
26X-CC		227.7	R	P																					P
27X-CC		237.3	R	M			P																		P
28X-CC		246.9	R	P			P		P																P
29X-CC		250.1	C	G		P	P			P															P
30X-CC		256.6	A	G			P		P																P
31X-CC		266.2	R	P			P																		P
32X-CC		275.8	F	M			P																		P
33X-CC		285.5	R	M						P															P
34X-CC		295.1	A	G			P	P	P	P	P														P
35X-CC		304.8	R	P			P																		P
36X-CC		314.4	R	P			P																		P
37X-CC		324.1	A	G		P	P		P																P
38X-CC		333.7	A	G			P			P															P
39X-CC		343.4	C	G																					P
Unzoned		40X-CC	353.0	R	P																				
	41X-CC	362.6	R	P																					
	42X-CC	372.2	R	P																					
	44X-CC	391.0	R	P																					
	45X-CC	401.0	B																						
	46X-CC	410.5	B																						
	47X-CC	420.2	B																						
	48X-CC	429.8	B																						
	49X-CC	439.4	B																						
	50X-CC	449.0	B																						

stratigraphy” section, this chapter). The strong influence of calcium carbonate on the bulk-density values can be seen in Figure 20.

Heat Flow

Thermal conductivity measurements were made to 77.95 mbsf in Hole 1014B at an average of three per core (Table 18 on CD-ROM in the back pocket of this volume). Three downhole temperature measurements were taken with the APC Adara temperature tool in Hole 1014B: 5.6°C at 31.7 mbsf, 6.8°C at 50.7 mbsf, and 8.2°C at 69.7 mbsf in Cores 167-1014B-4H, 6H, and 8H, respectively (Fig. 21). The bottom-water temperature was measured during the run for Core 167-1014B-6H, leaving the tool at the mudline for approximately 12 min before piston coring. The data indicate a bottom-water temperature of 4.1°C ± 0.1°C. The four data points yield a thermal gradient

of 58°C/km (Fig. 22). Using an average measured thermal conductivity of 0.842 W/(m·K) provides a heat-flow estimate of 49 mW/m² at Site 1014.

Color Reflectance

Reflectance measurements were taken at 4- to 8-cm intervals in Holes 1014A, 1014B, and 1014C. A composite color reflectance record to 150 mcd for the 650–700-nm band average is included in the “Composite Depths and Sedimentation Rate” section (this chapter). Color reflectance data from Hole 1014A were used to predict high-resolution calcium carbonate content. Two separate regression equations were used, one based on Site 1012 reflectance and calcium carbonate data and the other based on a combined data set from Sites 1012 and 1013. The combined equation was an effort to compensate

Table 9. Distribution and relative abundances of radiolarians in Hole 1014B.

Zone	Core, section, interval	Depth (mbsf)	Abundance	Preservation	<i>Acrosphaera murrayana</i>	<i>Actinomma popofskii</i>	<i>Botryostrobos aquilonaris</i>	<i>Botryostrobos praetunidulus</i>	<i>Botryostrobos tumidulus</i>	<i>Ceratocypris hisiricosa</i>	<i>Ceratocypris hyperborea</i>	<i>Clathrocyclas b. bicornis</i>	<i>Clathrocyclas b. bicincta</i>	<i>Cycladophora d. davisiana</i>	<i>Cyrtocapsella cornuta</i>	<i>Eucyrtidium adereces</i>	<i>Eucyrtidium acuminatum</i>	<i>Eucyrtidium calvertense</i>	<i>Eucyrtidium erythromystax</i>	<i>Eucyrtidium matuyamai</i>	<i>Eucyrtidium teuscheri</i>	<i>Lamprocyclus haddros</i>	<i>Lamprocyclus junonis</i>	<i>Lamprocyrtis danieliae</i>	<i>Lamprocyrtis heteroporos</i>
<i>B. aquilonaris/ S. univertus</i>	167-1014B-1H-CC	3.2	B																						
	2H-CC	12.7	R	P	P																				
	3H-CC	22.2	B																						
	5H-CC	41.2	B																						
	6H-CC	50.7	R	P			P																		P
<i>E. matuyamai</i>	7H-CC	60.2	R	P																					
	8H-CC	69.7	R	M																					
	9H-CC	79.2	R	P																					
	10H-CC	88.7	R	G			P																		
	11H-CC	98.2	C	G			P			P															
	12H-CC	105.2	R	P																					
	13X-CC	114.2	R	P																					
	14X-CC	120.7	F	G																					
	15X-CC	129.7	A	G			P	P											P						
	16X-CC	139.3	A	G			P	P				P													
	17X-CC	148.9	A	G			P	P		P		P													
	18X-CC	158.6	A	G			P	P				P							P	P					P
	<i>S. langii</i>	19X-CC	168.1	R	P																				
20X-CC		177.7	R	P																					
21X-CC		187.3	A	G			P	P																	
22X-CC		196.9	A	G			P	P		P		P													
23X-CC		206.5	F	G			P	P																	
24X-CC		216.1	A	G			P	P																	
25X-CC		225.8	A	G			P	P																	
26X-CC		235.4	C	G			P	P																	
27X-CC		245.0	A	G			P	P																	

Notes: P = present; more detailed abundance information not available. See “Explanatory Notes” chapter for other abbreviations.

for the effect of the high organic carbon content at Site 1014. Organic carbon levels at Site 1014 (average ~5.0%) are generally higher than those at Sites 1013 (average ~3.9%) and 1012 (average ~2.6%).

A comparison of the downhole predictions and measured calcium carbonate data to 100 mbsf is given in Figure 23. Calcium carbonate content is simulated well by both equations, generally matching the laboratory measurements in both amplitude and phase. Careful examination of Figure 23 shows that the Site 1012 equation tends to overestimate calcium carbonate content at Site 1014, whereas the combined regression equation is more prone to underestimation.

Digital Color Video

Cores from all Site 1014 holes were imaged with the ODP digital imaging system over 20-cm intervals to provide a 0.25 mm pixel.

DOWNHOLE MEASUREMENTS

Logging Operations and Log Quality

Hole 1014A was logged with the density-porosity combined tool string, sonic-FMS, and GHMT tool strings after the hole was flushed of debris with a sepiolite pill and the drill pipe was set at 84 mbsf (Table 19). One full pass (pass 1: 98–443 mbsf) and a shorter repeat pass (pass 2: 0–325 mbsf) of the density-porosity combination tool string and one full pass of the sonic-FMS tool string (103–444 mbsf) were conducted. Two full passes of the GHMT tool string were conducted (passes 1 and 2: 75–445 mbsf). Sea-state conditions were moderate (2-m swells), and the wireline heave compensator was used on all passes.

Borehole caliper measurements conducted during the density-porosity combination and sonic-FMS passes indicate that the borehole was nearly at drill-bit diameter throughout most of the hole (12–13 in.) with significant, isolated washouts of up to 14–16 in below ~225 mbsf (Fig. 24). Overall log quality at this site is very good with the exception of the sonic velocity log, which was unable to measure formation velocities. Preliminary shipboard processing of the sonic data was also unsuccessful for extracting valid velocity data. As at Hole 1011B, the raw sonic velocity log data at this hole must be considered unreliable until further shore-based processing is completed.

The TLT was run during both passes of the density-porosity combination tool string. The temperature logs were linked to the actual logging depths using the time-depth log recorded at the logging unit. The raw TLT results show a minimum downhole thermal gradient of 29°C/km (Fig. 25). This is an underestimate because of the cooling effect of seawater circulation during drilling. In situ temperature measurements using the Adara probe indicate a thermal gradient near 58°C/km at this site (see “Physical Properties” section, this chapter).

Lithology

The transition from lithostratigraphic Subunit IA to Subunit IB near 145 mbsf is reflected as an increase in sediment density and reduced porosity, which most likely results from the enhanced carbonate content of sediments in Subunit IB (Fig. 24; see “Lithostratigraphy” section, this chapter). Although this subunit boundary was placed at 140 mbsf on the basis of core descriptions, the associated increases in log density would suggest that this gradual transition occurs slightly deeper in the section, near 160 mbsf. The ooze to chalk transition near 310 mbsf can be identified as a small and gradual in-

Table 9 (continued).

Zone	Core, section, interval	Depth (mbsf)	Abundance	Preservation	<i>Lamprocyrtis neoheteroporos</i>	<i>Lamprocyrtis nigrinatae</i>	<i>Lychmocanoma nipponica sakai</i>	<i>Phormostichoartus crustula</i>	<i>Phormostichoartus intermedium</i>	<i>Prunopyle tryppopyena</i>	<i>Pseudocubus warreni</i>	<i>Pterocanium auritum</i>	<i>Pterocorys clausus</i>	<i>Rhizosphaera aquatica</i>	<i>Rhopalastrum profundum</i>	<i>Siphocampe arachnea</i>	<i>Sphaeropyle langii</i>	<i>Stichocorys delmontensis</i>	<i>Stichocorys peregrina</i>	<i>Stylocarium acquilonium</i>	<i>Stylatractus univertus</i>	<i>Stylochlamidium venustum</i>	<i>Stylocidrya validispina</i>	
<i>B. aquilonaris/ S. univertus</i>	167-1014B-1H-CC	3.2	B																					
	2H-CC	12.7	R	P																				
	3H-CC	22.2	B																					
	5H-CC	41.2	B																					
	6H-CC	50.7	R	P										P			P			P			P	
<i>E. matuyamai</i>	7H-CC	60.2	R	P																				
	8H-CC	69.7	R	M	P	P						P					P							
	9H-CC	79.2	R	P					P									P						
	10H-CC	88.7	R	G	P		P														P			
	11H-CC	98.2	C	G	P		P	P						P							P		P	
	12H-CC	105.2	R	P																				
	13X-CC	114.2	R	P																				
	14X-CC	120.7	F	G	P										P		P					P	P	
	15X-CC	129.7	A	G	P																		P	
	16X-CC	139.3	A	G	P						P							P					P	
	17X-CC	148.9	A	G	P				P		P							P					P	
	18X-CC	158.6	A	G	P			P		P	P							P					P	
	<i>S. langii</i>	19X-CC	168.1	R	P																			P
20X-CC		177.7	R	P			P																P	
21X-CC		187.3	A	G	P			P	P						P		P						P	
22X-CC		196.9	A	G	P			P	P						P		P						P	
23X-CC		206.5	F	G	P										P		P						P	
24X-CC		216.1	A	G	P		P								P		P						P	
25X-CC		225.8	A	G	P						P				P								P	
26X-CC		235.4	C	G	P				P						P			P					P	
27X-CC		245.0	A	G	P				P						P									P

crease in bulk density. Three dolostone stringers within Subunit IB are clearly apparent in the log density, porosity, and resistivity data; depths and thicknesses can be estimated from the sonic-FMS microresistivity images (FMS logging depth [thickness]: 224.6–225.1 mbsf [50 cm]; 251.6–252.3 mbsf [70 cm]; and 353.3–353.8 mbsf [50 cm]).

The magnetic susceptibility log data from the two GHMT passes are shown in Figure 26. Repeatability between the two passes is excellent, and the broad-scale susceptibility variations (intrinsic resolution of the log measurement is ~1 m) are similar to the core-based susceptibility measurements. The log susceptibility measurements exhibit periodic ~2- to 3-m variations throughout much of the hole (Fig. 26). Value differences between the two passes are real and reflect changes in internal tool temperature as the tool warms in the borehole, an effect that can be corrected after processing.

Comparison of Core and Log Data

Broad variations in sediment composition are apparent from the log data. Variations in calcium carbonate percentage are strongly correlated with the density (RHOB), corrected gamma ray (CGR), and photoelectric factor (PEF) log measurements. The PEF log is of particular interest because it is one of the highest resolution logs, with an intrinsic resolution approaching 20 cm. The photoelectric effect is caused by absorption by atomic nuclei of lower energy gamma rays, which have reduced velocities resulting from multiple Compton (“billiard ball”) atomic collisions. Higher atomic number elements can more efficiently capture low-energy gamma rays. Because calcium has a relatively large capture cross section, the PEF log can be useful in delineating variations in calcium carbonate abundances (Fig. 27A), reflecting the influence of calcium abundance (CaCO₃)

on low-energy gamma-ray absorption. The standard (PEF; 15-cm sample interval) and high-resolution photoelectric effect (HPEF; processed 2-cm sample interval) log data are shown adjacent to the digital color reflectivity measurements for the 160–175 mbsf interval at Hole 1014A (Fig. 28). The HPEF log is processed to higher resolution using the source–near detector spacing standard PEF count-rate data (from the HLDT tool). Digital color reflectivity at this site is closely correlated to carbonate abundance (see “Lithostratigraphy” section, this chapter), so the similarity between core reflectivity and the PEF and HPEF log data reflects variable sedimentary CaCO₃ abundance. The sub-meter-scale correlations between the core reflectivity and the HPEF logs demonstrate the quantitative lithostratigraphic potential of these high-resolution log data.

Similarly, the log data can be used to estimate variations in organic carbon input using the uranium (U) log from the natural gamma-ray tool (Fig. 27). The solubility of U in interstitial waters is dependent upon the sedimentary redox conditions; highly reducing organic-rich sediments typically fix authigenic U. Core-based organic carbon concentration and log-based U content at Site 1014 are extremely high, reaching up to 10% and 16 ppm, respectively, and are closely covariant (Fig. 27). The U signal is so strong that it overwhelms the terrigenous K and Th natural gamma-ray contributions (Fig. 29). Note that the total gamma-ray curve dominantly reflects U concentration variations tied to variation in organic carbon content (e.g., Fig. 27). The CRG variations reflect combined K and contributions from variations in terrigenous mineral abundance and are anticorrelated with CaCO₃ content at Hole 1014A.

The core and log measurements of sediment bulk density are similar over their common interval, whereas the core porosity data are significantly lower than the log (neutron) measurements (Fig. 30). The log porosities are significantly higher because the neutron log

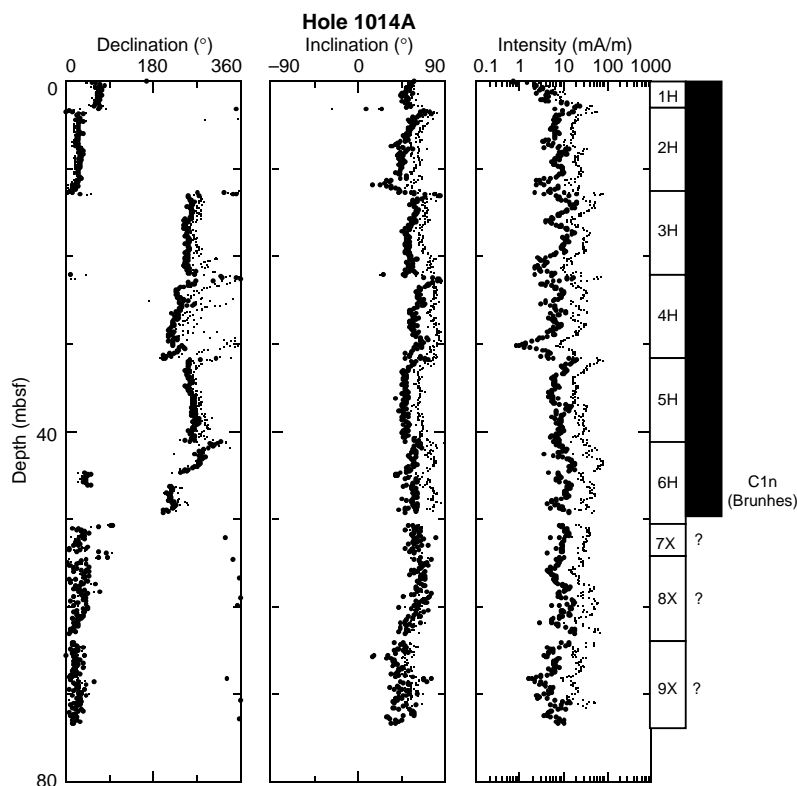


Figure 7. Plots of magnetic declination, inclination, and intensity of cores from Hole 1014A. Small and large dots represent magnetic declination, inclination, and intensity before and after AF demagnetization at 20 mT, respectively.

porosity data reflect measurement of both free water (interstitial space) and molecularly bound water associated with abundant clay mineral content in the formation. Hence, the neutron porosity tends to overestimate porosity in very clay-rich formations such as at Hole 1014A.

SUMMARY

At Site 1014, in the Tanner Basin of the California Borderland, we drilled a high-resolution, upper Neogene sedimentary section to study upper intermediate waters at the basin sill depth of 1160 mbsf, near the actual depth of the drill site (1176 mbsf; Fig. 31). Site 1014 has a higher time resolution than Site 1013, with sedimentation rates of 80 m/m.y. or more to 3 Ma, and older sediments than at Site 1013 were sampled. The base of the sediment column is probably late Miocene in age. Site 1014 forms a good paleoceanographic comparison to Site 1013 because the two have similar sill depths. Site 1013 bottom waters flow for a significant distance through the borderland province, whereas Site 1014 receives relatively pristine waters from across the Patton Escarpment.

Four holes were drilled at Site 1014, with four cores penetrating from 0 to 19 mbsf (~0–0.25 Ma), three cores penetrating 19–121 mbsf (~0.25–1.7 Ma), and two cores penetrating 121–245 mbsf (~1.7–2.7 Ma). The deepest hole penetrated to a depth of 449 mbsf, which may be as old as 7.5 Ma, based on extrapolation of the sedimentation rate between 328 and 382 mbsf. An excellent paleomagnetic reversal sequence in the APC section and calcareous biostratigraphy form the primary stratigraphy at Site 1014. However, foraminifers are absent below 353 mbsf, and poorly diagnostic nannofossil assemblages at the base of the hole leave the basal age in doubt. Siliceous microfossils, while present, are never abundant and rarely age diagnostic. The high quality of the paleomagnetic record was surpris-

ing, as it was at Sites 1012 and 1013, because of the high sedimentary organic carbon content (averaging 5%–6% or higher) and significant organic matter diagenesis within the sediment column, as indicated by the interstitial water analyses. Typical magnetic minerals should have been reduced in the upper sediment column by diagenetic reactions.

Site 1014 has a sedimentary column similar to that at Site 1012, although it accumulated at somewhat faster rates. Distinctive features to note within the lithostratigraphic column at Site 1014 are the higher amounts of siliceous microfossils than at Sites 1012 and 1013 and the high organic carbon contents, higher than any of the other California Borderland basins. Rhythmic layering is prominent here primarily as a result of changes in calcium carbonate content. High-resolution studies of orbital climate forcing should be achievable at this site.

REFERENCES

- Bordovskiy, O.K., 1965. Accumulation and transformation of organic substances in marine sediment, 2. Sources of organic matter in marine basins. *Mar. Geol.*, 3:5–31.
- Cande, S.C., and Kent, D.V., 1995. Revised calibration of the geomagnetic polarity timescale for the Late Cretaceous and Cenozoic. *J. Geophys. Res.*, 100:6093–6095.
- Emerson, S., and Hedges, J.I., 1988. Processes controlling the organic carbon content of open ocean sediments. *Paleoceanography*, 3:621–634.
- Emery, K.O., 1960. *The Sea Off Southern California: A Modern Habitat of Petroleum*. New York (Wiley).
- Kennett, J.P., Baldauf, J.G., and Lyle, M. (Eds.), 1995. *Proc. ODP, Sci. Results*, 146 (Pt. 2): College Station, TX (Ocean Drilling Program).
- Lyle, M., Gallaway, P.J., Liberty, L.M., Mix, A., Stott, L., Hammond, D., Gardner, J., Dean, W., and the EW9504 Scientific Party, 1995a. Data submission. W9406 and EW9504 site surveys of the California margin proposed drillsites, Leg 167 (Vol. 1): Site maps and descriptions. Boise State Univ., *CGISS Tech. Rep.*, 95–11.

_____, 1995b. Data submission. W9406 and EW9504 site surveys of the California margin proposed drillsites, Leg 167 (Vol. 2): Seismic profiles. Boise State Univ., *CGISS Tech. Rep.*, 95-12.
 Poore, R.Z., McDougall, K., Barron, J.A., Brabb, E.E., and Kling, S.A., 1981. Microfossil biostratigraphy and biochronology of the type Relizian and Luisian Stages of California. In Garrison, R.E., Douglas, R.G., Pis-ciotto, K.E., Isaacs, C.M., and Ingle, J.C. (Eds.), *The Monterey Forma-*

tion and Related Siliceous Rocks of California. Proc. SEPM Res. Pacific Sect., Soc. Econ. Paleontol. Mineral., 55-70.

Ms 167IR-108

NOTE: For all sites drilled, core-description forms (“barrel sheets”) and core photographs can be found in Section 3, beginning on page 499. Smear-slide data can be found in Section 4, beginning on page 1327. See Table of Contents for material contained on CD-ROM.

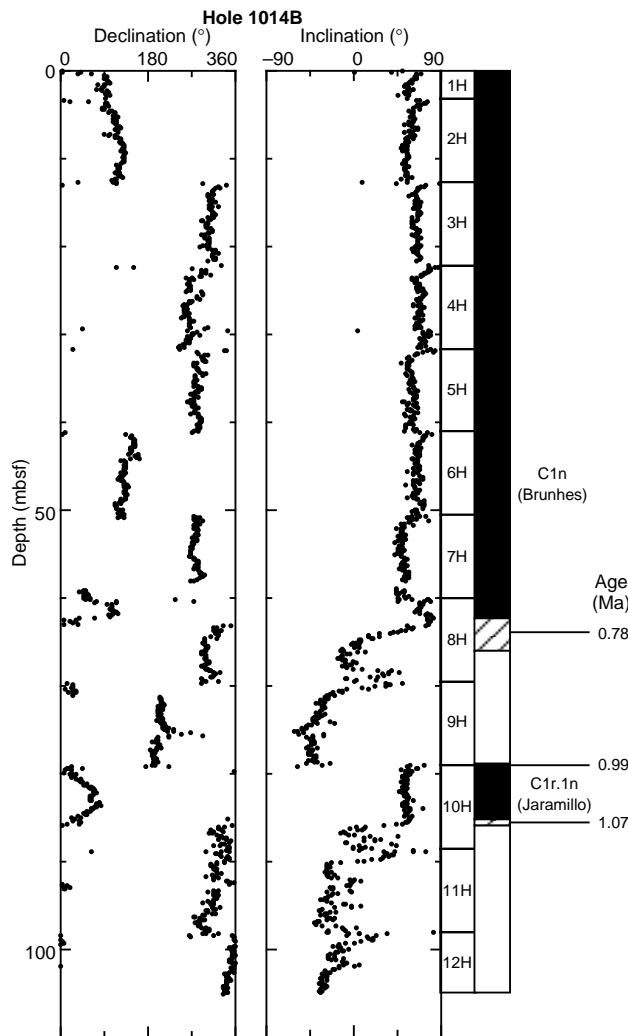


Figure 8. Plots of magnetic declination and inclination of cores from Hole 1014B with the magnetostratigraphic polarity interpretation. Ages in Ma of the reversal boundaries are from Cande and Kent (1995). Small and large dots represent magnetic declination and inclination before and after AF demagnetization at 20 mT, respectively.

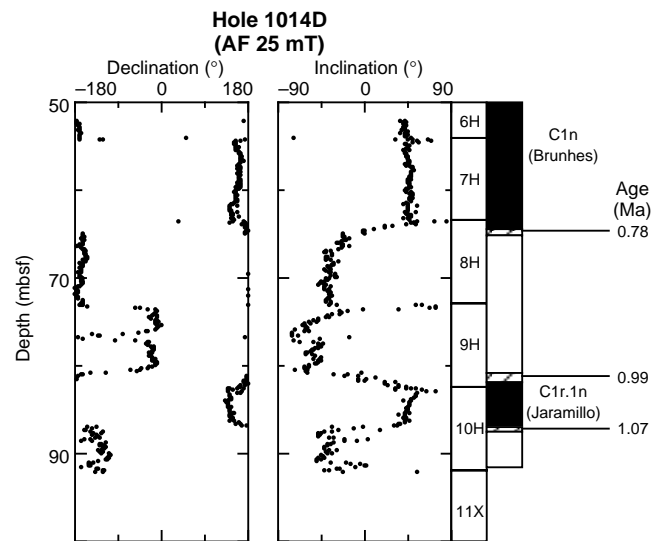


Figure 9. Plots of magnetic declination and inclination of cores from Hole 1014D after AF demagnetization at 25 mT. Also shown is the magnetostratigraphic polarity interpretation with the ages of the reversal boundaries (Cande and Kent, 1995).

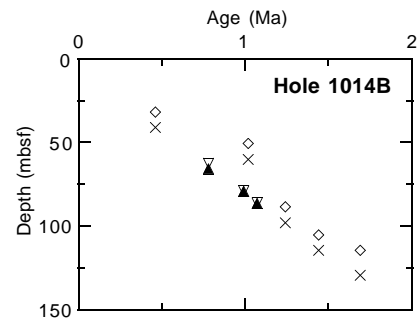


Figure 10. Age/depth plot for Hole 1014B. Open and solid triangles show the upper and lower limit for each of the three polarity transitions. Also shown are the upper (diamonds) and lower (×) limits of the nannofossil datum events (see “Biostratigraphy” section, this chapter). The sedimentation rate is constant at 79 m/m.y.

Table 10. Magnetostratigraphic datum levels in Holes 1014B and 1014D.

Chronozone boundary	Age (Ma)	Upper limit			Lower limit		
		Core, section	Level (cm)	Depth (mbsf)	Core, section	Level (cm)	Depth (mbsf)
		167-1014B-			167-1014B-		
C1n Brunhes (o)	0.780	8H-2	55	62.25	8H-4	125	65.95
Clr.1n Jaramillo (t)	0.990	9H-7	35	79.05	10H-1	5	79.25
Clr.1n Jaramillo (o)	1.070	10H-5	85	86.05	10H-6	5	86.75
		167-1014D-			167-1014D-		
C1n Brunhes (o)	0.780	8H-1	85	64.35	8H-2	5	65.05
Clr.1n Jaramillo (t)	0.990	9H-6	25	80.75	9H-6	145	81.95
Clr.1n Jaramillo (o)	1.070	10H-3	135	86.85	10H-4	35	87.35

Notes: o = onset; t = termination; the assigned ages of the reversal boundaries are according to the time scale of Cande and Kent (1995). The upper and lower limits define the range within which a reversal occurs.

Table 11. Site 1014 composite depth section.

Hole, core, section	Depth (mbsf)	Offset (m)	Depth (mcd)	Hole, core, section	Depth (mbsf)	Offset (m)	Depth (mcd)
167-1014A-				167-1014B-			
1H-1	0.00	0.00	0.00	1H-1	0.00	0.00	0.00
2H-1	3.10	0.65	3.75	2H-1	3.20	0.27	3.47
3H-1	12.60	1.16	13.76	3H-1	12.70	0.91	13.61
4H-1	22.10	1.31	23.41	4H-1	22.20	1.17	23.37
5H-1	31.60	1.60	33.20	5H-1	31.70	1.12	32.82
6H-1	41.10	2.97	44.07	6H-1	41.20	2.00	43.20
7X-1	50.60	3.00	53.60	7H-1	50.70	2.50	53.20
8X-1	54.30	2.67	56.97	8H-1	60.20	1.81	62.01
9X-1	64.00	2.03	66.03	9H-1	69.70	1.91	71.61
10X-1	73.80	2.31	76.11	10H-1	79.20	1.23	80.43
11X-1	83.50	1.91	85.41	11H-1	88.70	1.71	90.41
12X-1	93.10	2.21	95.31	12H-1	98.20	4.52	102.72
13X-1	102.80	1.96	104.76	13X-2	106.15	4.52	110.67
14X-1	112.40	0.12	112.52	14X-1	114.70	-0.59	114.11
15X-2	122.20	-3.64	118.56	15X-1	120.10	-1.04	119.06
16X-1	131.60	-7.00	124.60	16X-1	129.70	-0.28	129.42
17X-1	141.20	-4.74	136.46	17X-1	139.30	1.30	140.60
18X-1	150.80	-3.87	146.93	18X-1	148.90	6.87	155.77
19X-1	160.40	-3.87	156.53	19X-1	158.60	5.51	164.11
20X-1	170.00	-4.56	165.44	20X-1	168.10	5.51	173.61
21X-1	179.60	-4.56	175.04	21X-2	177.98	5.51	183.49
22X-1	189.20	-4.49	184.71	22X-1	187.30	5.51	192.81
23X-2	199.21	-4.49	194.72	23X-1	196.90	5.51	202.41
24X-1	208.40	-6.60	201.80	24X-1	206.50	5.51	212.01
25X-1	218.00	-6.60	211.40	25X-1	216.10	5.51	221.61
26X-1	223.50	-6.60	216.90	26X-1	225.80	5.51	231.31
27X-1	227.70	-6.60	221.10	27X-1	235.40	5.51	240.91
28X-1	237.30	-6.60	230.70				
29X-1	246.90	-6.60	240.30	167-1014C-			
30X-1	250.10	-6.60	243.50	1H-1	0.00	1.31	1.31
31X-1	256.60	-6.60	250.00	2H-1	9.50	2.20	11.70
32X-1	266.20	-6.60	259.60	167-1014D-			
33X-1	275.80	-6.60	269.20	1H-1	0.00	0.00	0.00
34X-1	285.50	-6.60	278.90	2H-1	6.50	0.03	6.53
35X-1	295.10	-6.60	288.50	3H-1	16.00	-0.05	15.95
36X-1	304.80	-6.60	298.20	4H-1	25.50	0.21	25.71
37X-2	314.80	-6.60	308.20	5H-1	35.00	0.17	35.17
38X-1	324.10	-6.60	317.50	6H-1	44.50	0.92	45.42
39X-1	333.70	-6.60	327.10	7H-1	54.00	0.37	54.37
40X-2	343.77	-6.60	337.17	8H-1	63.50	0.71	64.21
41X-1	353.00	-6.60	346.40	9H-1	73.00	0.75	73.75
42X-1	362.60	-6.60	356.00	10H-1	82.50	0.50	83.00
44X-1	381.80	-6.60	375.20	11X-1	92.00	1.01	93.01
45X-2	392.34	-6.60	385.74	12X-1	101.70	1.01	102.71
46X-1	401.00	-6.60	394.40	13X-1	111.30	-1.30	110.00
47X-3	412.64	-6.60	406.04				
48X-1	420.20	-6.60	413.60				
49X-1	429.80	-6.60	423.20				
50X-1	439.40	-6.60	432.80				

Note: This table is also on CD-ROM, back pocket, this volume.

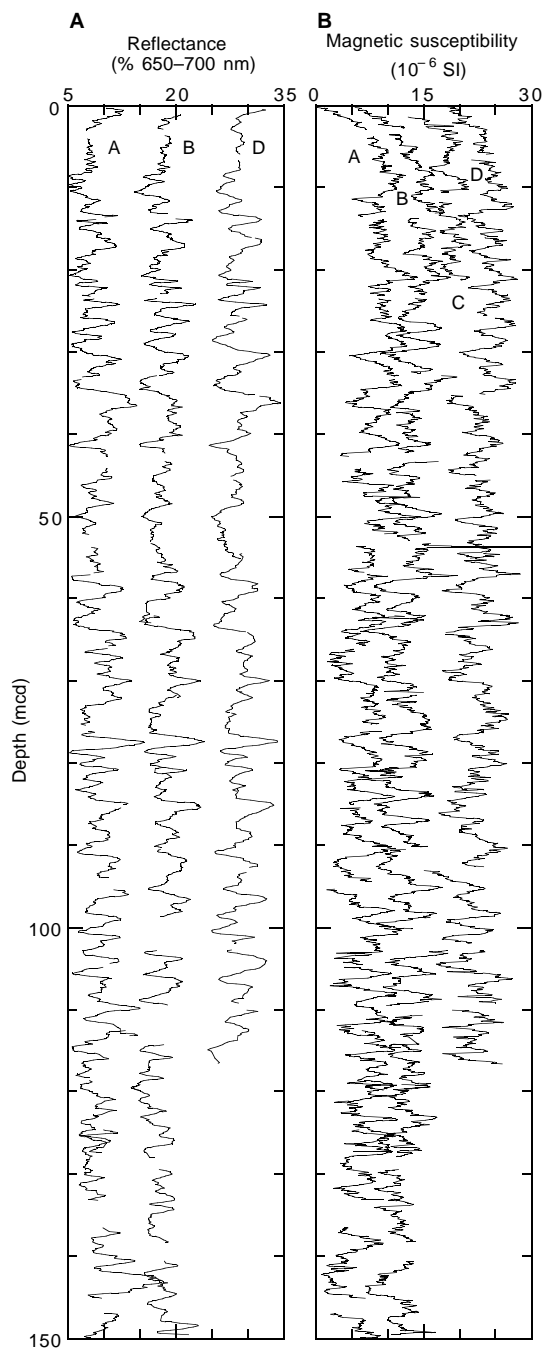


Figure 11. **A.** Smoothed (5-point running average) color reflectance (650–700 nm band) data for the upper 150 m from Site 1014 on the mcd scale. Holes 1014A, 1014B, and 1014D are offset from each other by a constant (10%). **B.** Smoothed (15-cm Gaussian) magnetic susceptibility data for the upper 150 m from Site 1014 on the mcd scale. Holes 1014A to 1014D are offset from each other by a constant (10×10^{-6} SI).

Table 12. Site 1014 splice tie points.

Hole, core, section, interval (cm)	Depth		tie to	Hole, core, section, interval (cm)	Depth	
	(mbsf)	(mcd)			(mbsf)	(mcd)
1014D-1H-5, 62	5.12	5.12	tie to	1014B-2H-2, 15	4.85	5.12
1014B-2H-6, 83	11.53	11.8	tie to	1014D-2H-4, 77	11.77	11.8
1014D-2H-6, 37	14.37	14.4	tie to	1014B-3H-1, 79	13.49	14.4
1014B-3H-6, 51	20.71	21.62	tie to	1014D-3H-4, 117	21.67	21.62
1014D-3H-6, 87	24.37	24.32	tie to	1014B-4H-1, 95	23.15	24.32
1014B-4H-7, 11	31.31	32.48	tie to	1014D-4H-5, 77	32.27	32.48
1014D-4H-6, 122	34.22	34.43	tie to	1014B-5H-2, 11	33.31	34.43
1014B-5H-6, 127	40.47	41.59	tie to	1014D-5H-5, 37	41.42	41.59
1014D-5H-6, 127	43.86	44.03	tie to	1014B-6H-1, 83	42.03	44.03
1014B-6H-6, 123	49.99	51.99	tie to	1014D-6H-5, 57	51.07	51.99
1014D-6H-6, 127	53.27	54.19	tie to	1014B-7H-1, 99	51.69	54.19
1014B-7H-5, 99	57.69	60.19	tie to	1014D-7H-4, 132	59.82	60.19
1014D-7H-6, 77	62.27	62.64	tie to	1014B-8H-1, 63	60.83	62.64
1014B-8H-6, 87	68.57	70.38	tie to	1014D-8H-5, 17	69.67	70.38
1014D-8H-7, 17	72.67	73.38	tie to	1014B-9H-2, 27	71.47	73.38
1014B-9H-6, 111	78.31	80.22	tie to	1014D-9H-5, 47	79.47	80.22
1014D-9H-7, 17	82.17	82.92	tie to	1014B-10H-2, 99	81.69	82.92
1014B-10H-6, 99	87.69	88.92	tie to	1014D-10H-4, 142	88.42	88.92
1014D-10H-7, 22	91.72	92.22	tie to	1014B-11H-2, 31	90.51	92.22
1014B-11H-4, 35	93.55	95.26	tie to	1014D-11X-2, 97	94.47	95.48
1014D-11X-6, 62	100.12	101.13	tie to	1014A-12X-5, 59	99.11	101.32
1014A-12X-6, 119	101.21	103.42	tie to	1014B-12H-1, 83	99.03	103.55
1014B-12H-3, 23	101.43	105.95	tie to	1014A-13X-1, 127	104.07	106.03
1014A-13X-5, 83	109.63	111.59	tie to	1014D-13X-2, 37	113.17	111.87
1014D-13X-4, 92	116.05	114.75	tie to	1014B-14X-1, 71	115.41	114.82
1014B-14X-4, 119	120.39	119.8	tie to	1014A-15X-2, 127	123.47	119.83
1014A-15X-5, 131	128.01	124.37	tie to	1014B-15X-4, 87	125.47	124.43
1014B-15X-5, 35	126.45	125.41	tie to	1014A-16X-2, 31	132.49	125.49
1014A-16X-6, 35	138.53	131.53	tie to	1014B-16X-2, 63	131.83	131.55
1014B-16X-6, 95	138.15	137.87	tie to	1014A-17X-1, 143	142.63	137.89
1014A-17X-6, 115	149.85	145.11				

Note: This table is also on CD-ROM, back pocket, this volume.

Table 13. Site 1014 sedimentation rate age control points.

Event	Chron/ subchron	Depth (mcd)	Age (Ma)
T <i>P. lacunosa</i>		37.79	0.46
B Brunhes	C1n	65.66	0.78
T Jaramillo	C1r.1n	81.58	0.99
B Jaramillo	C1r.1n	87.62	1.07
T large <i>Gephyrocapsa</i>		95.26	1.24
B large <i>Gephyrocapsa</i>		115.40	1.44
B <i>G. oceanica</i>		121.16	1.69
T <i>D. surculus</i>		212.86	2.61
T <i>D. iamalís</i>		254.80	2.76
B <i>L. neoheteroporos</i>		322.30	3.06
B <i>Ceratolithus</i> spp.		375.00	5.03

Note: T = top, B = bottom.

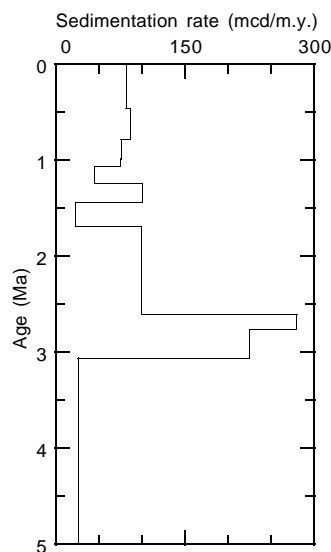


Figure 12. Sedimentation rate vs. age at Site 1014 based on the age control points from Table 12.

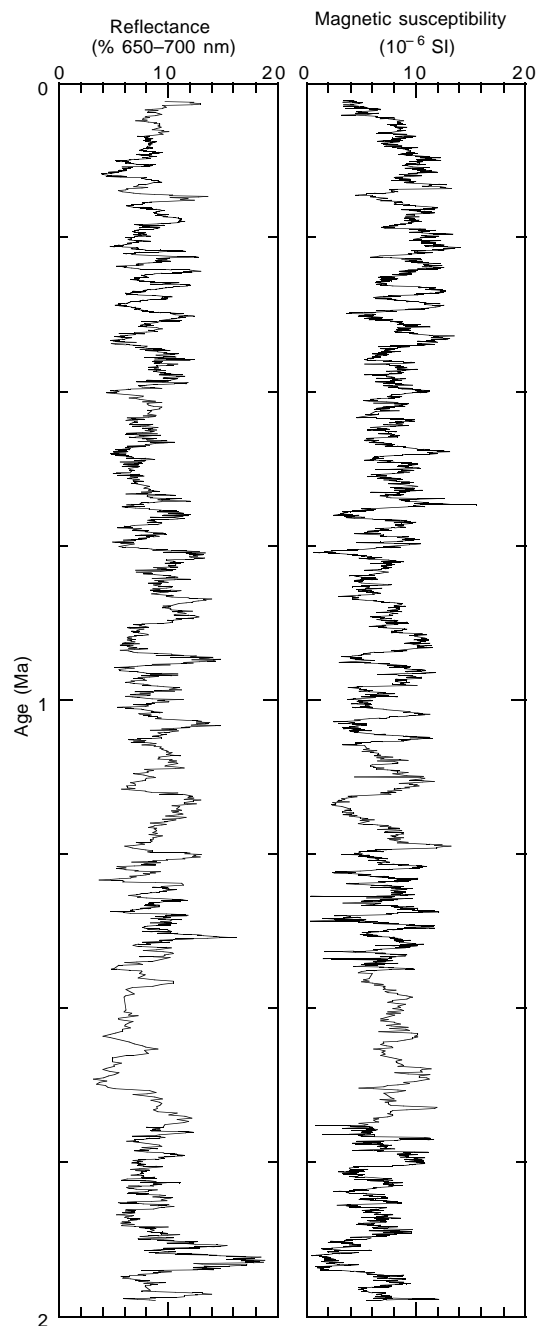


Figure 13. Site 1014 spliced records of color reflectance and magnetic susceptibility vs. age based on age control points from Table 12.

Table 14. Interstitial water geochemical data, Hole 1014A.

Core, section, interval (cm)	Depth (mbsf)	pH	Alkalinity (mM)	Salinity	Cl ⁻ (mM)	Na ⁺ (mM)	SO ₄ ²⁻ (mM)	HPO ₄ ²⁻ (μM)	NH ₄ ⁺ (mM)	H ₄ SiO ₄ (μM)	Ca ²⁺ (mM)	Mg ²⁺ (mM)	Sr ²⁺ (μM)	Li ⁺ (μM)	K ⁺ (mM)
167-1014A-															
1H-1, 145-150	1.45	7.47	3.63	34.0	546	470	27.7	7	<0.2	325	10.2	52.1	87	28	10.2
2H-3, 145-150	7.55	7.23	29.5	34.0	555	780	10.0	98	3.0	571	6.29	51.0	90	32	9.5
3H-3, 145-150	17.05	7.17	52.0	34.0	561	489	<1	142	6.0	660	3.79	53.2	113	36	10.4
4H-3, 145-150	26.55	7.31	56.6	34.5	555	486	<1	171	7.6	712	3.47	53.6	120	44	11.1
5H-3, 145-150	36.05	7.21	58.6	34.5	548	483	<1	158	9.9	858	2.82	53.6	110	58	11.0
7X-1, 145-150	52.05	7.27	69.5	35.0	548	487	<1	154	15.7	916	3.50	56.4	117	78	11.0
10X-3, 145-150	78.25	7.14	82.0	35.5	547	489	<1	183	19.4	905	4.27	60.5	123	103	10.8
13X-3, 145-150	107.25	7.18	97.2	37.0	550	495	<1	201	23.1	953	5.68	65.0	137	122	10.9
16X-4, 145-150	136.63	6.91	111	38.0	548	497	<1	205	22.5	1011	7.15	68.3	163	140	10.8
19X-3, 145-150	164.85	6.90	113	38.0	549	504	<1	177	25.9	984	6.79	67.1	163	154	10.6
22X-1, 145-150	190.65	6.79	112	40.0	549	503	<1	163	28.2	1103	7.32	65.3	180	172	13.0
25X-3, 145-150	222.45	7.40	102	37.0	545	504	<1	132	32.0	1118	7.13	58.0	183	187	12.9
28X-1, 145-150	238.75	6.70	96.6	37.0	545	502	<1	97	30.1	1136	7.01	55.8	196	200	13.6
31X-3, 145-150	259.91	6.64	96.1	37.0	545	511	<1	79	31.7	1148	6.22	52.5	190	209	13.2
34X-3, 145-150	289.95	7.53	83.8	36.0	542	505	<1	72	31.9	1118	6.57	47.3	180	220	13.2
50X-3, 140-150	443.51	7.65	95.4	36.0	545	521	<1	52	38.0	1317	9.51	43.6	246	278	13.2

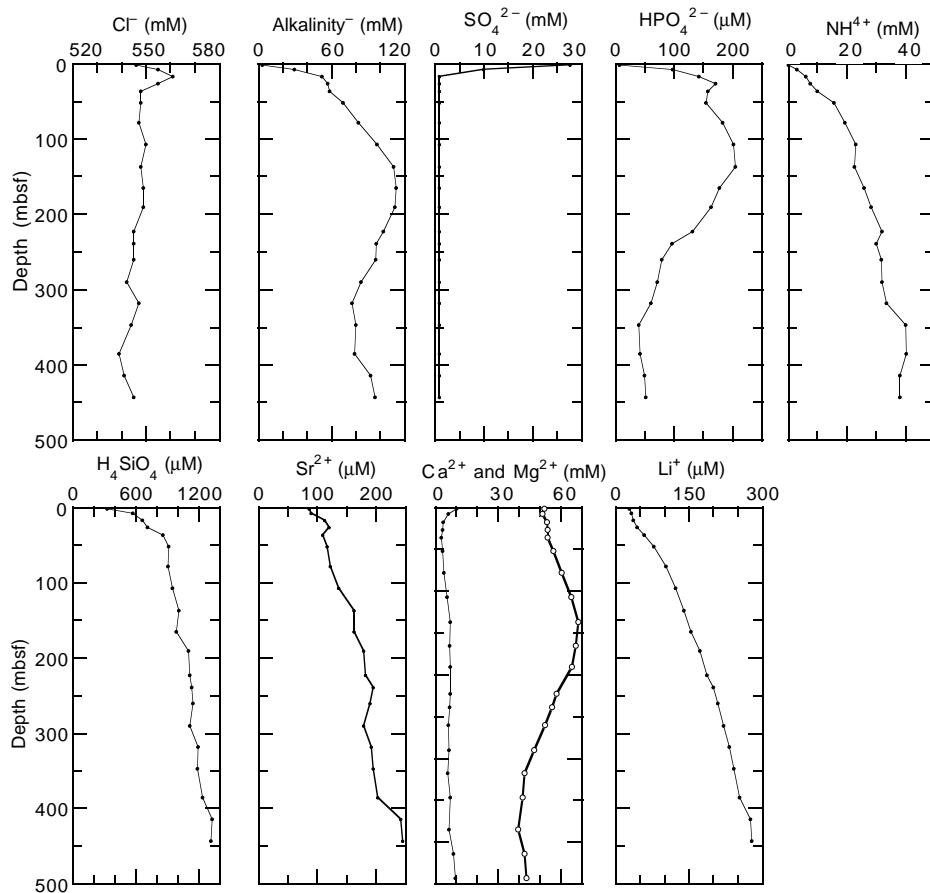


Figure 14. Interstitial water geochemical data, Site 1014. Solid circles = Ca, open circles = Mg.

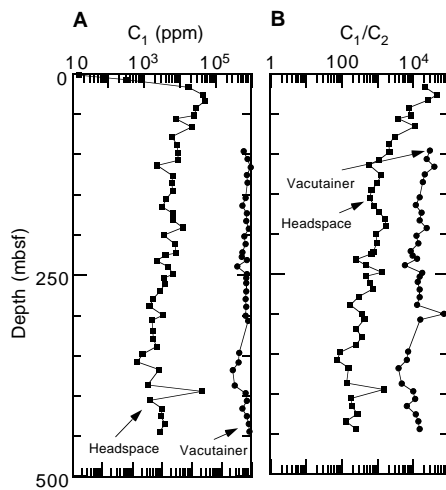


Figure 15. **A.** Concentrations of methane (C₁) obtained by the headspace and vacutainer techniques from Hole 1014A. **B.** Methane/ethane ratios of headspace and vacutainer measurements from Hole 1014A.

Table 15. Concentrations of methane (C₁), ethene (C₂₌), ethane/ethylene (C₂), propene (C₃₌), and propane/propylene (C₃) obtained by the headspace and vacutainer techniques from Hole 1014A.

Core, section, interval (cm)	Depth (mbsf)	C ₁ (ppm)	C ₂₌ (ppm)	C ₂ (ppm)	C ₃₌ (ppm)	C ₃ (ppm)	C ₁ /C ₂	C ₁ /C ₂₊
Headspace								
167-1014A-								
1H-2, 0-5	1.53	15						
2H-4, 0-5	7.63	310						
3H-4, 0-5	17.13	17,468		0.8			21,835	21,835
4H-4, 0-5	26.63	46,354		1			46,354	46,354
5H-3, 145-150	36.08	50,881	1	1		1	25,441	16,960
6H-5, 0-5	47.13	29,583	1	3		3	7,396	4,226
7X-2, 0-5	52.13	25,109	1	2		1	8,370	6,277
8X-4, 0-5	58.83	7,846		2			3,923	3,923
9X-4, 0-5	68.53	22,288		2		1	11,144	7,429
10X-4, 0-5	78.33	6,192		2			3,096	3,096
11X-4, 0-5	88.03	8,602	1	3		2	2,151	1,434
12X-4, 0-5	97.63	8,761	1	3		2	2,190	1,460
13X-4, 0-5	107.33	9,146	2	6		6	1,143	653
14X-2, 0-5	113.93	2,390	1	3		3	598	341
15X-3, 0-5	125.03	6,305	1	4		4	1,261	701
16X-5, 0-5	137.63	6,042	1	5		5	1,007	549
17X-3, 0-5	144.23	6,246	2	7	1	8	694	347
18X-4, 0-5	155.33	4,240	2	5		5	606	353
19X-4, 0-5	164.93	3,227	1	3		3	807	461
20X-3, 0-5	173.03	6,698	1	5		5	1,116	609
21X-2, 0-5	181.13	6,459	1	3		3	1,615	923
22X-2, 0-5	190.73	12,376	1	6		5	1,768	1,031
23X-2, 0-5	200.33	3,594	1	3		3	899	513
24X-3, 0-5	211.43	7,529	2	6		6	941	538
25X-4, 0-5	222.53	7,850	2	8		7	785	462
26X-2, 0-5	225.03	4,084	1	5		4	681	408
27X-4, 0-5	232.23	2,283	2	7		7	254	143
28X-2, 0-5	239.23	4,694	2	8		7	469	276
29X-2, 0-5	248.43	6,590	1	4		4	1,318	732
30X-3, 0-5	253.13	3,533	1	6		5	505	294
31X-4, 0-5	261.13	3,812	1	5		6	635	318
32X-3, 0-5	269.23	2,921	1	3		2	730	487
33X-3, 0-5	278.83	1,805	1	5		5	301	164
34X-4, 0-5	290.03	1,437	2	6		5	180	111
35X-4, 0-5	299.63	3,363	1	8		7	374	210
36X-2, 0-5	306.33	1,716	1	3		2	429	286
37X-4, 0-5	318.93	1,755	1	6		5	251	146
38X-4, 0-5	328.63	1,835	1	4		4	367	204
39X-3, 145-150	338.18	2,304	2	7		6	256	154
40X-4, 0-5	347.93	914	2	8		7	91	54
41X-2, 0-5	354.53	655	2	7		2	73	60
42X-4, 0-5	367.13	2,644	3	14		12	156	91
44X-4, 0-5	386.33	1,255	1	8		7	139	78
45X-3, 0-5	394.33	42,099	3	25	2	16	1,504	915
46X-4, 0-5	405.53	1,475	1	7		7	184	98
47X-4, 0-5	415.03	3,272	2	15		8	192	131
48X-4, 0-5	424.73	2,991	1	10		7	272	166
49X-4, 0-5	434.33	3,927	3	27	1	17	131	82
50X-4, 0-5	443.93	2,760	1	10		7	251	153
Vacutainer								
167-1014A-								
12X-3, 50-51	96.61	553,605		19		6	29,137	22,144
13X-3, 50-51	106.31	755,988		32		11	23,625	17,581
14X-3, 50-51	115.91	954,451		24		7	39,769	30,789
15X-3, 50-51	125.51	721,068		35		12	20,602	15,342
16X-3, 50-51	135.11	759,233		41		14	18,518	13,804
18X-3, 50-51	154.31	643,853		43		14	14,973	11,296
19X-3, 50-51	163.91	522,878		45		14	11,620	8,862
20X-3, 50-51	173.51	704,225		41		10	17,176	13,808
21X-3, 50-51	183.11	676,510		44		11	15,375	12,300
22X-3, 50-51	192.71	819,357		34		7	24,099	19,984
23X-3, 50-51	202.31	597,779		47		11	12,719	10,307
24X-3, 50-51	211.91	657,282		47		11	13,985	11,332
25X-3, 50-51	221.51	507,116		60		12	8,452	7,043
26X-3, 50-51	227.01	482,555		51		14	9,462	7,424
27X-3, 50-51	231.21	707,017		55		11	12,855	10,712
28X-2, 50-51	239.31	346,329		58		15	5,971	4,744
29X-2, 50-51	248.91	715,781		40		7	17,895	15,229
30X-3, 50-51	253.61	693,065		46		9	15,067	12,601
31X-3, 50-51	260.11	665,955		49		9	13,591	11,482
32X-3, 50-51	269.71	689,809		46		8	14,996	12,774
33X-3, 50-51	279.31	646,208		42		7	15,386	13,188
34X-3, 50-51	289.01	673,566		51		8	13,207	11,416
35X-4, 50-51	300.11	649,931		9		4	72,215	49,995
36X-2, 50-51	306.81	792,184		50		7	15,844	13,898
40X-3, 50-51	346.91	396,452		56		9	7,080	6,099
41X-4, 50-51	358.01	383,141		57		10	6,722	5,719
42X-4, 50-51	367.61	242,256		63		13	3,845	3,188
44X-4, 50-51	386.81	282,459		58		10	4,870	4,154
45X-4, 50-51	396.31	640,477		64		8	10,007	8,896
46X-4, 50-51	406.01	713,967		62		8	11,516	10,200
47X-4, 50-51	415.51	516,110		78		11	6,617	5,799
48X-4, 50-51	425.21	719,292		60		8	11,988	10,578
49X-4, 50-51	434.30	843,892		61		8	13,834	12,230
50X-4, 50-51	443.90	851,856		57		7	14,945	13,310

Table 16. Depth variations in concentrations of inorganic carbon, calcium carbonate, total carbon, total organic carbon, total nitrogen, and total sulfur in weight percent (wt%) in Hole 1014A .

Core, section, interval (cm)	Depth (mbsf)	Inorganic carbon (wt%)	CaCO ₃ (wt%)	Total carbon (wt%)	Total organic carbon (wt%)	Total nitrogen (wt%)	Total sulfur (wt%)	Total organic carbon/total nitrogen
167-1014A-								
1H-1, 30-31	0.3	5.24	43.6	10.83	5.59	0.65	0.75	8.6
1H-2, 30-31	1.8	3.84	32	8.33	4.49	0.53	1.05	8.5
2H-1, 30-31	3.4	3.09	25.7	7.34	4.25	0.45	1.29	9.4
2H-2, 30-31	4.9	3.41	28.4	8.34	4.93	0.51	1.2	9.7
2H-3, 30-31	6.4	3.34	27.8	8.1	4.76	0.58	1.48	8.2
2H-4, 30-31	7.9	2.59	21.6	8.83	6.24	0.72	1.82	8.7
2H-5, 30-31	9.4	2.05	17.1	8.12	6.07	0.61	1.99	10
2H-6, 30-31	10.9	4.28	35.7	9.39	5.11	0.52	1.31	9.8
2H-7, 30-31	12.4	2.93	24.4	8.9	5.97	0.59	1.91	10.1
3H-1, 30-31	12.9	2.71	22.6	8.57	5.86	0.58	1.81	10.1

Only part of this table is produced here. The entire table appears on CD-ROM, back pocket, this volume.

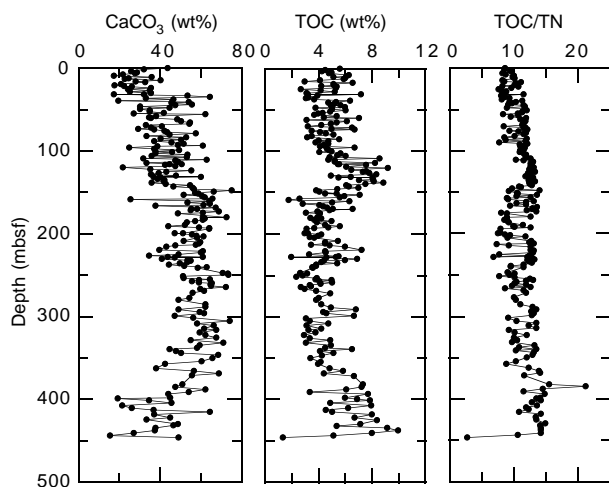


Figure 16. Depth variations of calcium carbonate, total organic carbon content, and TOC/TN ratio in sediments of Hole 1014A.

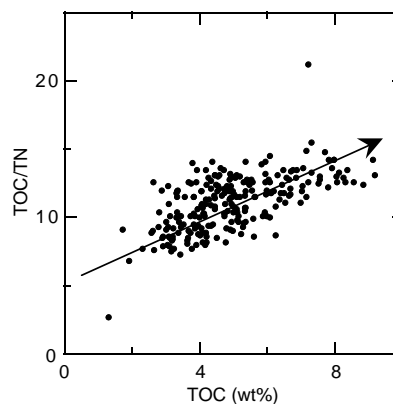


Figure 17. TOC/TN ratio vs. total organic carbon content (TOC) in sediments of Hole 1014A. Arrow indicates the slightly positive correlation between TOC and TOC/TN ratios.

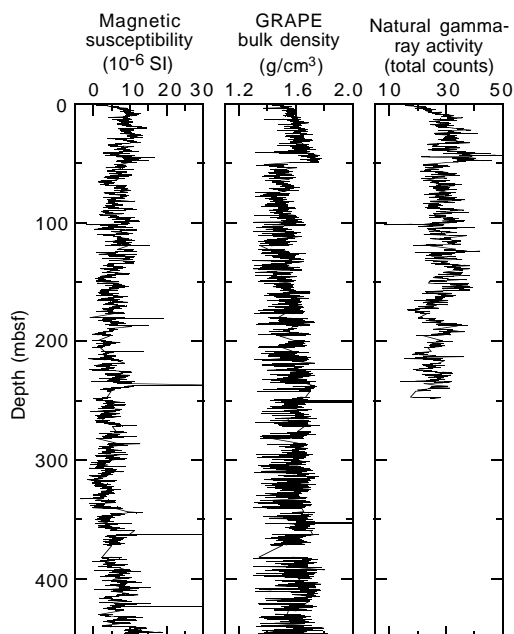


Figure 18. MST data from Hole 1014A.

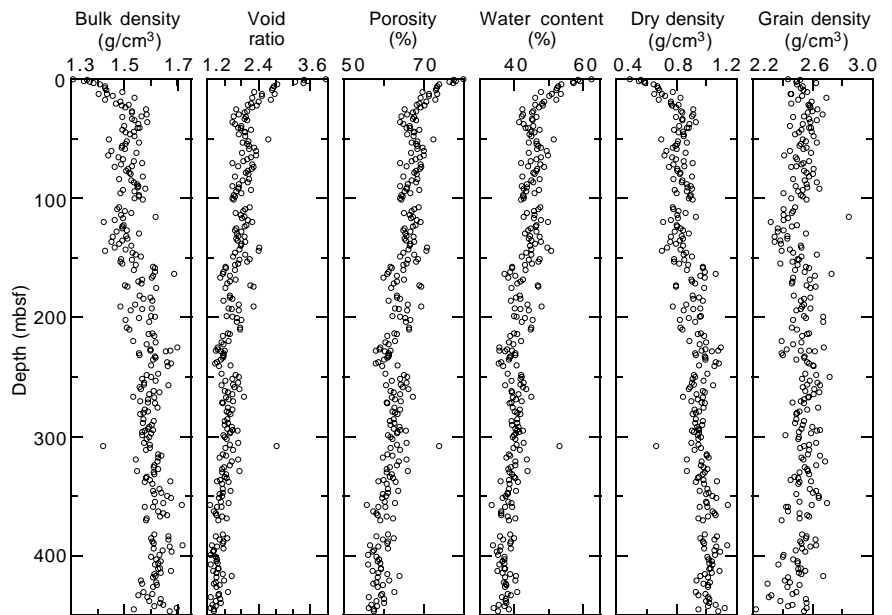


Figure 19. Index property data from Hole 1014A.

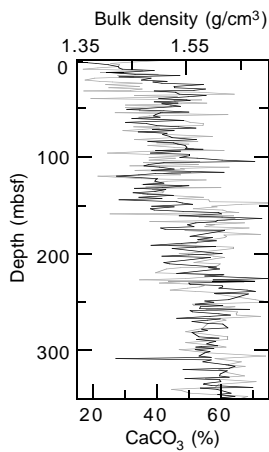


Figure 20. Gravimetric bulk density (dark line) vs. discrete calcium carbonate content (gray line) from Hole 1014A.

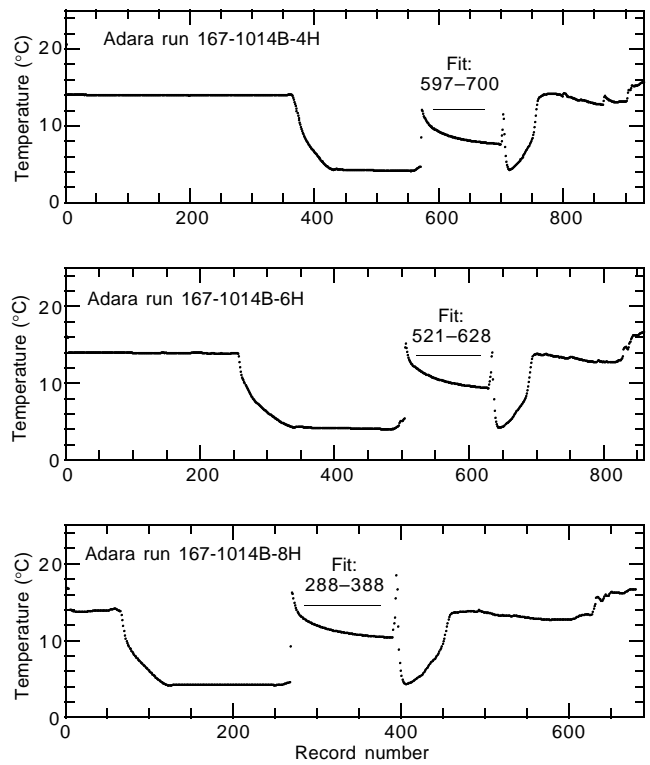


Figure 21. Hole 1014B downhole temperature vs. record number (5-s recording frequency) for each measurement run, showing the intervals fitted to determine downhole temperature.

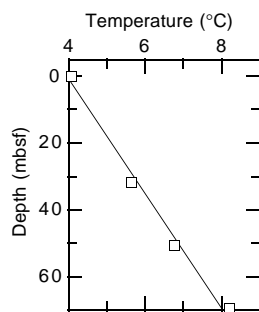


Figure 22. Downhole temperature gradient for Hole 1014B.

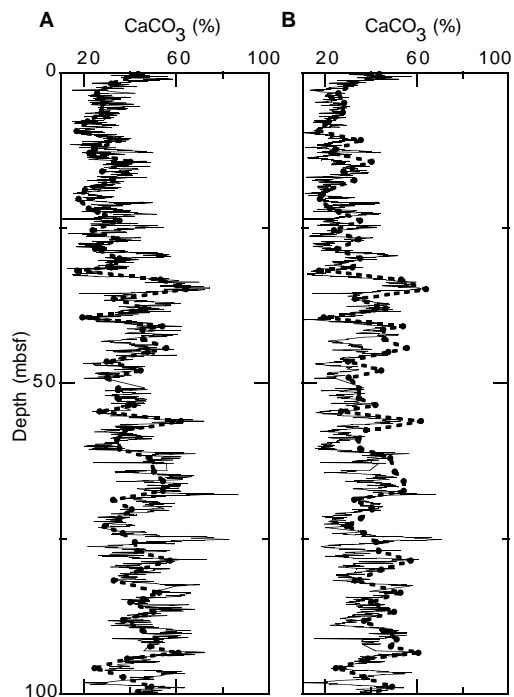


Figure 23. Summary of measured and estimated calcium carbonate values for 0–100 mbsf in Hole 1014A. **A.** Based on Site 1012 regression (solid line = estimated values, dashed line connects measured values). **B.** Based on a combined regression for Sites 1012 and 1013 (symbols as in part A).

Table 19. Downhole measurements at Hole 1014A.

Date, time	Description
10 May 1996	
0145	Set pipe at 84 mbsf, start wireline rig up, seas moderate (2-m swell).
0245	Finish wireline rig up, RIH density-porosity combination tool string.
0430	At TD (445 mbsf), wireline heave compensator on, start density-porosity pass 1 (98–443 mbsf); 300 m/hr.
0600	At TD (277.5 mbsf), wireline heave compensator on, start density-porosity pass 2 (0–325 mbsf), 300 m/hr continue log recording to mudline.
0730	Rig down density-porosity, rig up and RIH with sonic-FMS toolstring.
0930	At TD, wireline heave compensator on, begin sonic-FMS pass 1 (103–444 mbsf) at 300 m/hr.
1210	End sonic-FMS pass 1, POOH, rig up GHMT.
1435	At TD with GHMT, begin pass 1 (75–445 mbsf) at 1000 m/hr.
1530	At TD with GHMT, begin pass 2 (75–445 mbsf) at 1000 m/hr.
1535	End GHMT pass 2, POOH GHMT, rig down.

Note: RIH = run in hole, TD = total depth, FMS = Formation MicroScanner, POOH = pull out of hole, GHMT = geological high-sensitivity magnetic tool.

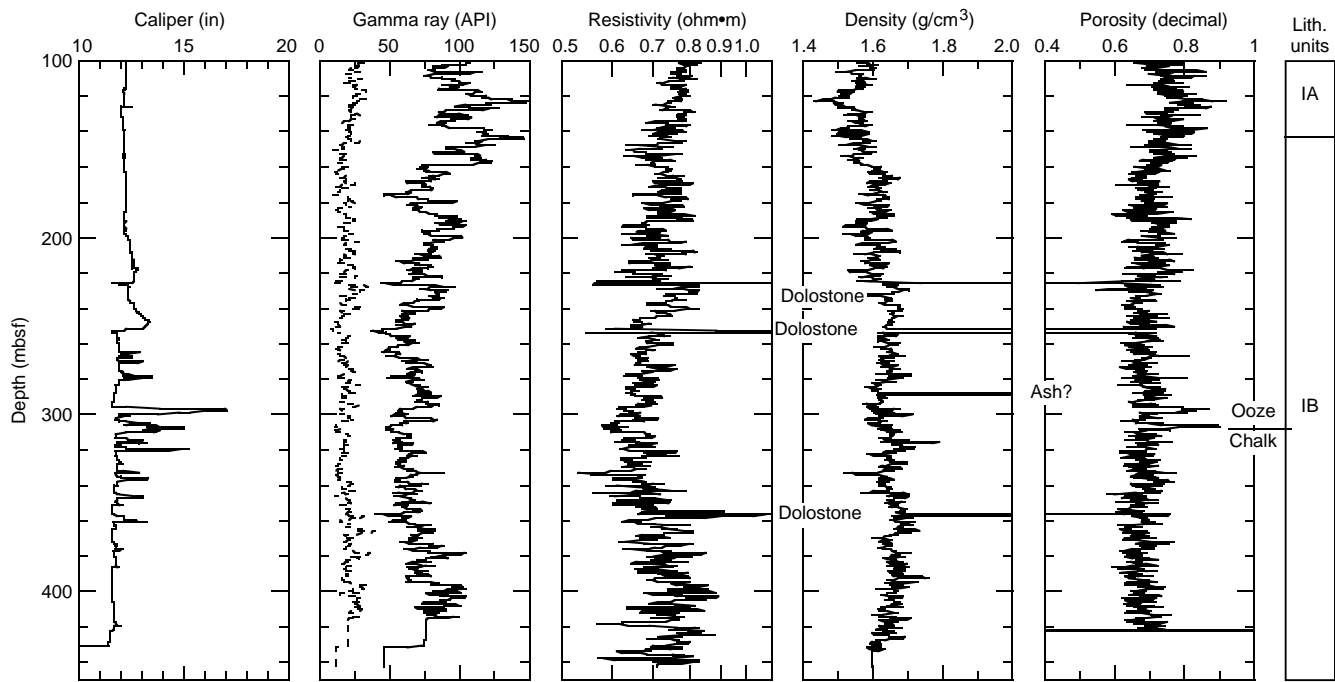


Figure 24. Downhole log data from the density-porosity combination tool string (pass 1) and a lithologic summary column at Hole 1014A (see “Lithostratigraphy” section, this chapter).

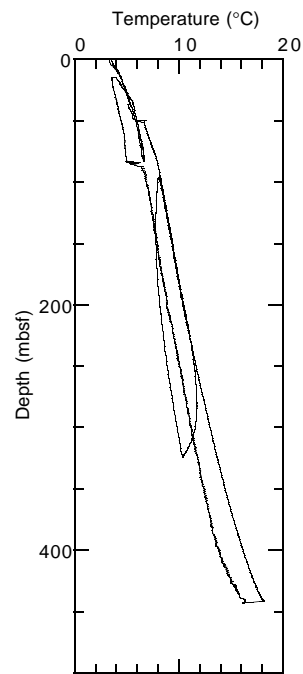


Figure 25. Borehole temperature measurements from the Lamont-Doherty temperature logging tool.

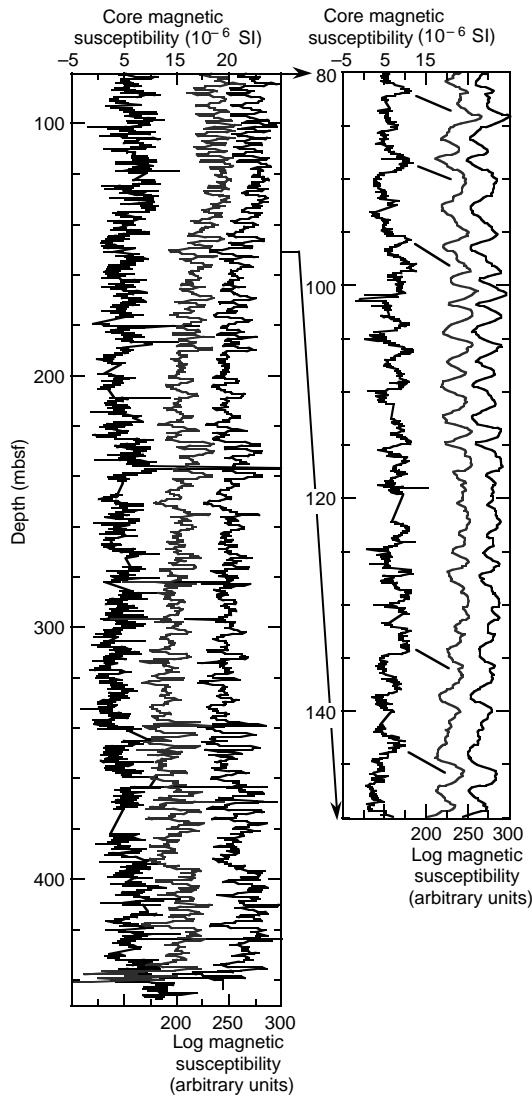


Figure 26. Hole 1014A magnetic susceptibility log data for passes 1 and 2.

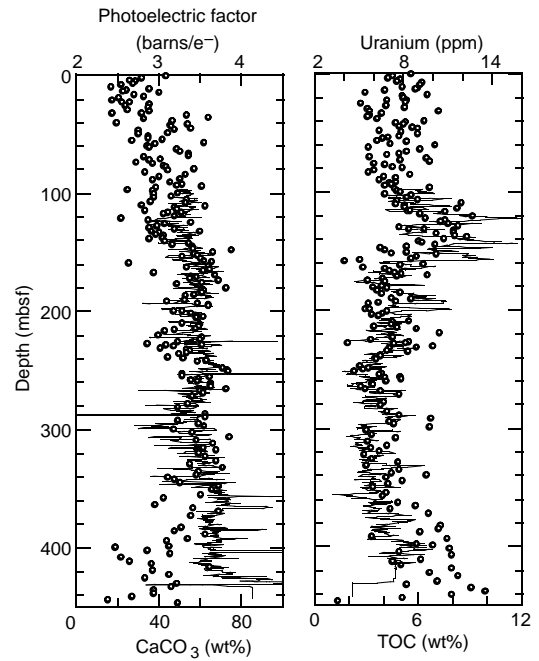


Figure 27. Log photoelectric effect (PEF) data compared to the calcium carbonate abundances measured at Hole 1014A.

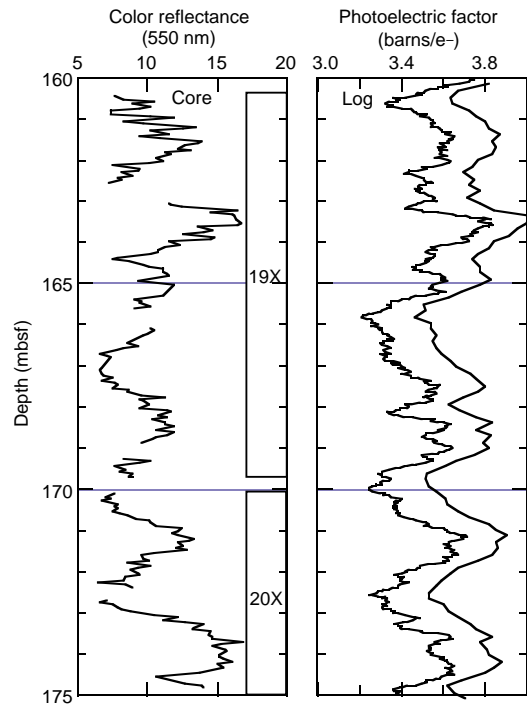


Figure 28. Comparison between the core-based color reflectivity data at Hole 1014A (550-nm channel) and the standard (PEF) and processed, high-resolution (HPEF) photoelectric effect log data for the 160–175 mbsf interval.

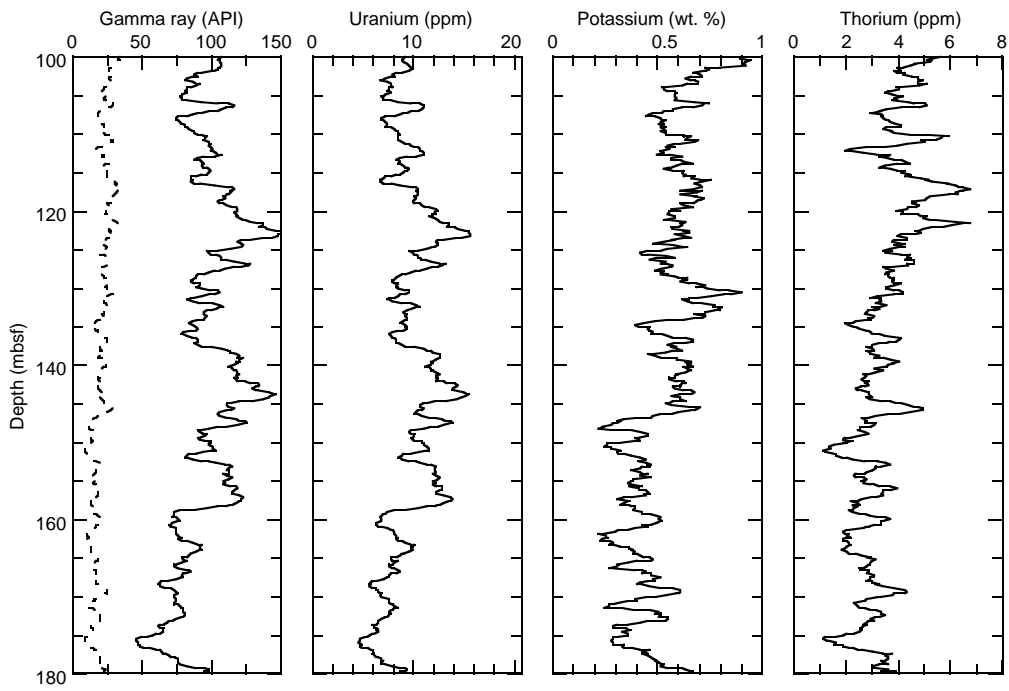


Figure 29. Log variations in total (HSGR) and uranium-corrected (HCGR) gamma-ray activities and individual K, U, and Th natural gamma-ray contributions at Hole 1014A.

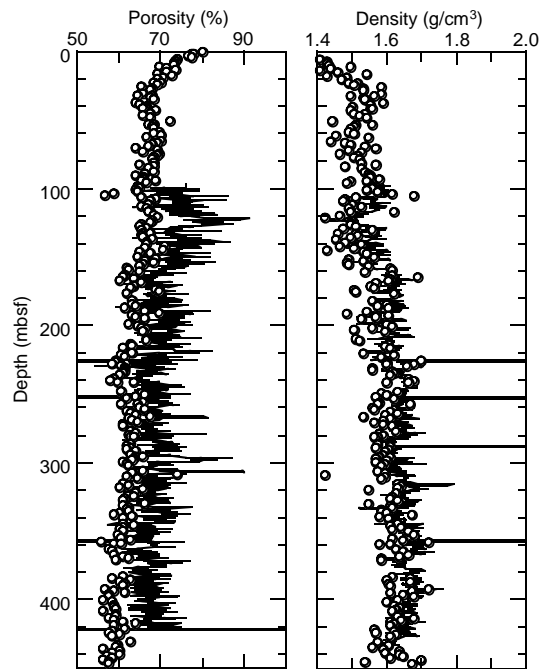


Figure 30. Comparison of core (open symbols) and log (line) physical properties data.

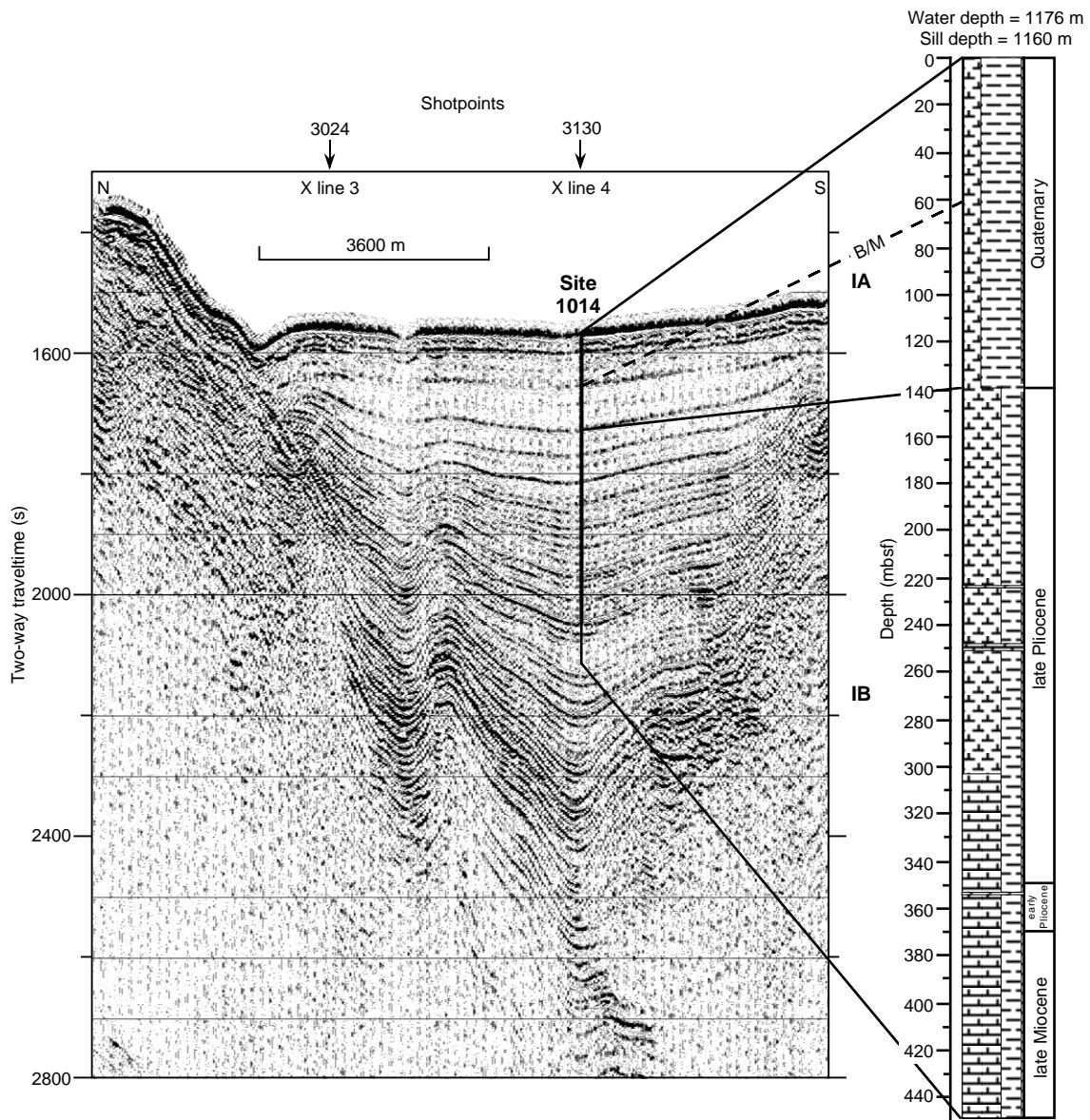


Figure 31. Comparison of the lithostratigraphic column at Site 1014 and a seismic profile through the site (Line EW9504 CA15-6; Lyle et al., 1995a, 1995b). Ties are calculated using measured seismic velocity profiles in Sites 1012 and 1013. On y-axis, (s) = milliseconds.

SHORE-BASED LOG PROCESSING

HOLE 1014A

Bottom felt: 1175.8 mbrf (used for depth shift to seafloor)

Total penetration: 449 mbsf

Total core recovered: 404.4 m (90%)

Logging Runs

Logging string 1: DIT/SDT/HLDT/APS/HNGS (2 passes)

Logging string 2: FMS/GPIT/SDT/NGT

Logging string 3: GHMT/NGT (2 passes)

Wireline heave compensator was used to counter ship heave.

Bottom-Hole Assembly

The following bottom-hole assembly depths are as they appear on the logs after differential depth shift (see "Depth shift" section) and depth shift to the seafloor. As such, there might be a discrepancy with the original depths given by the drillers onboard. Possible reasons for depth discrepancies are ship heave, use of wireline heave compensator, and drill string and/or wireline stretch.

DIT/SDT/HLDT/APS/HNGS: Did not reach bottom-hole assembly (pass 1).

DIT/SDT/HLDT/APS/HNGS: Bottom-hole assembly at ~55 mbsf (pass 2).

FMS/GPIT/SDT/NGT: Bottom-hole assembly at ~55 mbsf.

GHMT/NGT: Did not reach bottom-hole assembly (pass 1).

GHMT/NGT: Bottom-hole assembly at ~55 mbsf (pass 2).

Processing

Depth shift: Original logs have been interactively depth shifted with reference to NGT from DIT/HLDT/APS/HNGS pass 1, and to the seafloor (-1175.8 m).

Gamma-ray and environmental corrections: Corrections for borehole size and type of drilling fluid were performed on the NGT data from the FMS/GPIT/SDT/NGT and GHMT/NGT tool strings. HNGS data from the DIT/HLDT/APS/HNGS tool string were corrected in real-time during the recording.

Acoustic data processing: The array sonic tool was operated in standard depth-derived, borehole compensated, long-spacing (8-10-10-12 ft) and short-spacing (3-5-5-7 ft) mode. Because of the poor quality of the transit times, only one of the 10-ft spaced readings (LTT4) was edited and used to compute an uncompensated velocity value.

Quality Control

Data recorded through bottom-hole assembly, such as the HNGS data above 55 mbsf (pass 1) should be used qualitatively only because of the attenuation on the incoming signal.

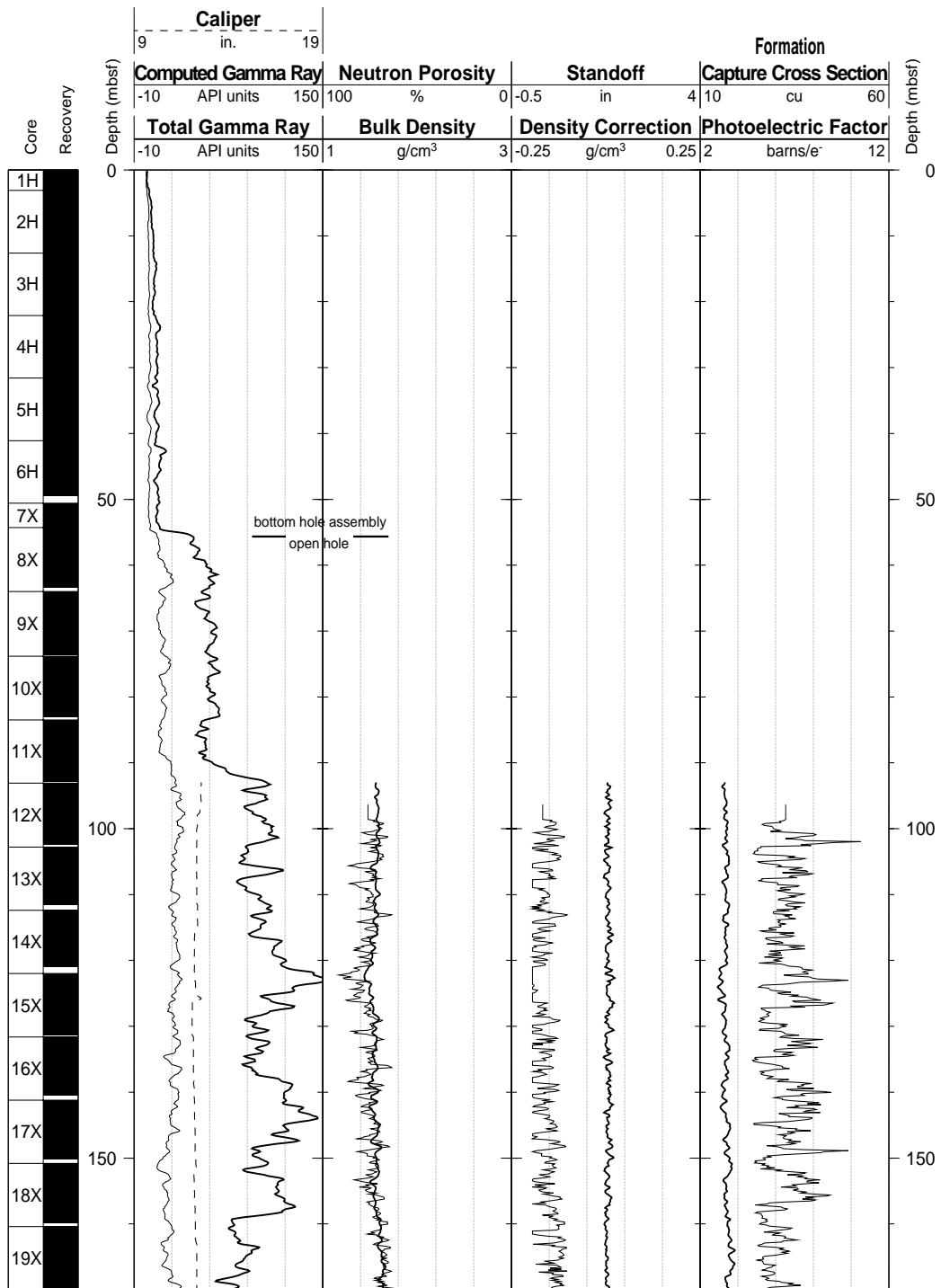
Hole diameter was recorded by the hydraulic caliper on the HLDT tool (CALI) and the caliper on the FMS string (C1 and C2).

Note: Details of standard shore-based processing procedures are found in the "Explanatory Notes" chapter, this volume. For further information about the logs, please contact:

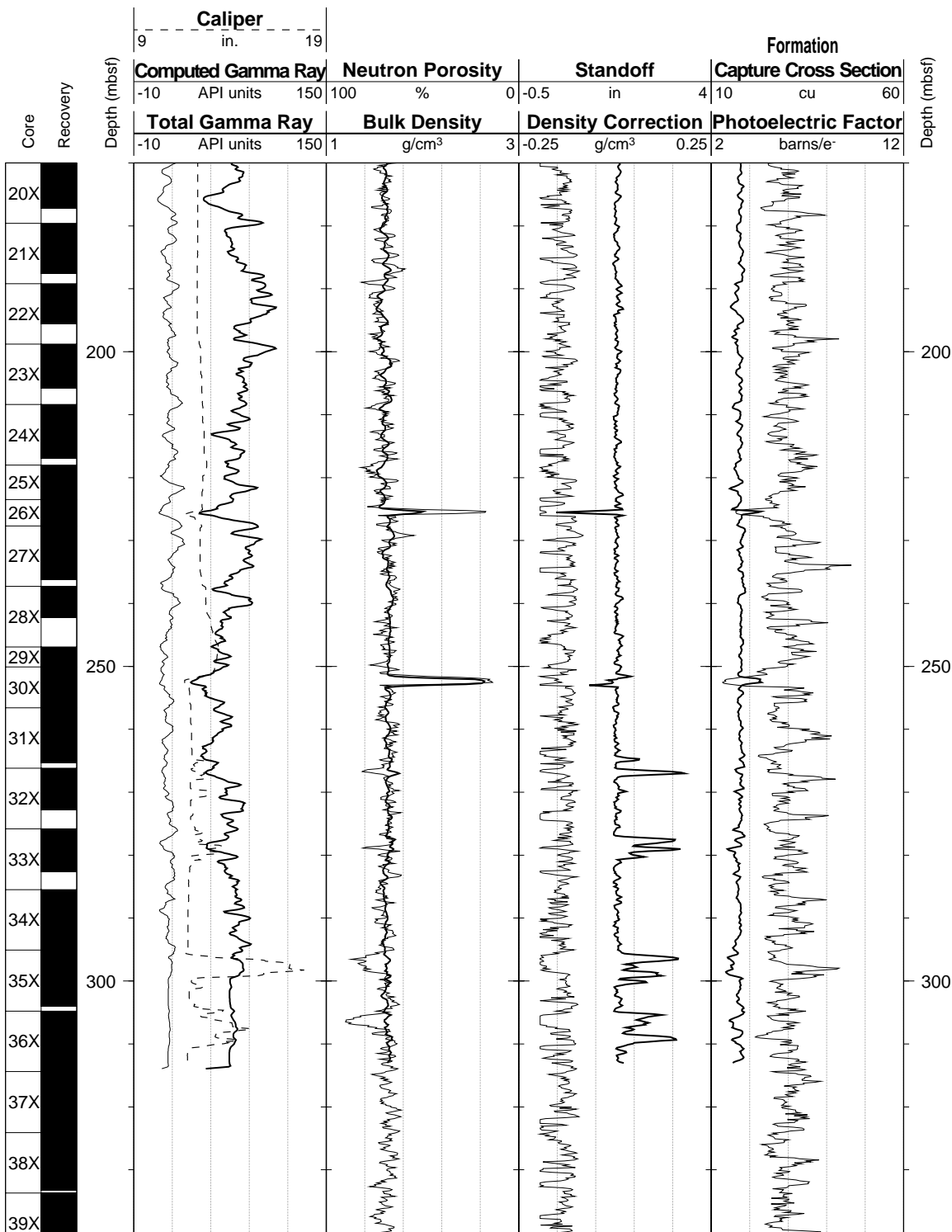
Cristina Broglia
Phone: 914-365-8343
Fax: 914-365-3182
E-mail: chris@ldeo.columbia.edu

Zhiping Tu
Phone: 914-365-8336
Fax: 914-365-3182
E-mail: ztu@ldeo.columbia.edu

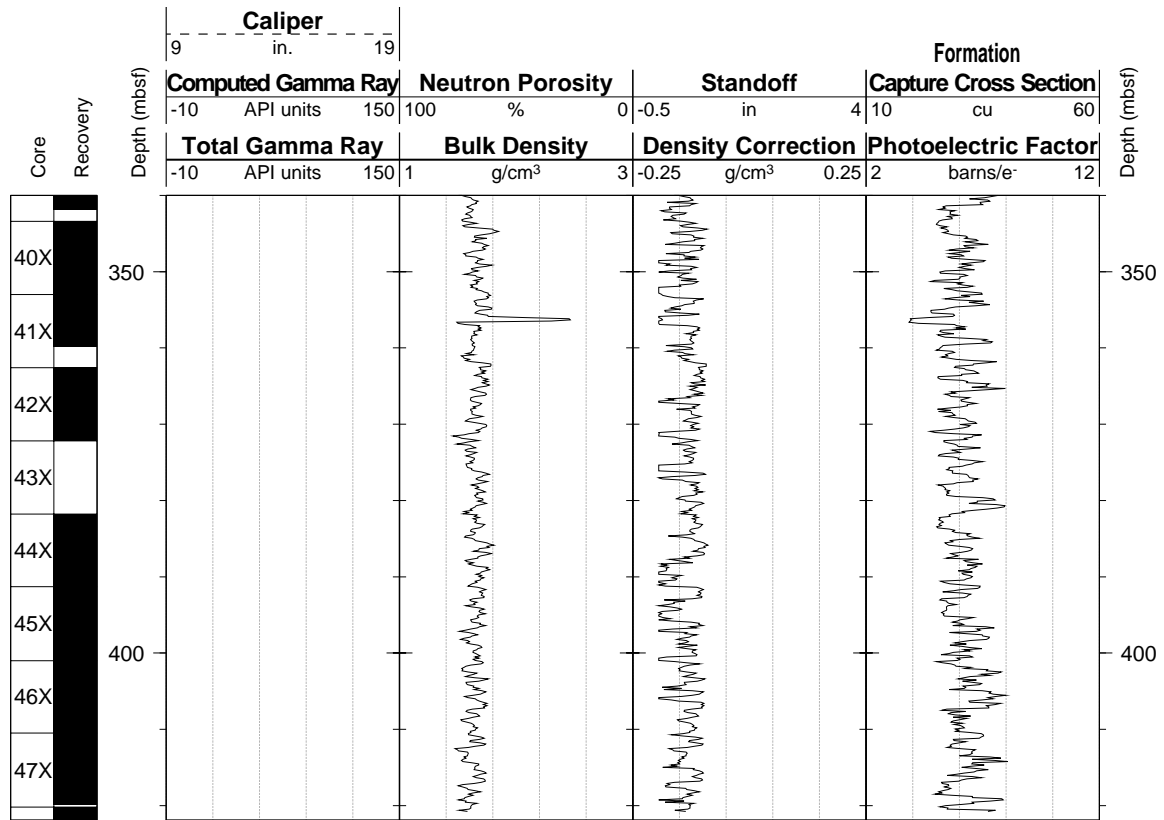
Hole 1014A: Natural Gamma Ray-Density-Porosity Logging Data-Pass 2



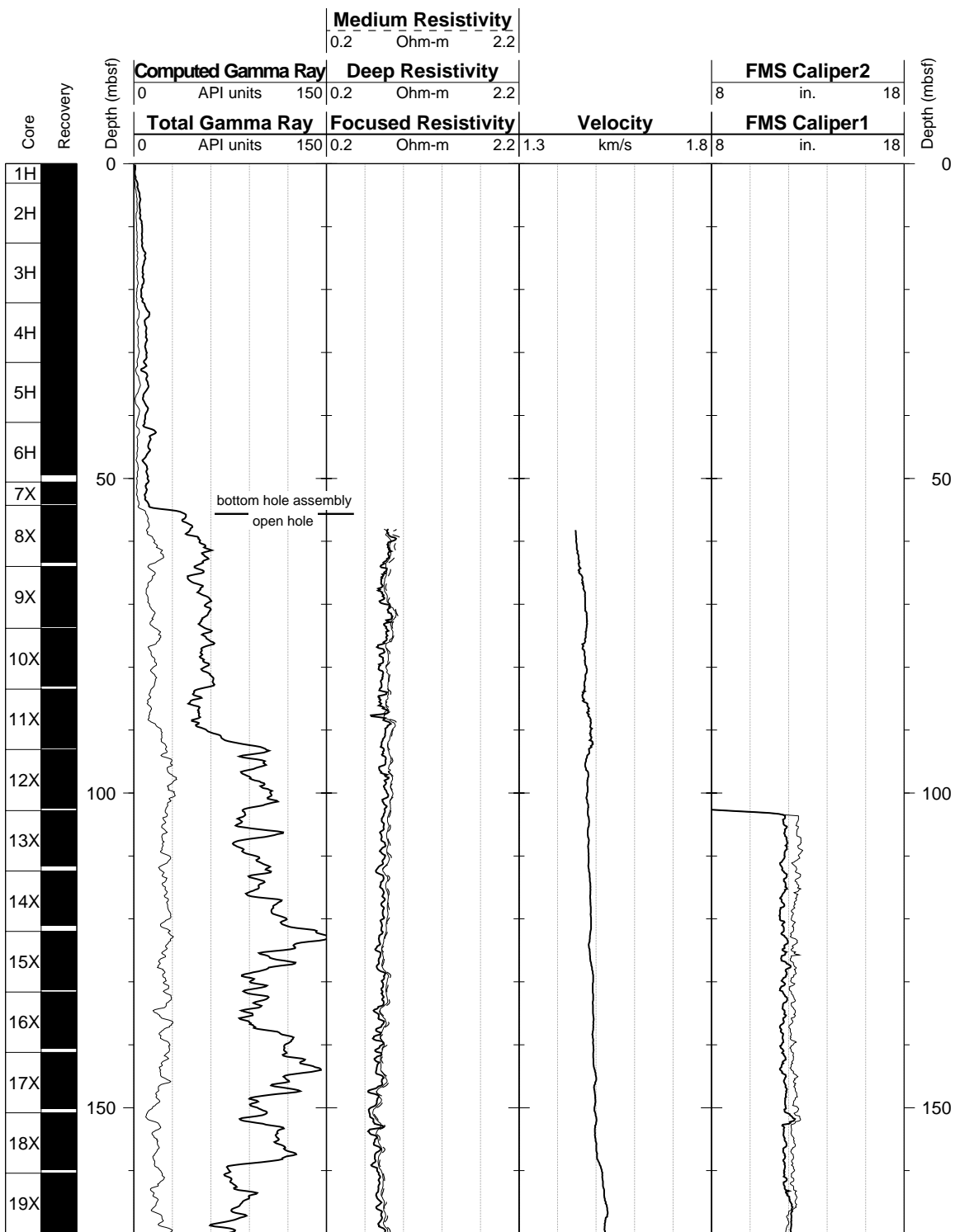
Hole 1014A: Natural Gamma Ray-Density-Porosity Logging Data-Pass 2 (cont.)



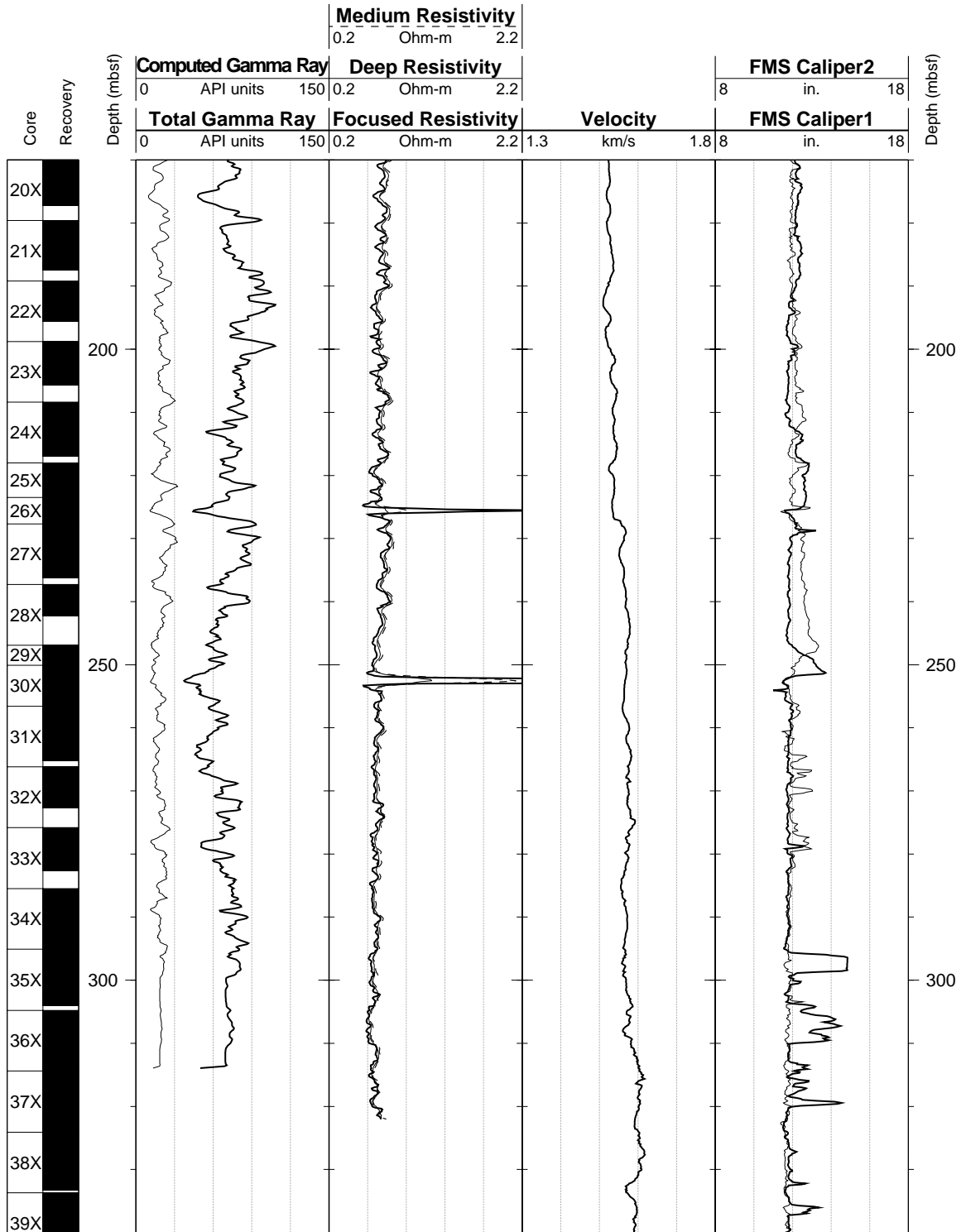
Hole 1014A: Natural Gamma Ray-Density-Porosity Logging Data-Pass 2 (cont.)



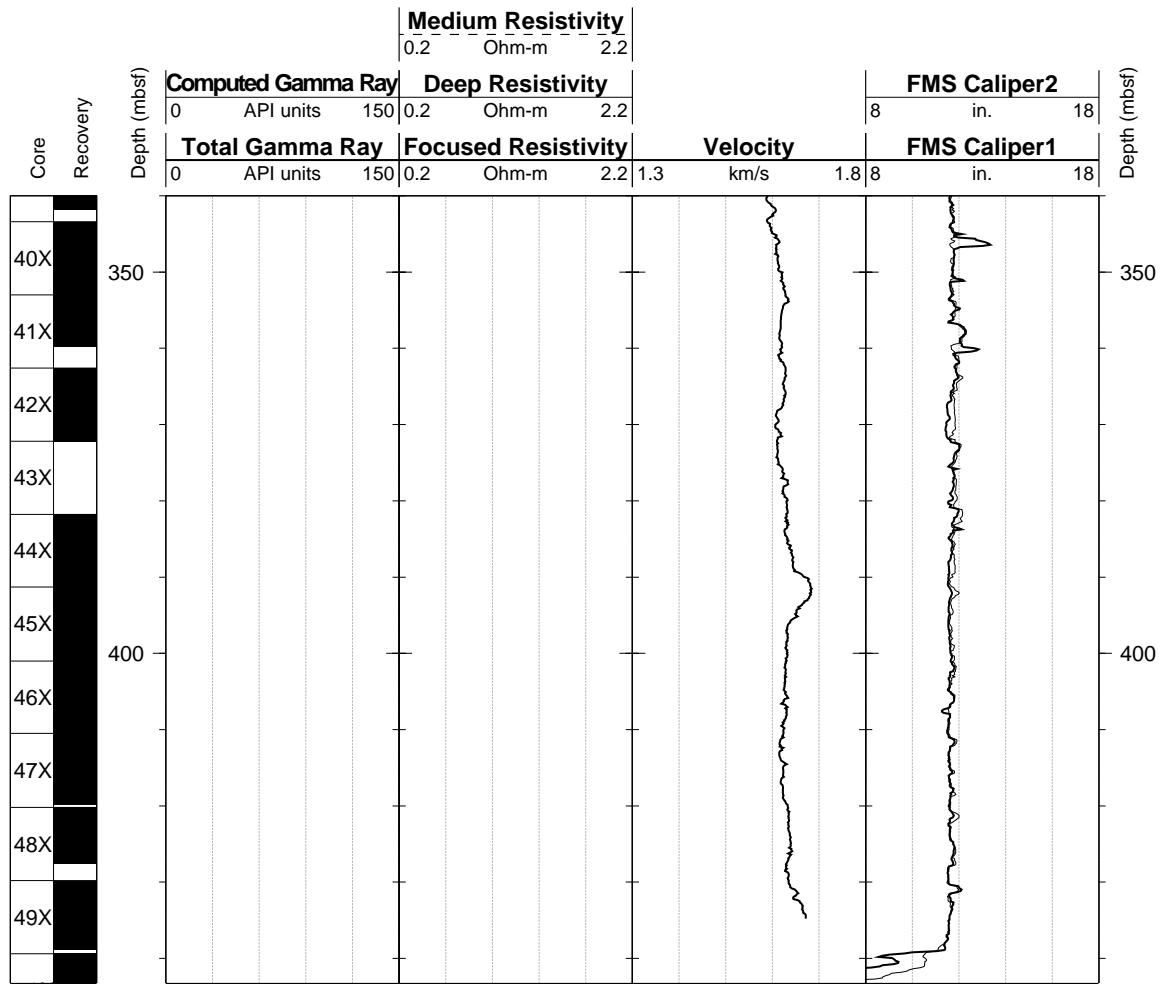
Hole 1014A: Natural Gamma Ray-Resistivity-Sonic Logging Data-Pass 2



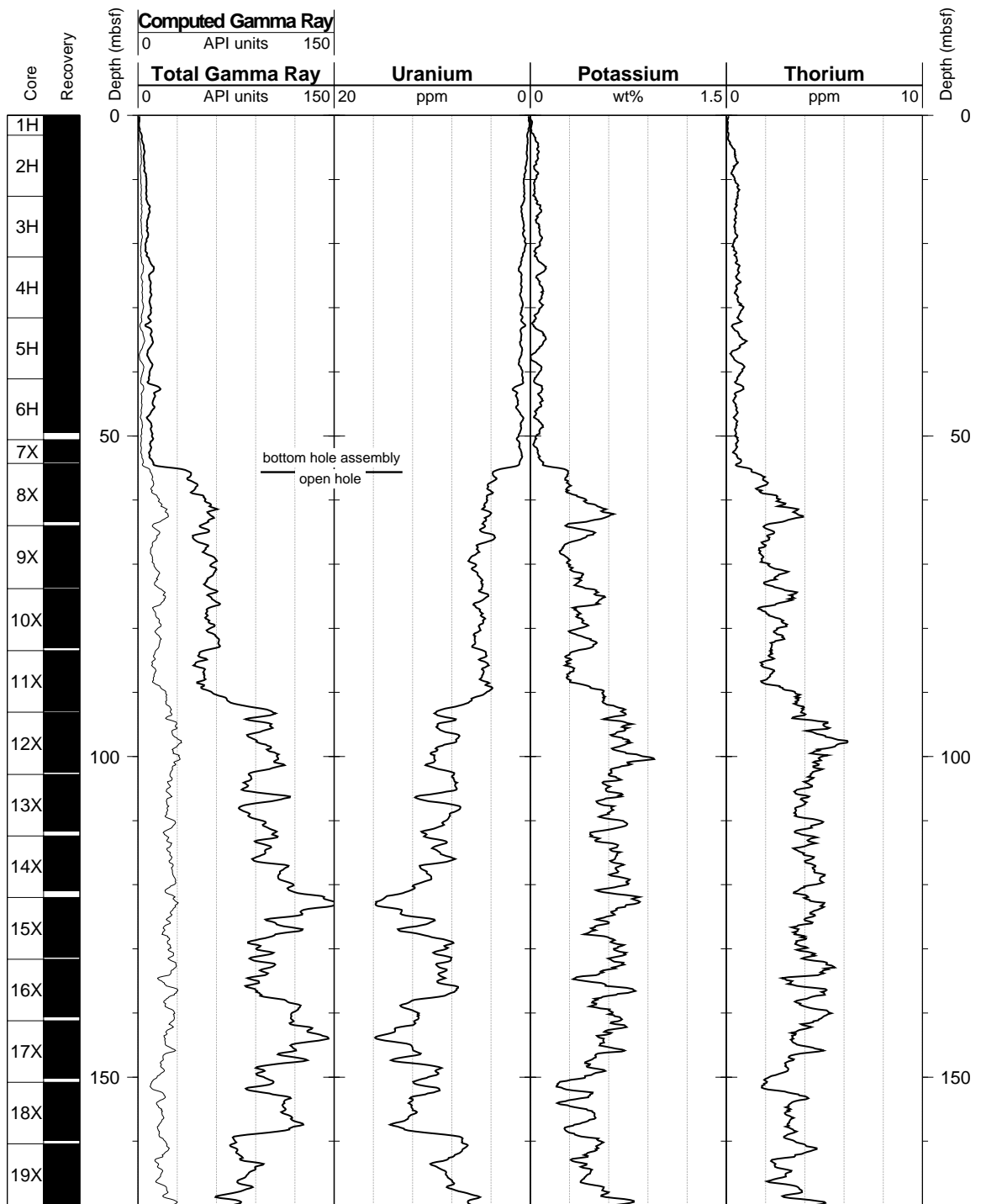
Hole 1014A: Natural Gamma Ray-Resistivity-Sonic Logging Data-Pass 2 (cont.)



Hole 1014A: Natural Gamma Ray-Resistivity-Sonic Logging Data-Pass 2 (cont.)



Hole 1014A: Natural Gamma Ray Logging Data-Pass 2



Hole 1014A: Natural Gamma Ray Logging Data-Pass 2 (cont.)

